(19) **United States**
(12) **Patent Application Publication**
Moslehi
(10) **Pub. No.: US 2009/0107545 A1**
(43) **Pub. Date: Apr. 30, 2009**

(54) **TEMPLATE FOR PYRAMIDAL THREE-DIMENSIONAL THIN-FILM SOLAR CELL MANUFACTURING AND METHODS OF USE**

(75) Inventor: **Mehrdad Moslehi**, Los Altos, CA (US)

Correspondence Address:
HULSEY IP INTELLECTUAL PROPERTY LAWYERS, P.C.
919 Congress Avenue, Suite 919
AUSTIN, TX 78701 (US)

(73) Assignee: **Soltaix, Inc.**

(21) Appl. No.: **11/868,492**

(22) Filed: **Oct. 6, 2007**

Related U.S. Application Data

(60) Provisional application No. 60/828,678, filed on Oct. 9, 2006, provisional application No. 60/886,303, filed on Jan. 24, 2007.

Publication Classification

(51) **Int. Cl.**
H01L 31/00 (2006.01)
H01L 21/02 (2006.01)

(52) **U.S. Cl.** **136/256**; 438/57; 257/E21.002

(57) **ABSTRACT**

A template **120** for pyramidal three-dimensional thin-film solar cell substrate formation for use in pyramidal three-dimensional thin-film solar cells. The template **120** comprises a substrate which comprises a plurality of pyramid trenches **122** between a plurality of posts **123**. The template **120** forms an environment for pyramidal three-dimensional thin-film solar cell substrate formation.

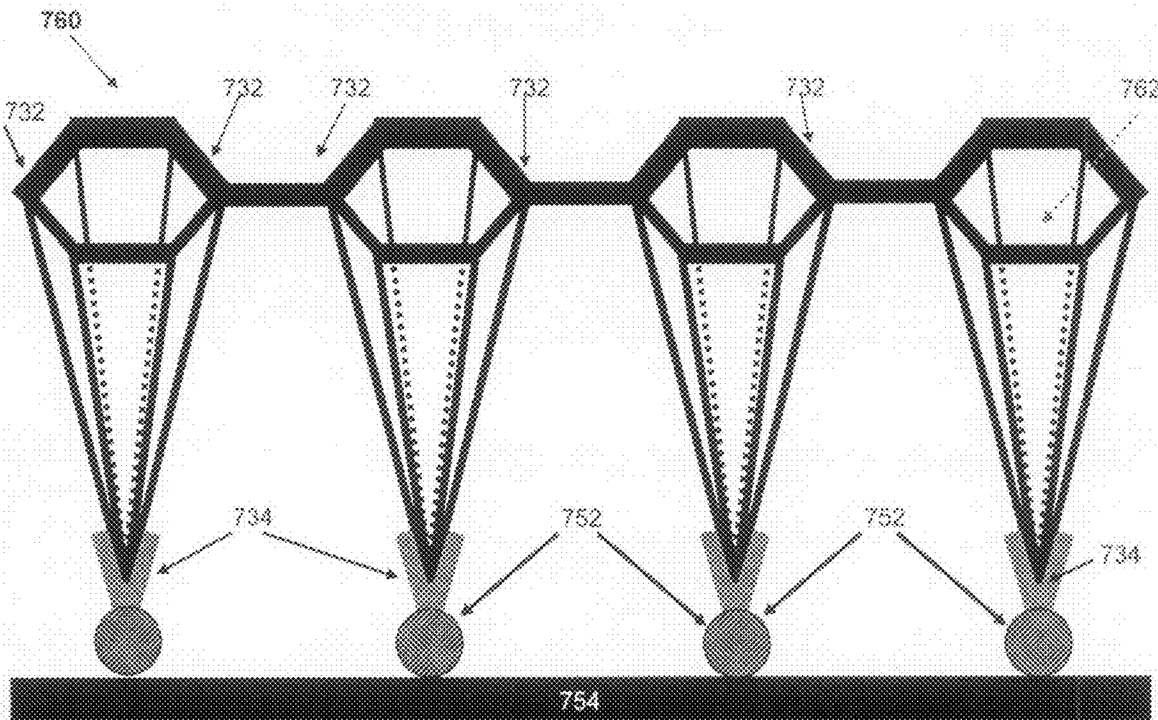

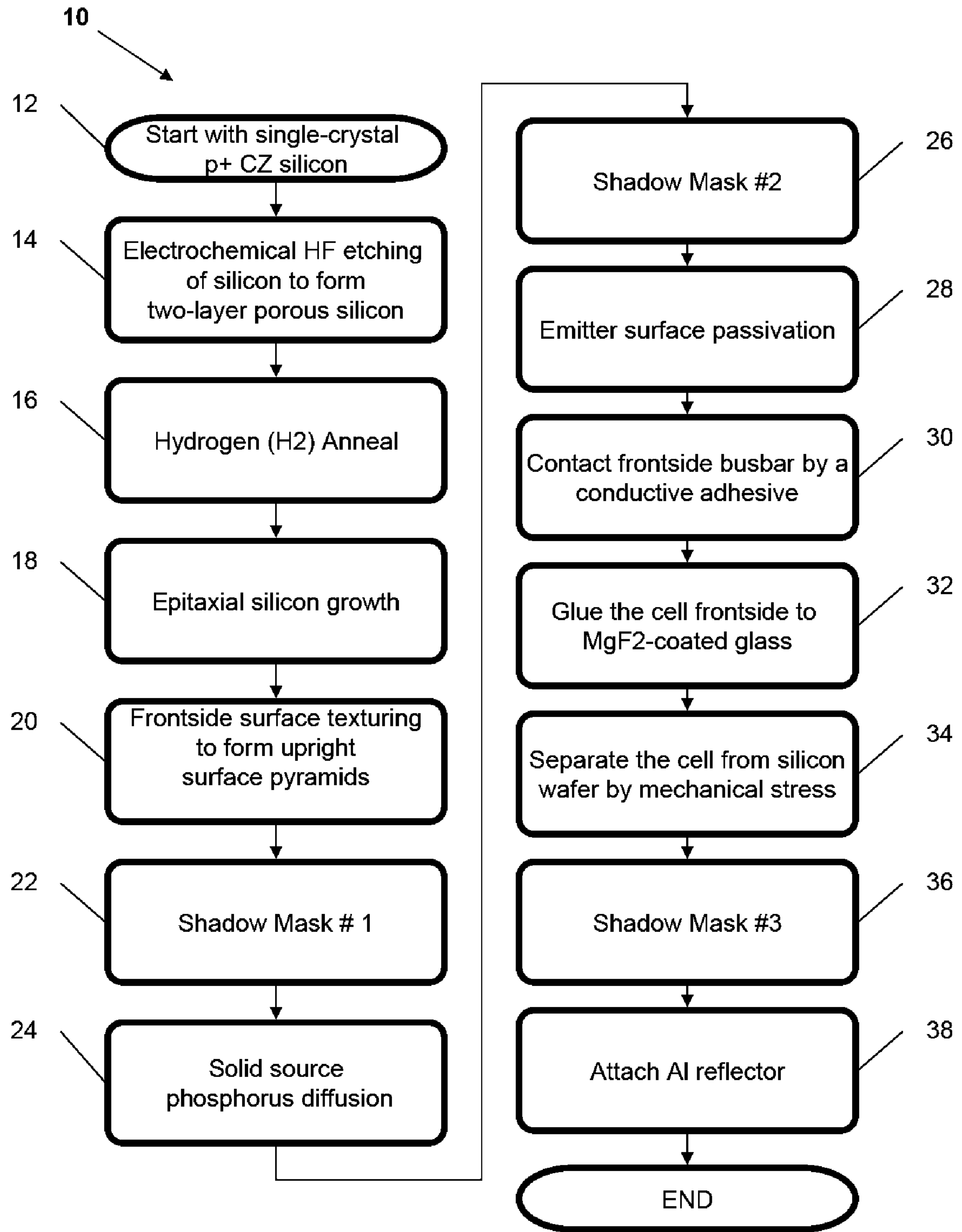

FIG. 1
(PRIOR ART)

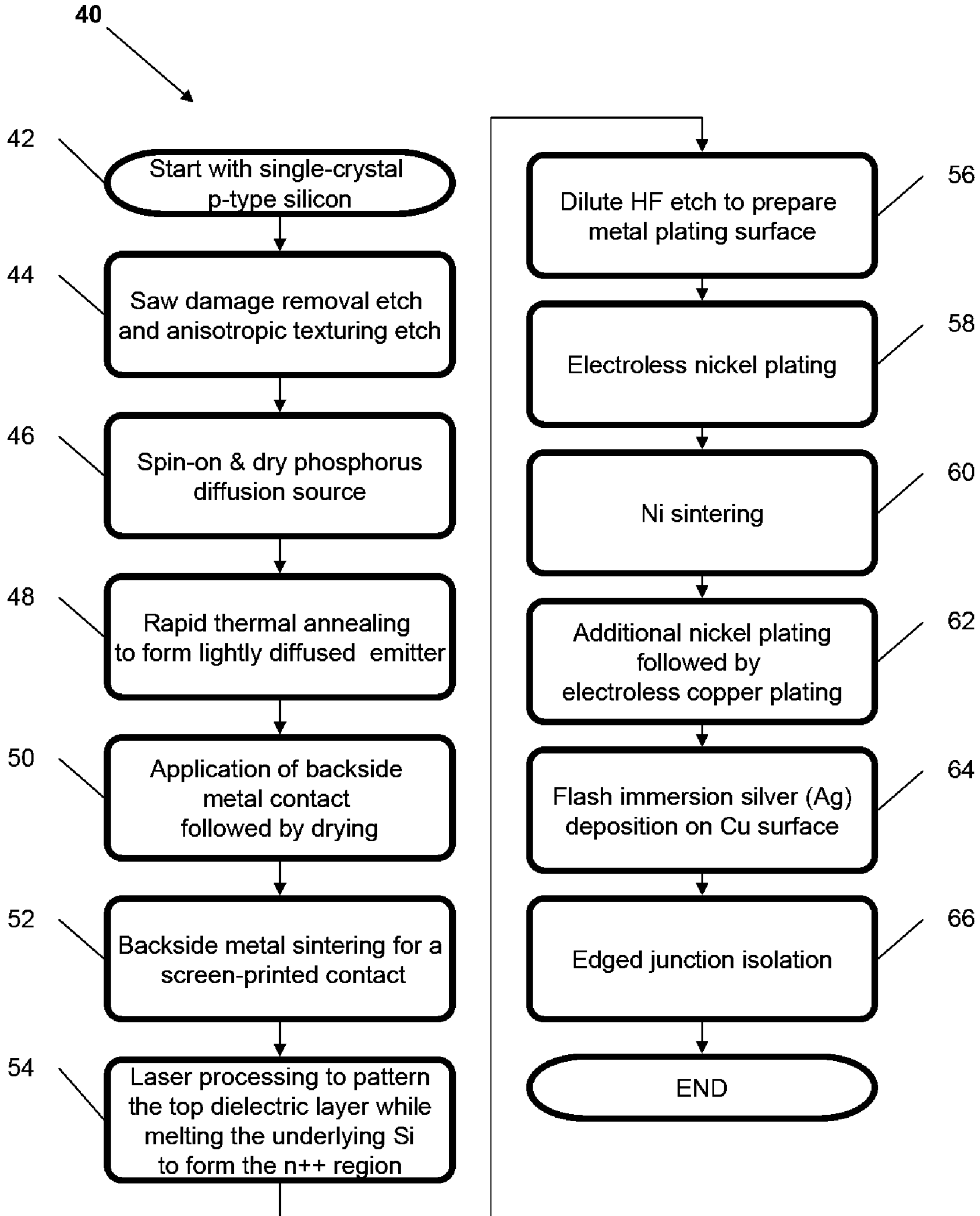

FIG. 2
(PRIOR ART)

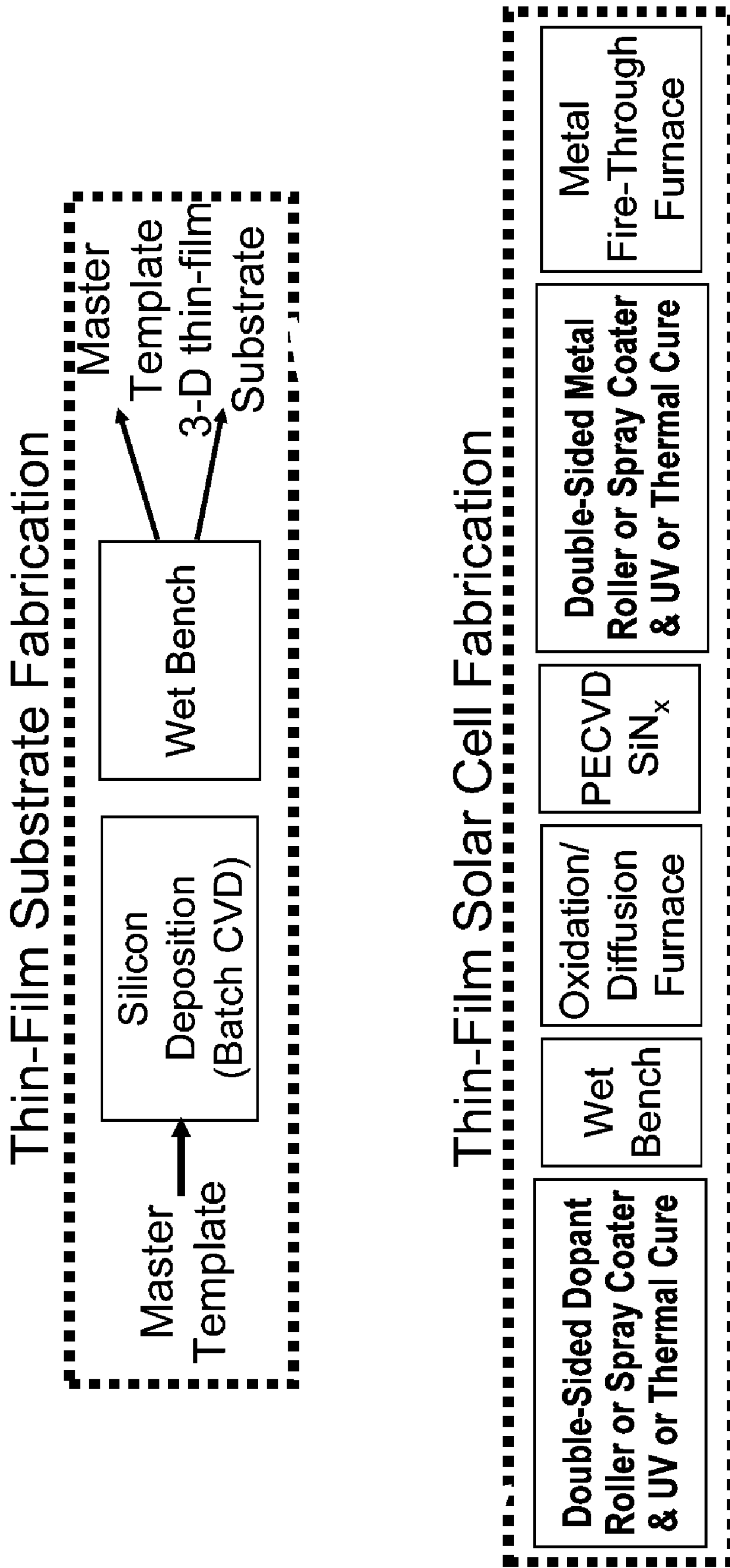

FIG. 3

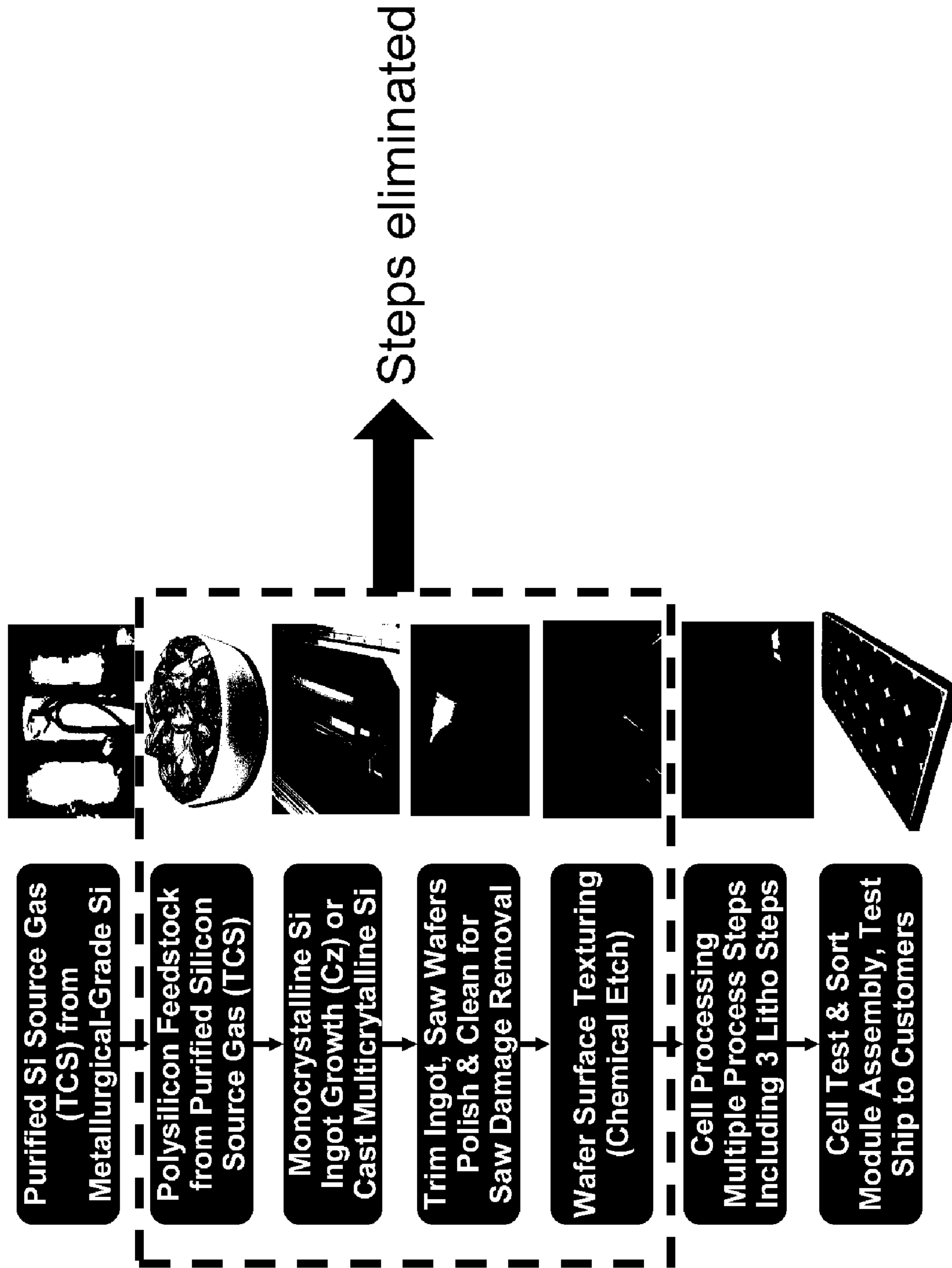

FIG. 4
(PRIOR ART)

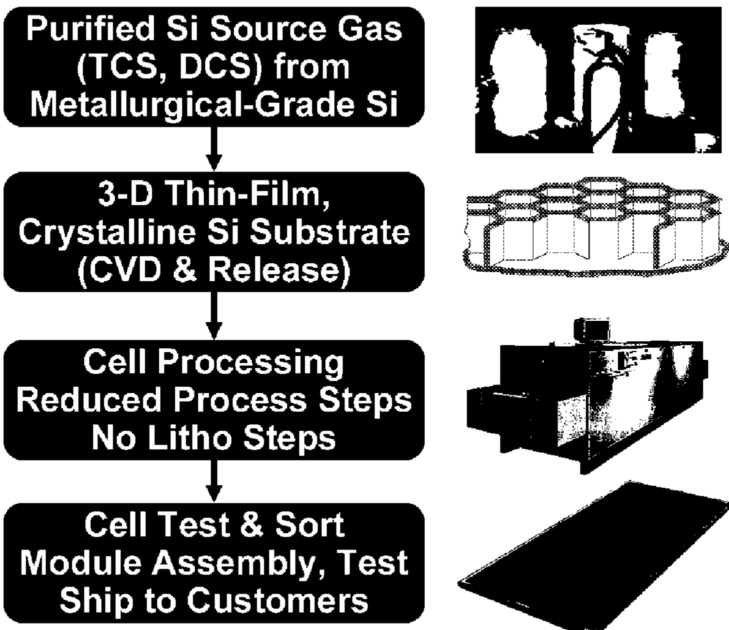

Competitive Advantages of Current Invention

1. < 1 gram of silicon per watt
2. Decoupled from silicon supply chain
3. No polysilicon feedstock cost
4. No crystal growth cost
5. No wire saw cost
6. No wafer saw damage removal cost
7. No texturing cost
8. No lithography cost for cell processing
9. Fewer process steps - self aligned flow
10. Reduced PV fab capital cost
11. >60% reduction in module mfg. cost/Wp
12. Ultra-high-efficiency cells & modules

FIG. 5

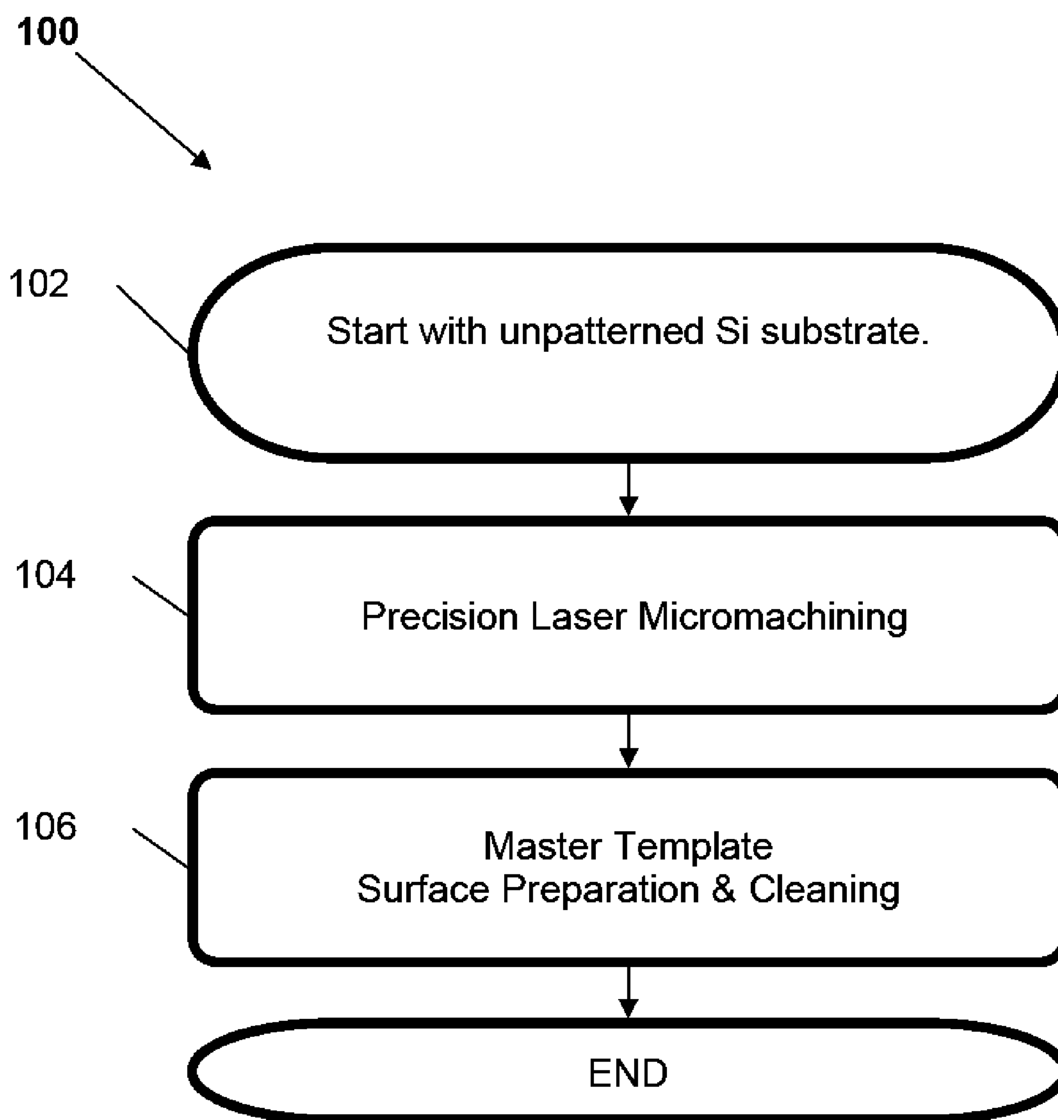

FIG. 6

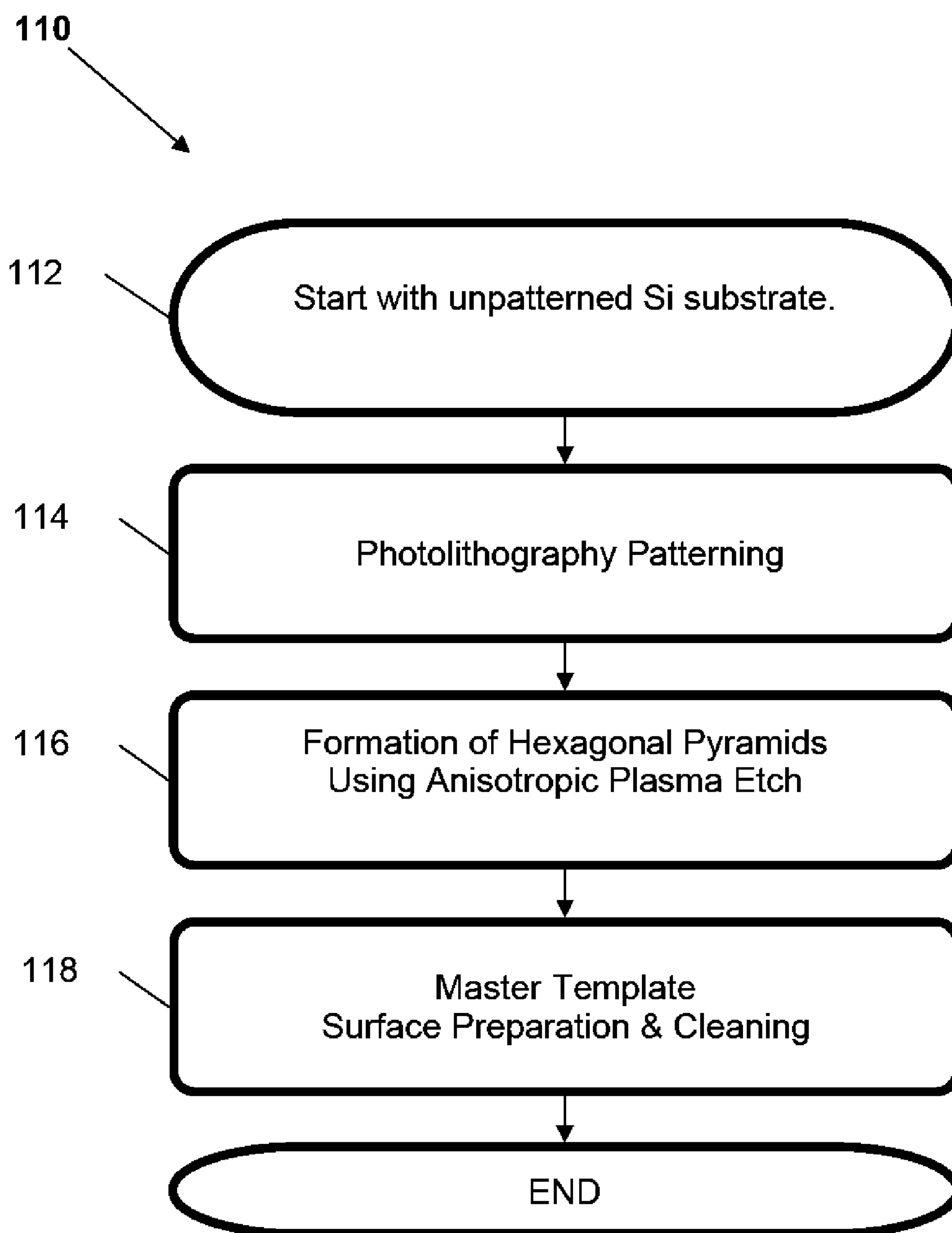

FIG. 7

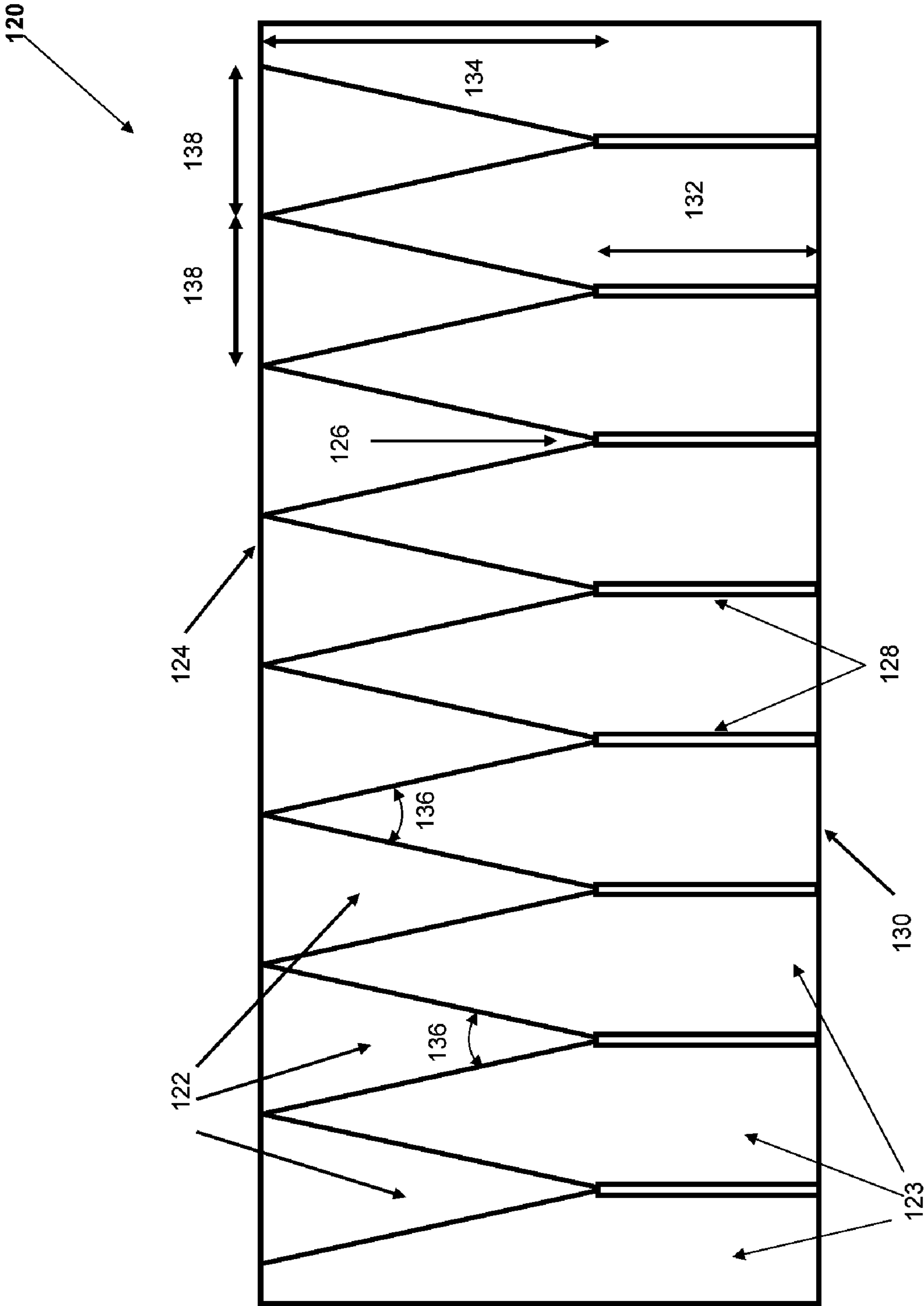

FIG. 8

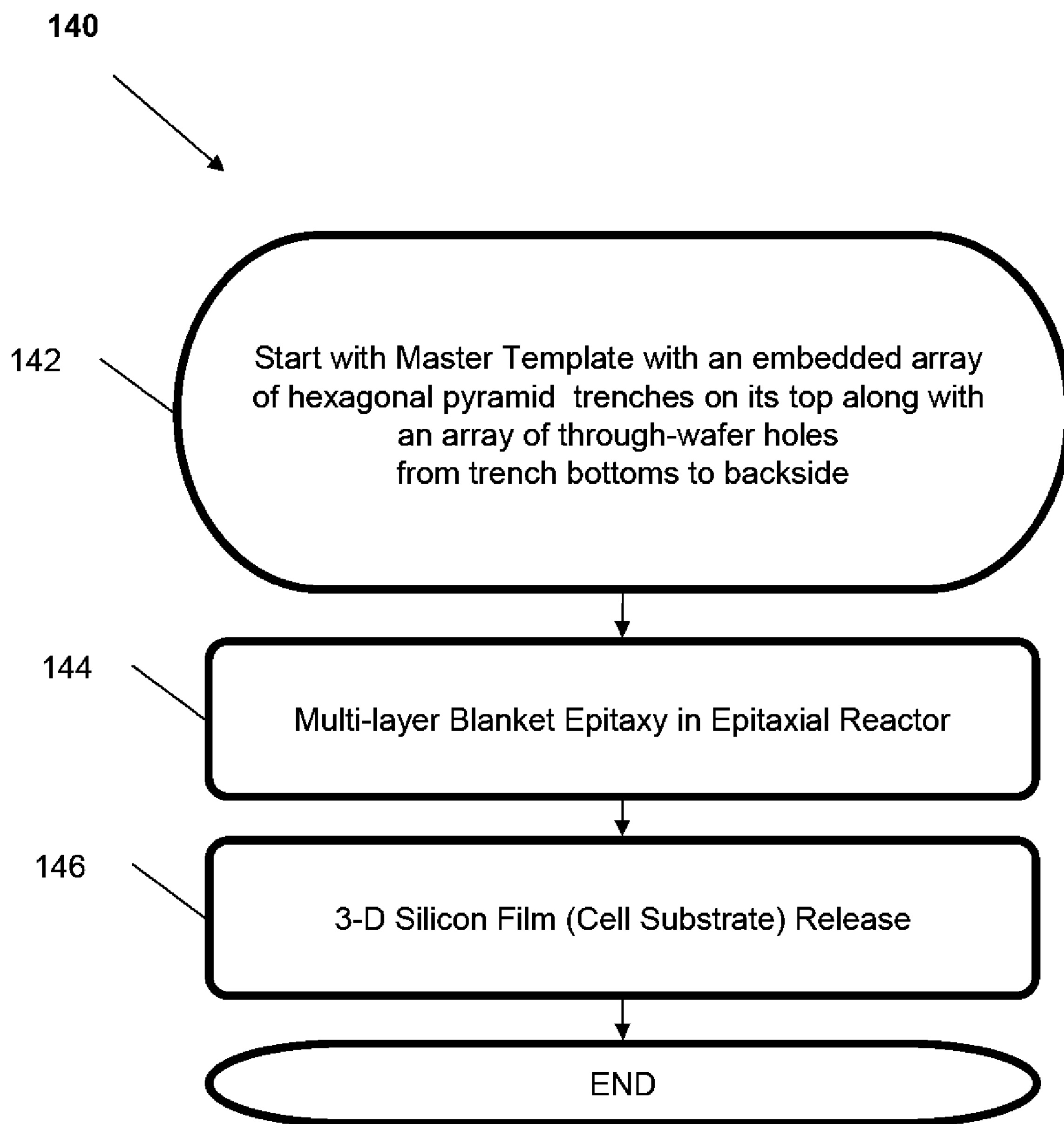

FIG. 9

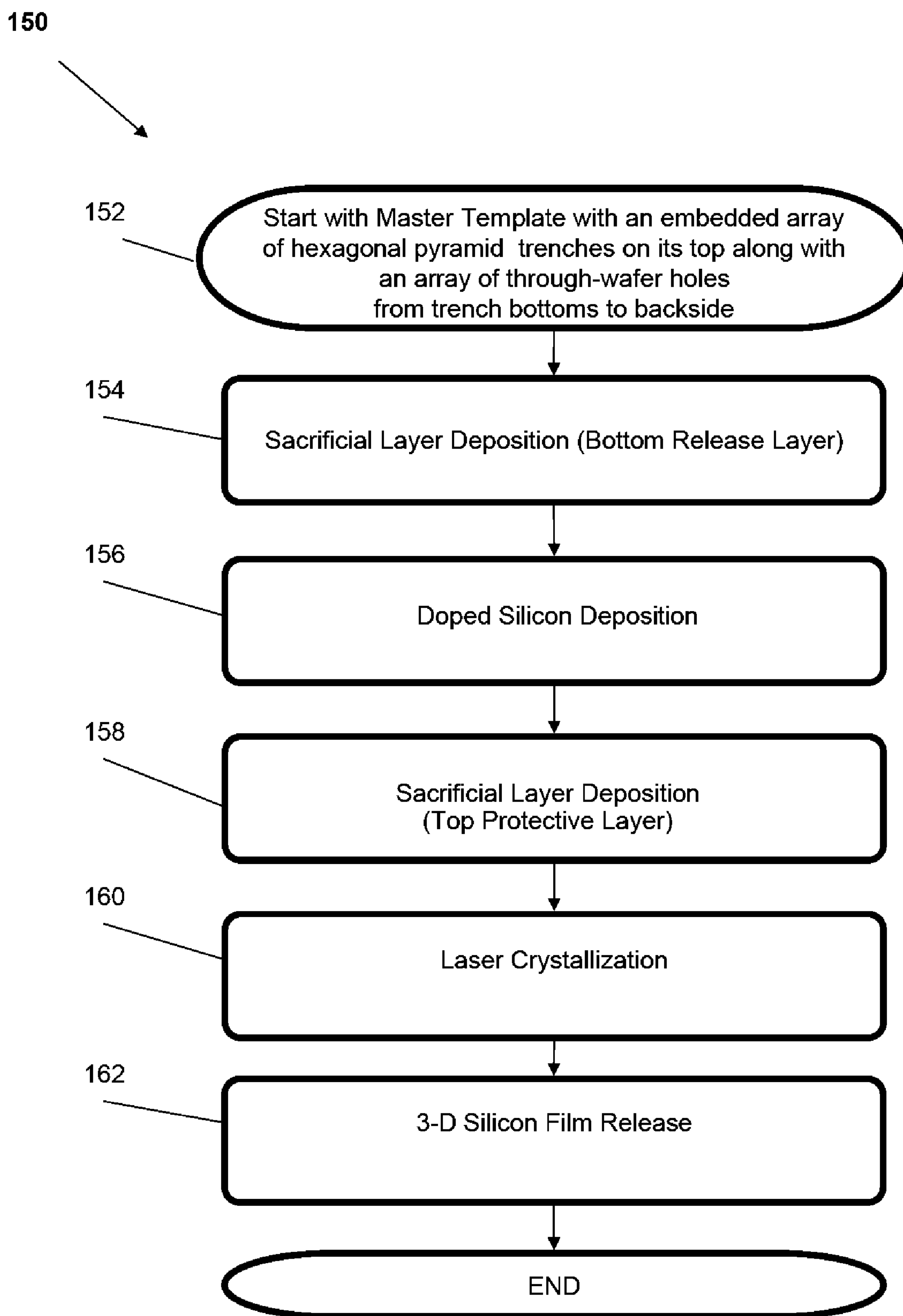

FIG. 10

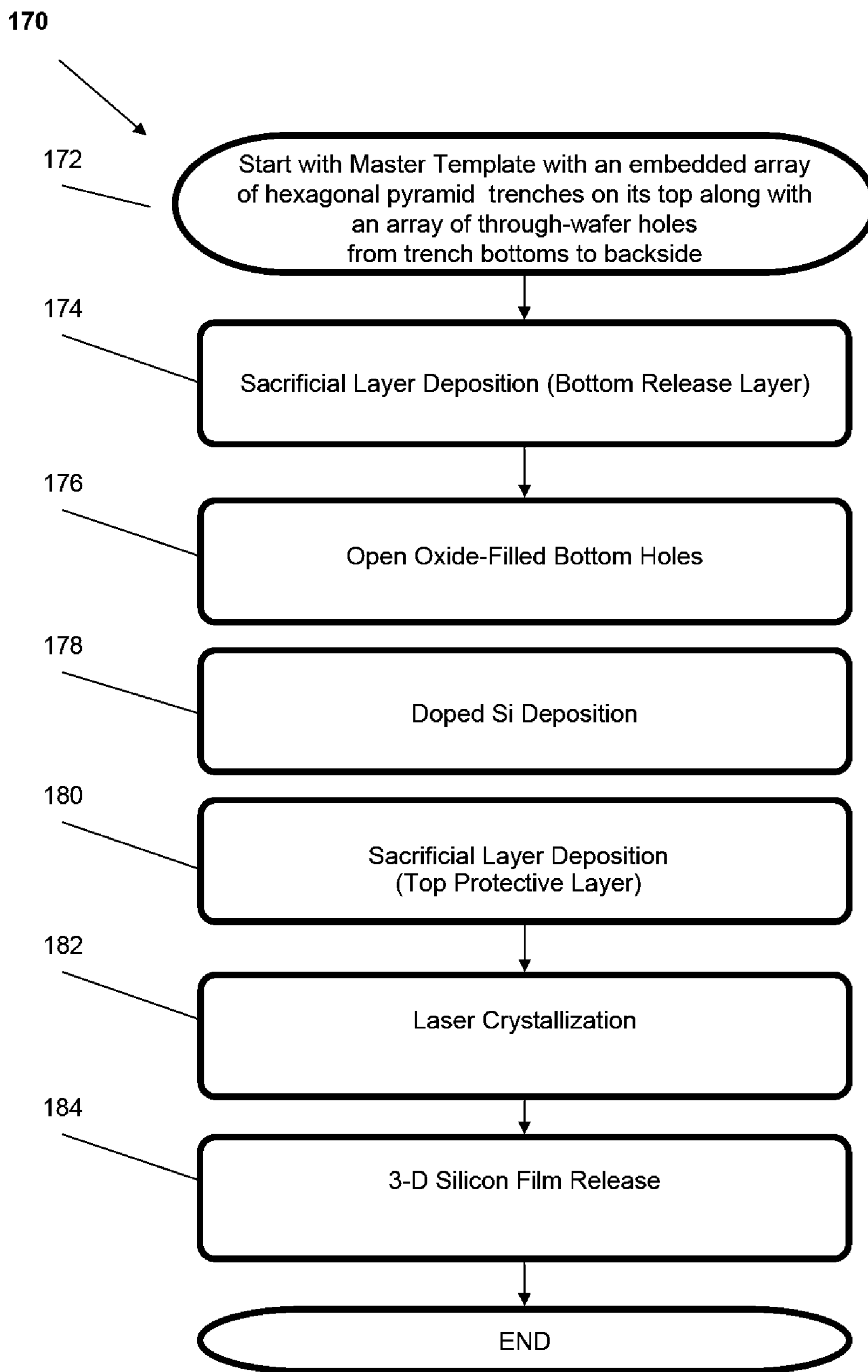

FIG. 11

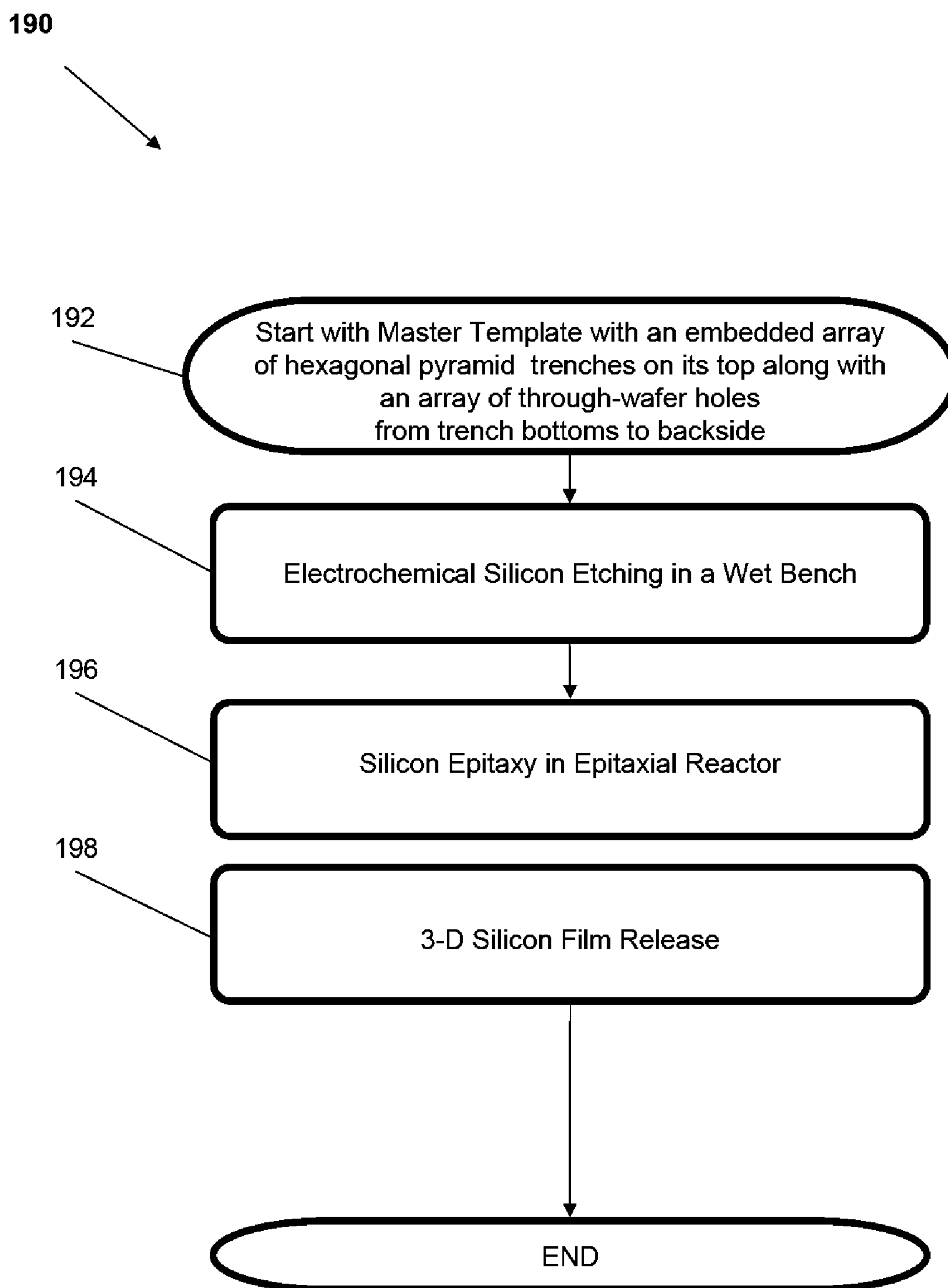

FIG. 12

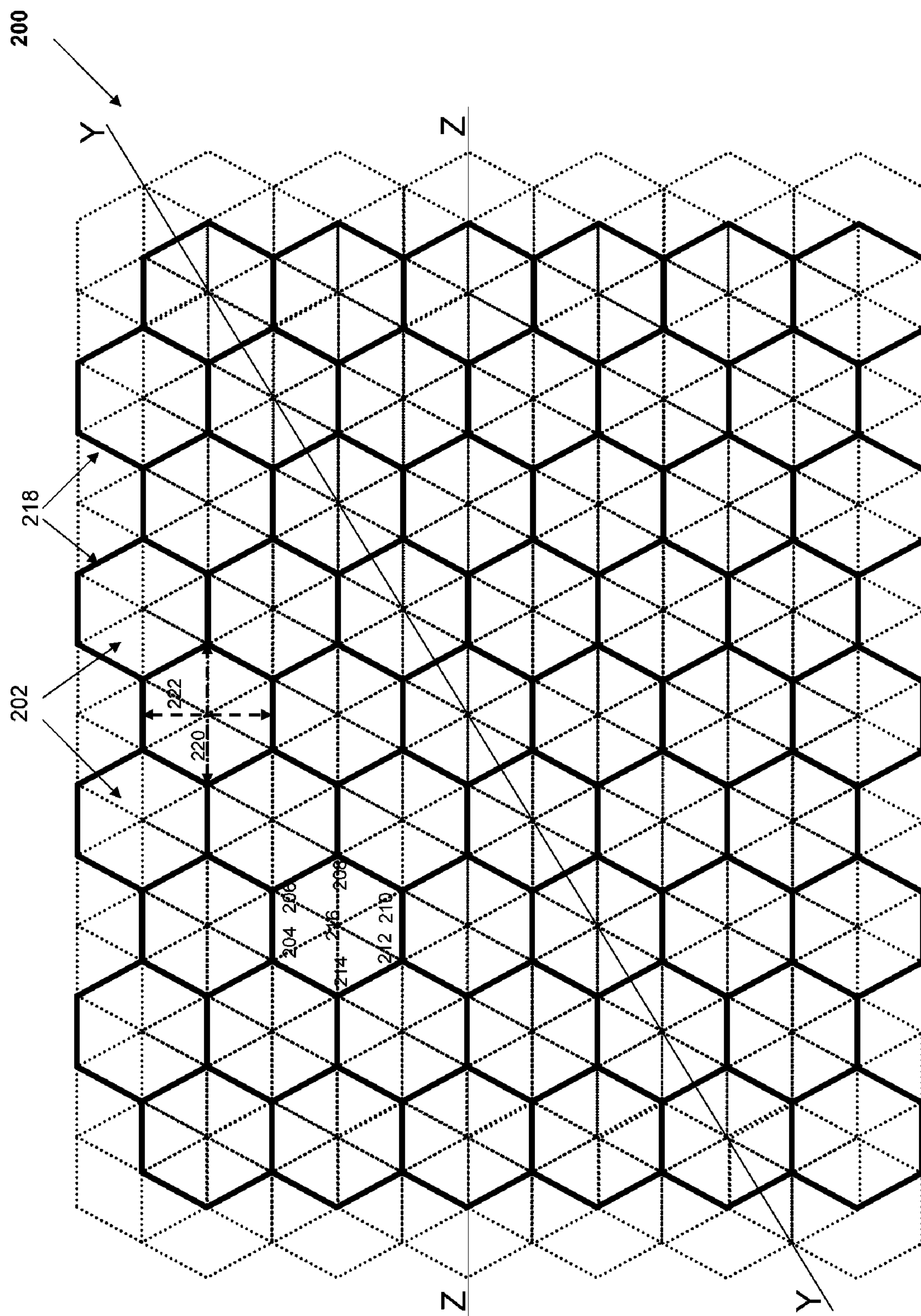

FIG. 13

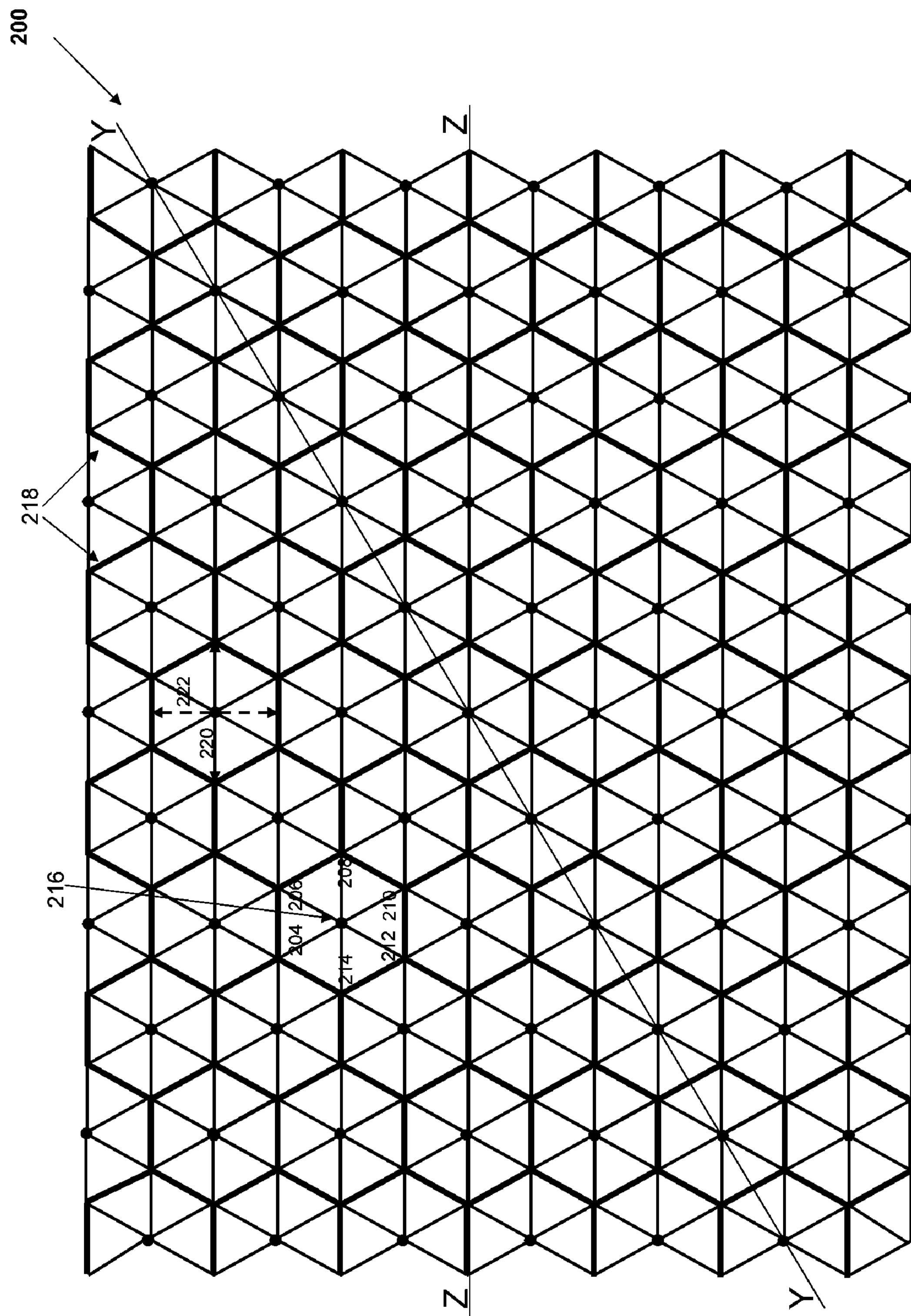

FIG. 14

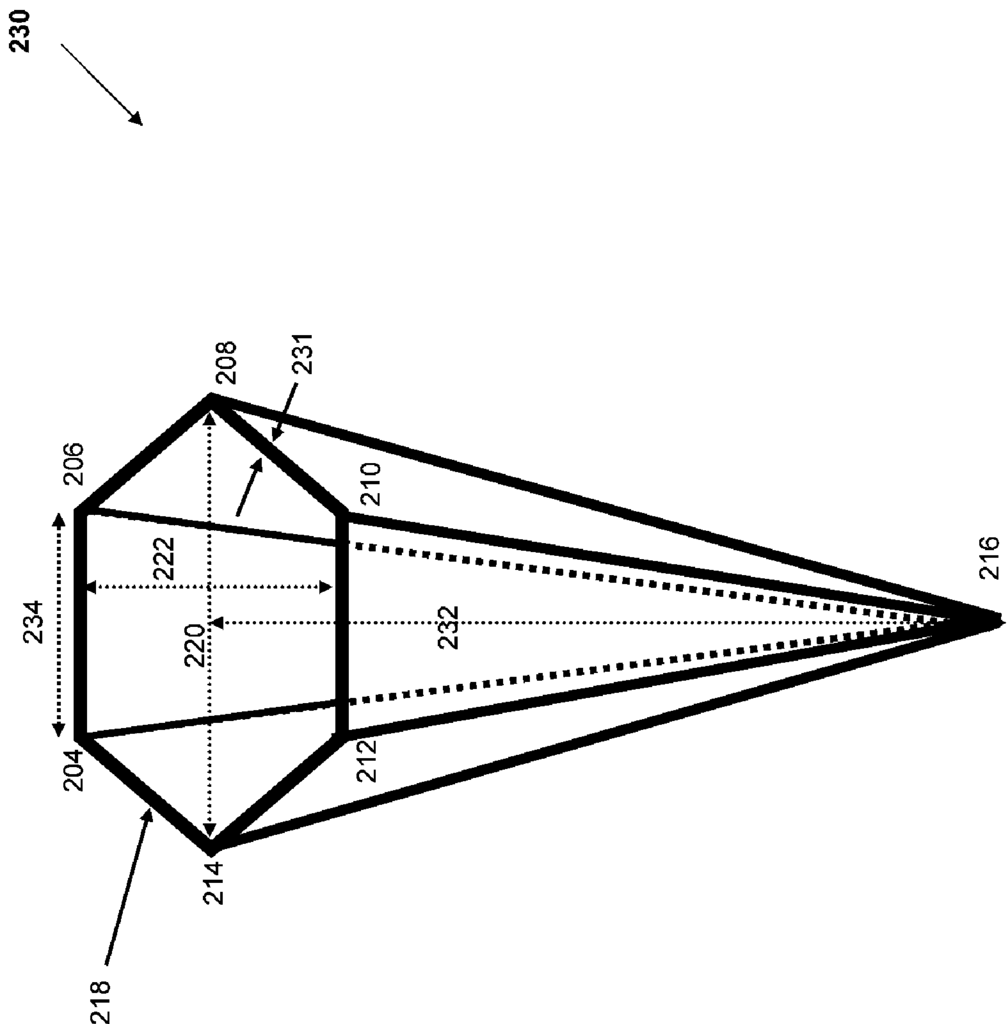

FIG. 15

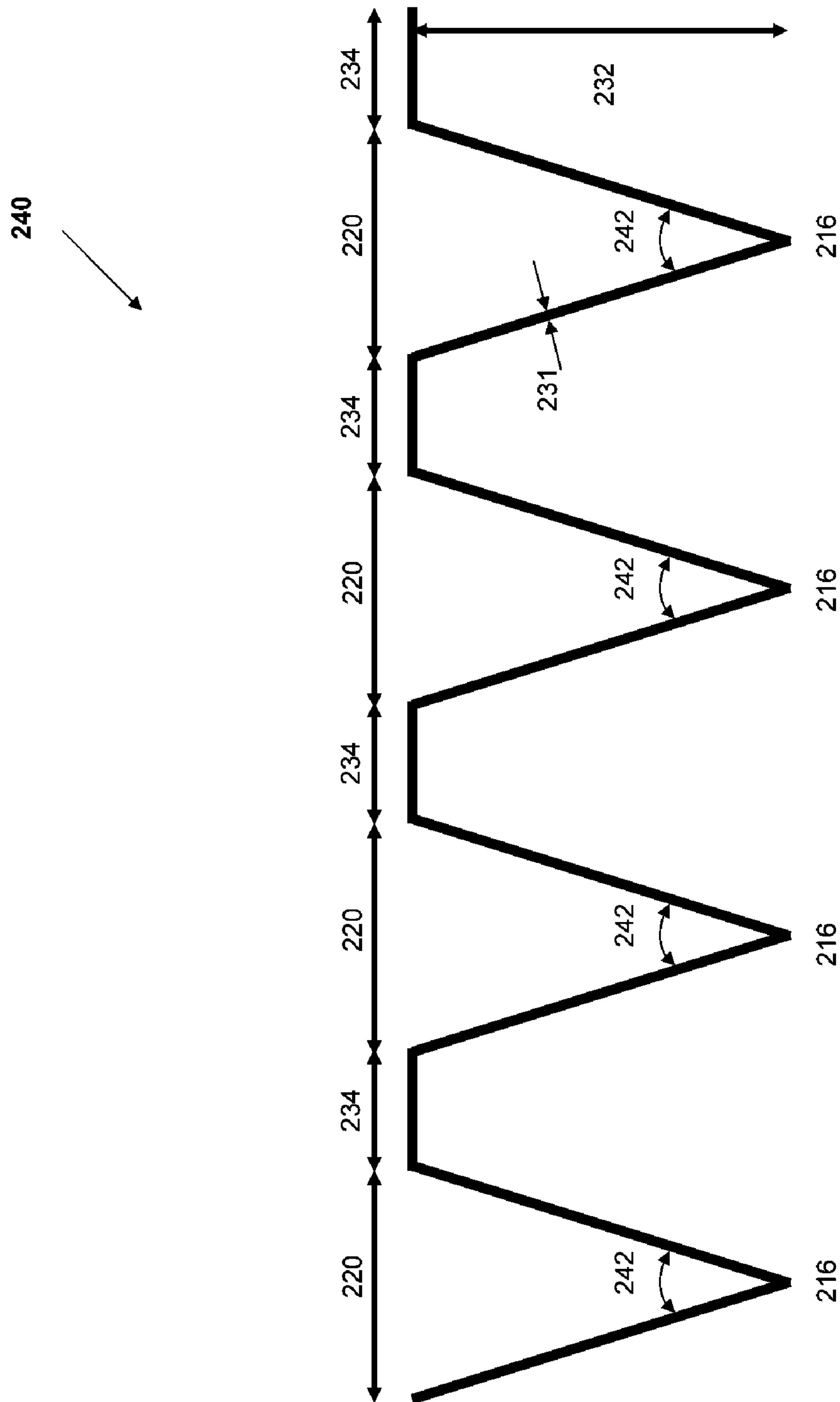

FIG. 16

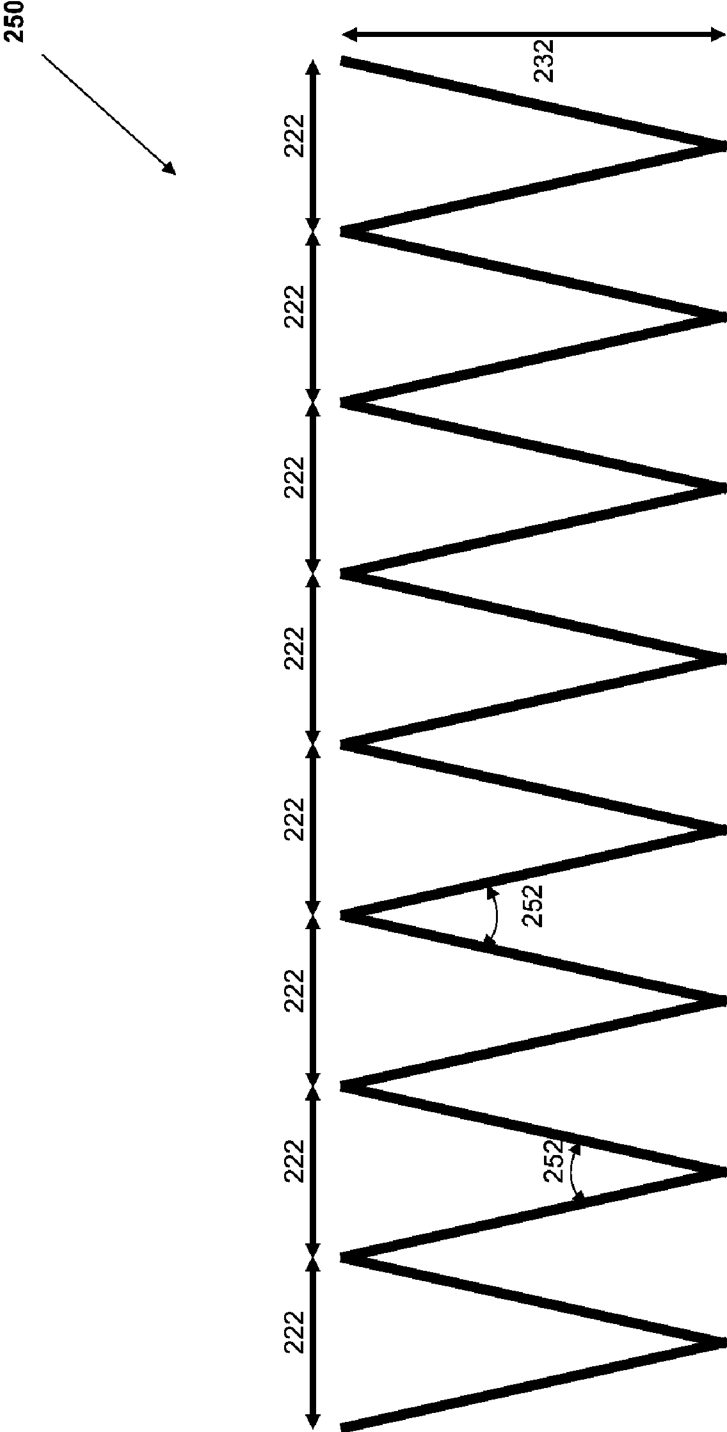

FIG. 17

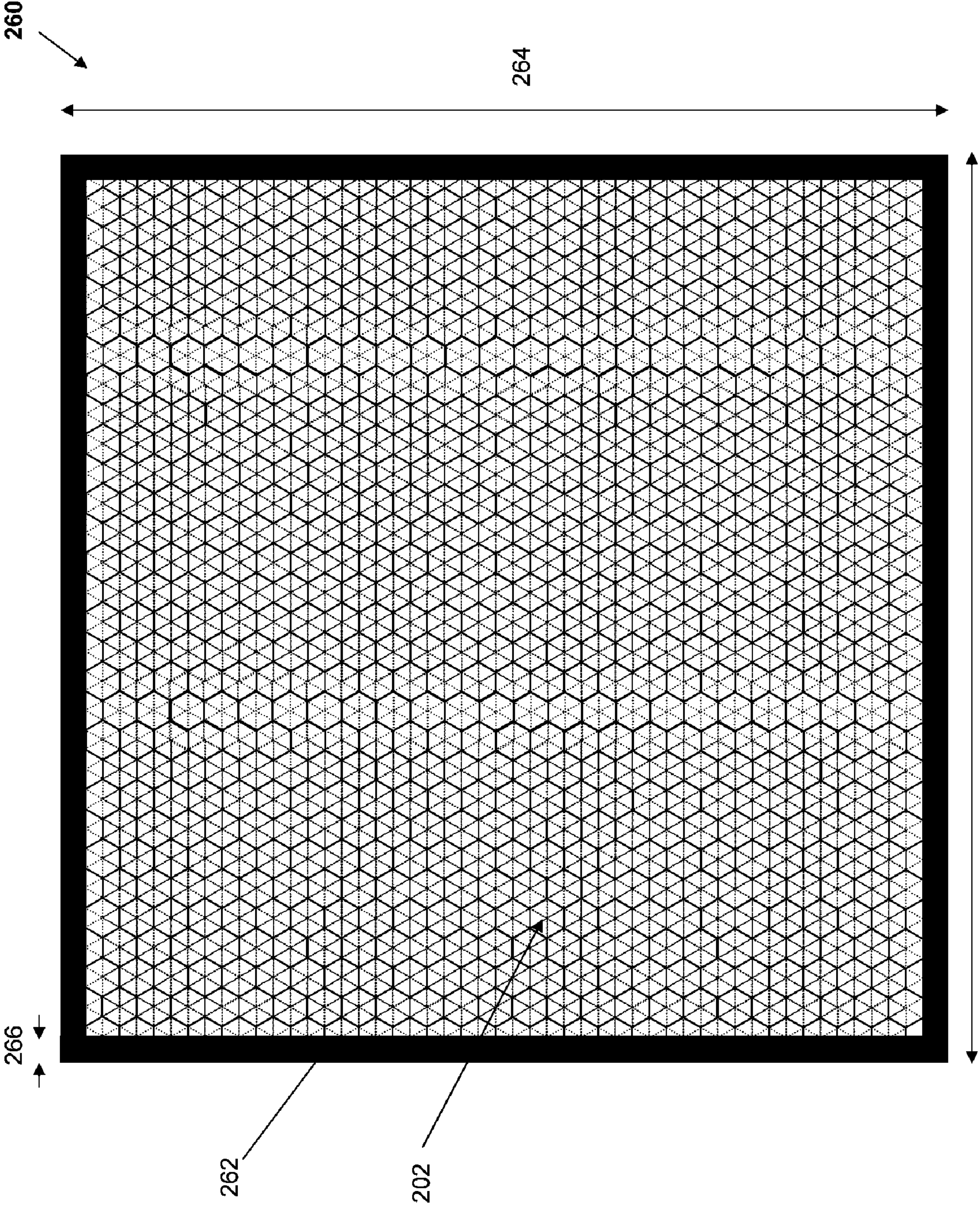

FIG. 18

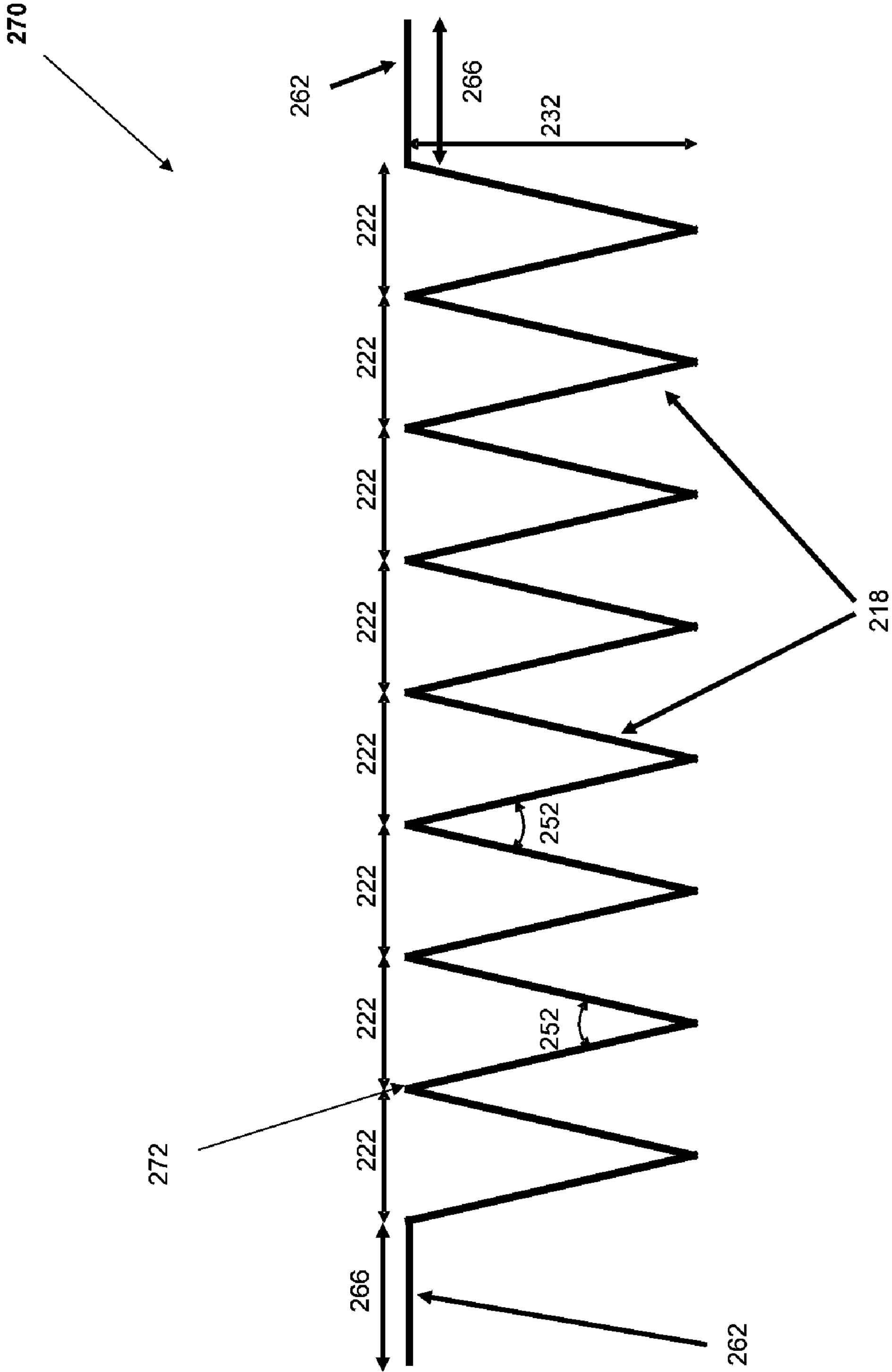

FIG. 19

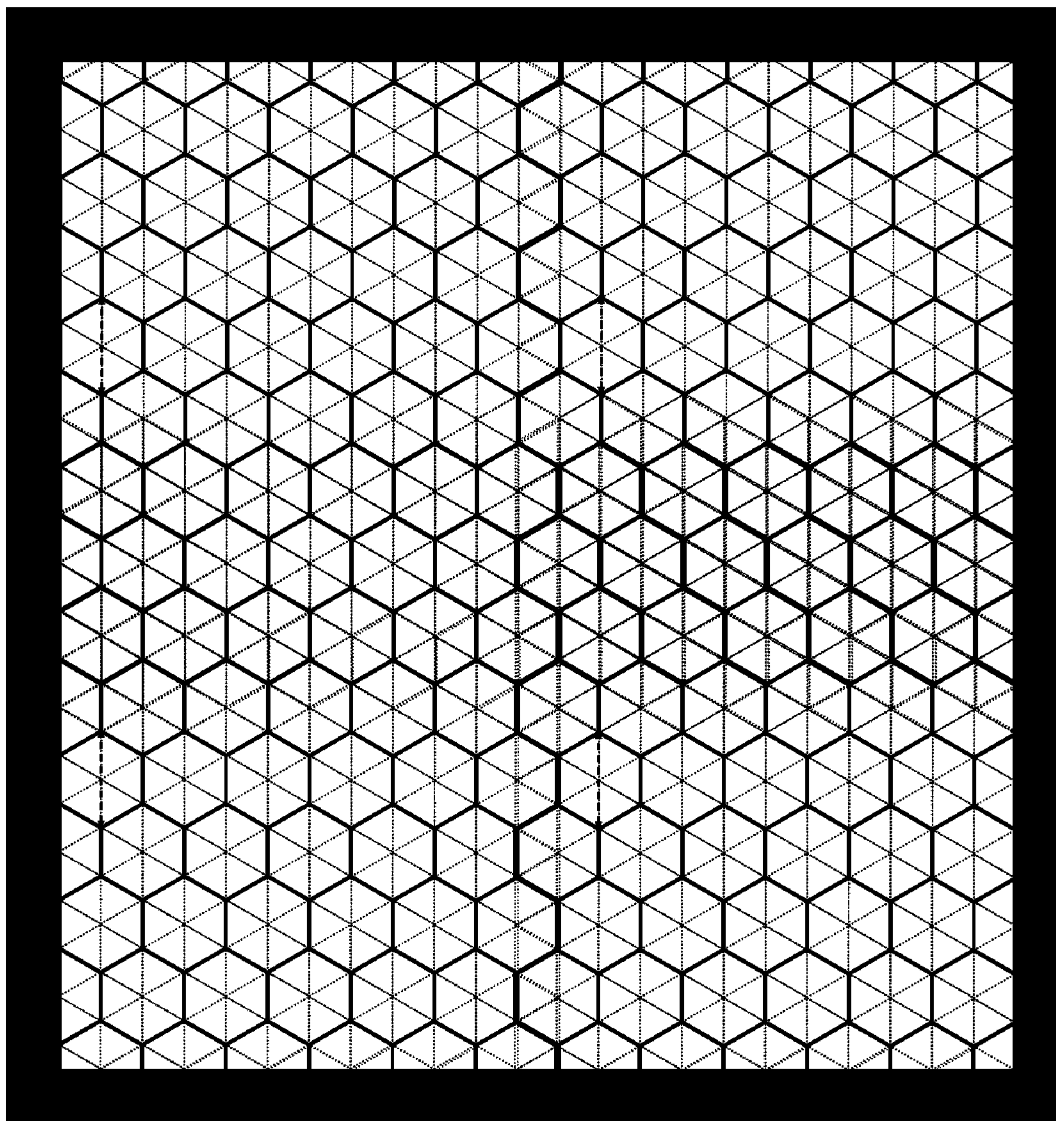

FIG. 20

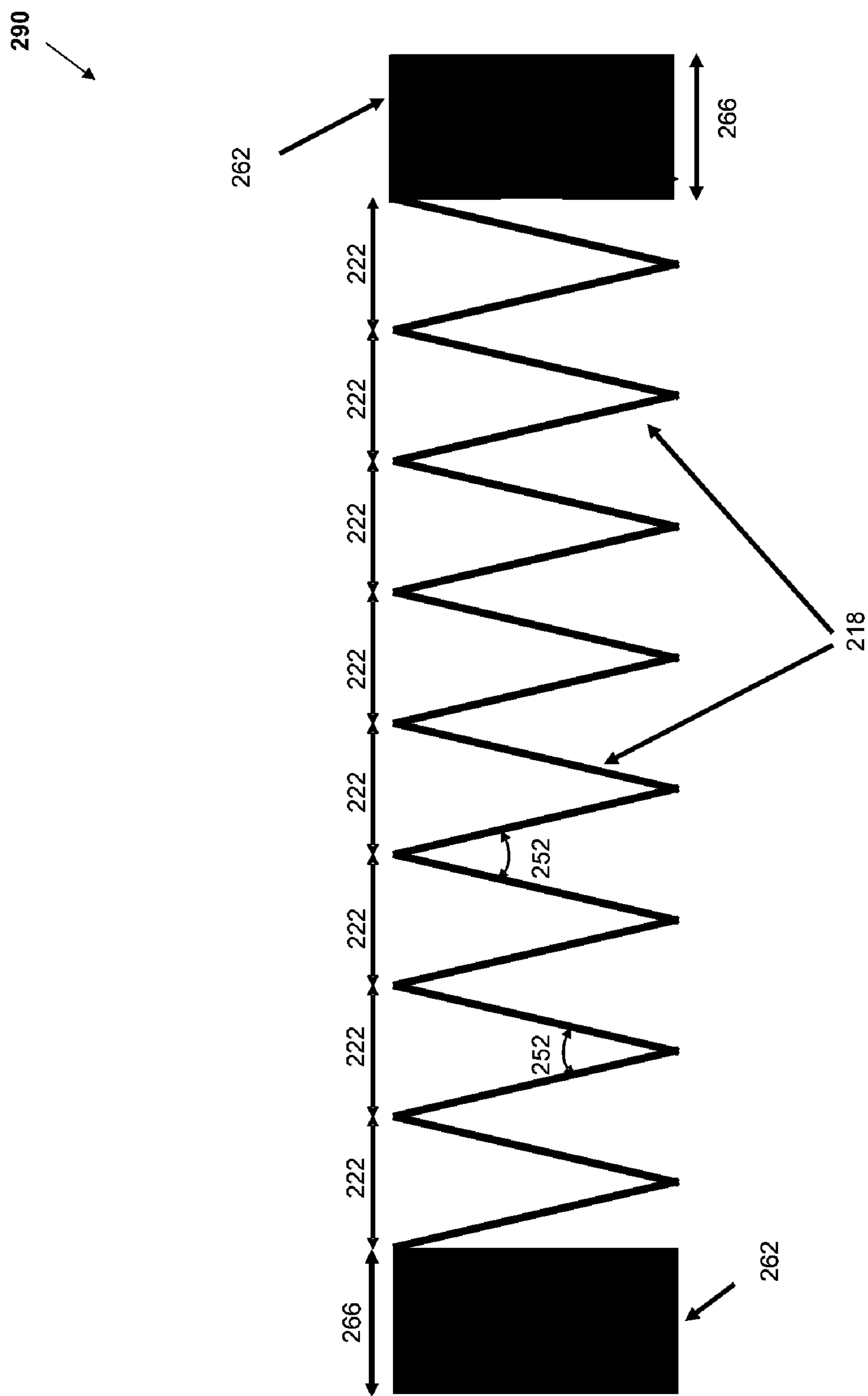

FIG. 21

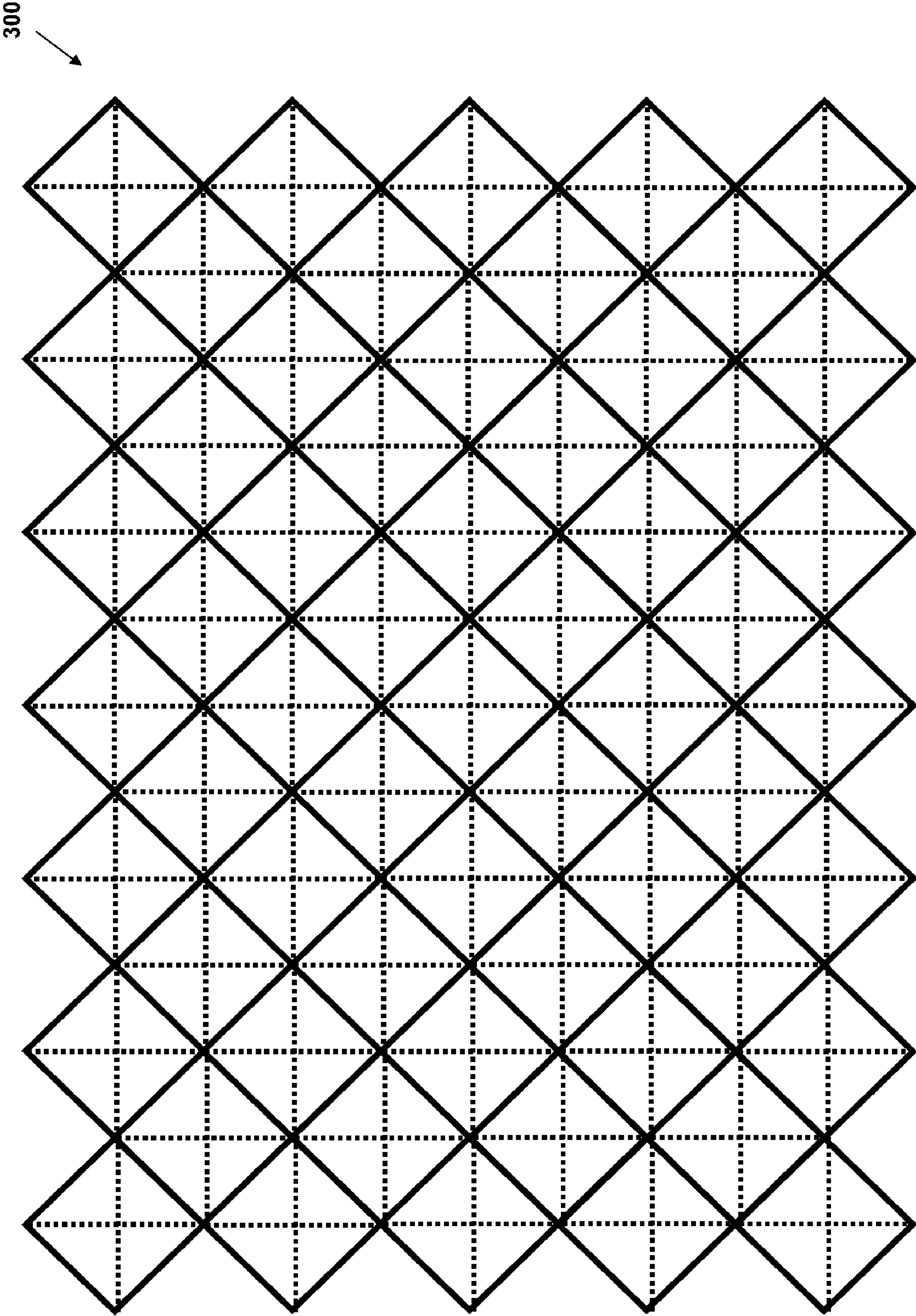

FIG. 22

FIG. 23

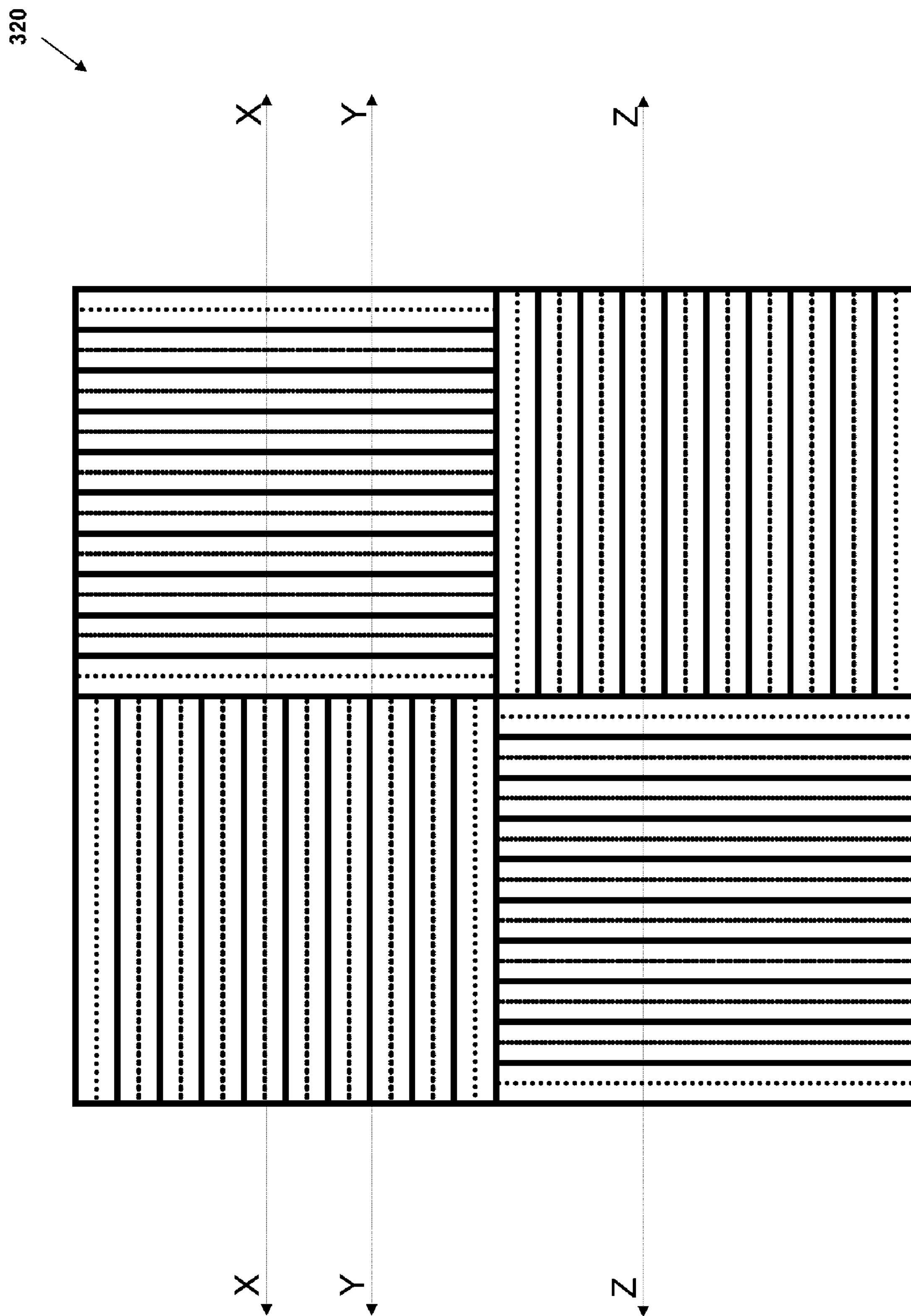

FIG. 24

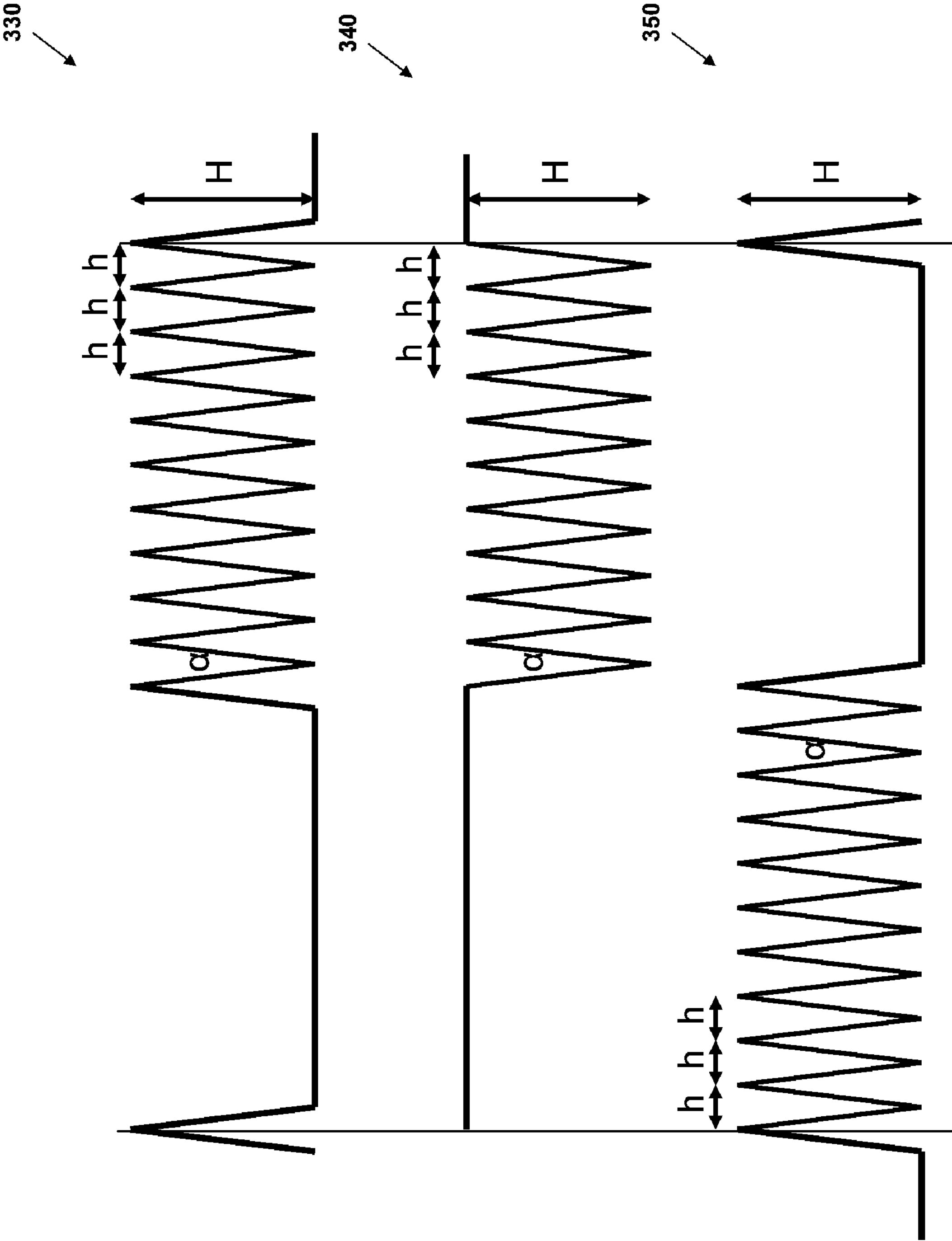

FIG. 25

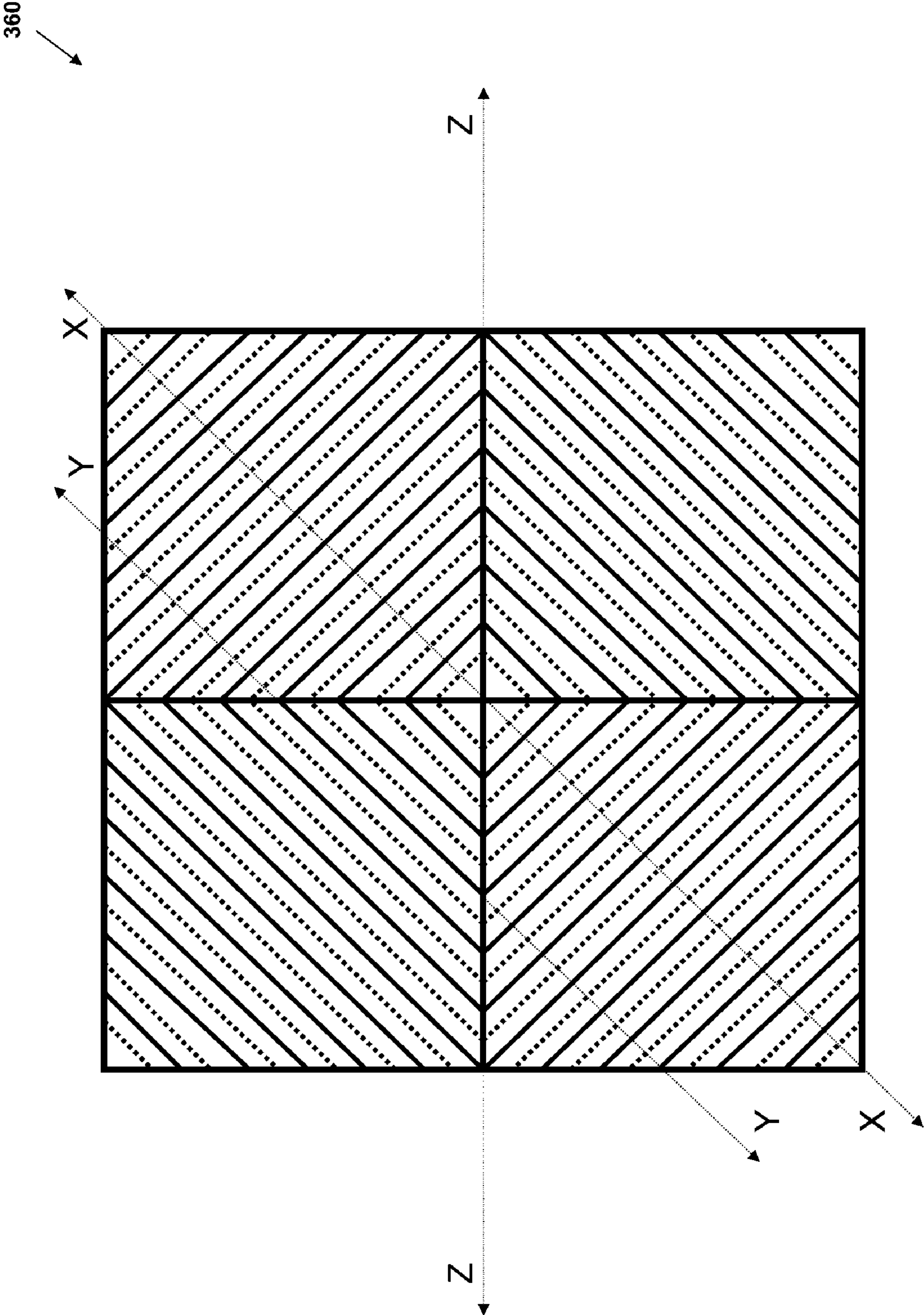

FIG. 26

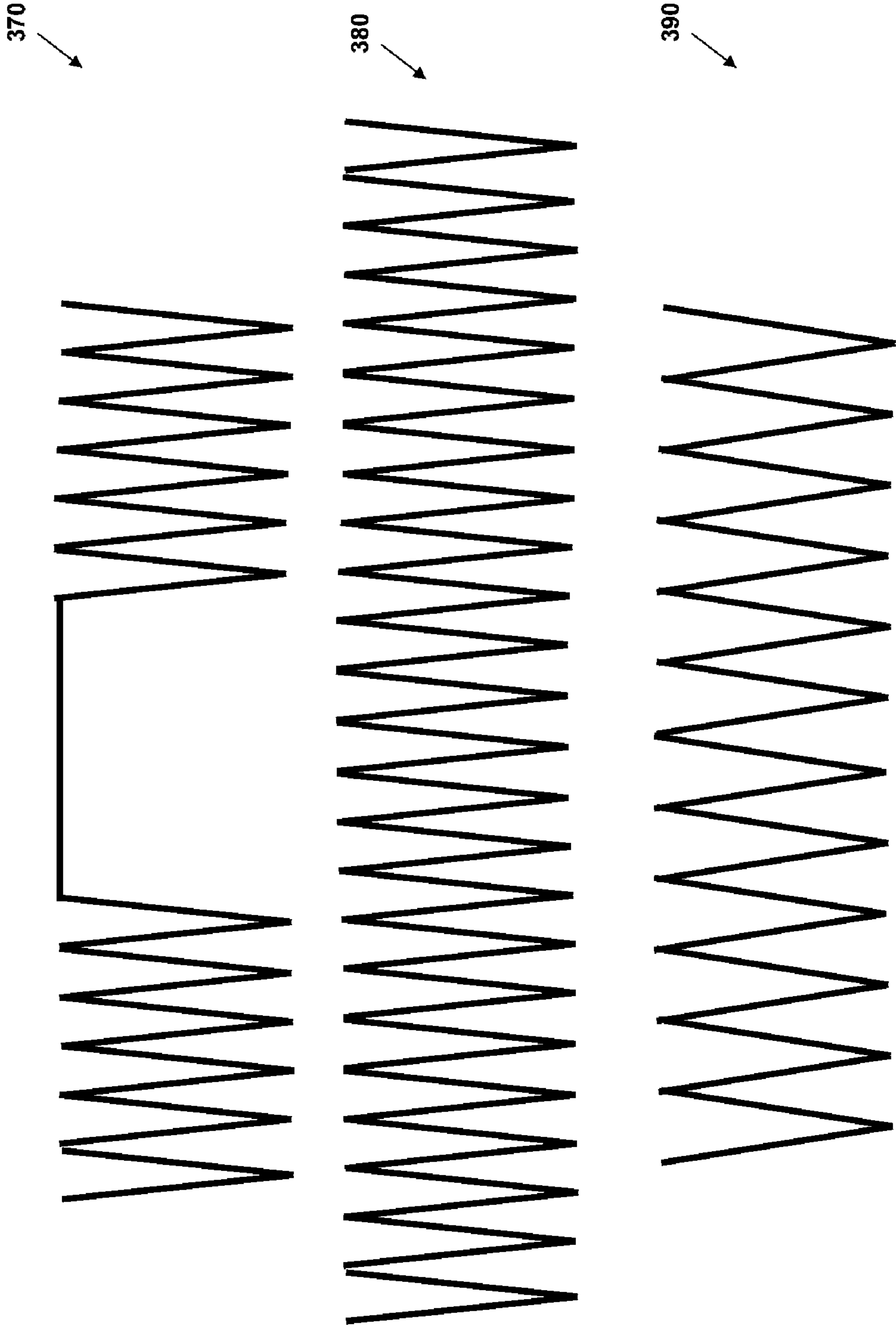

FIG. 27

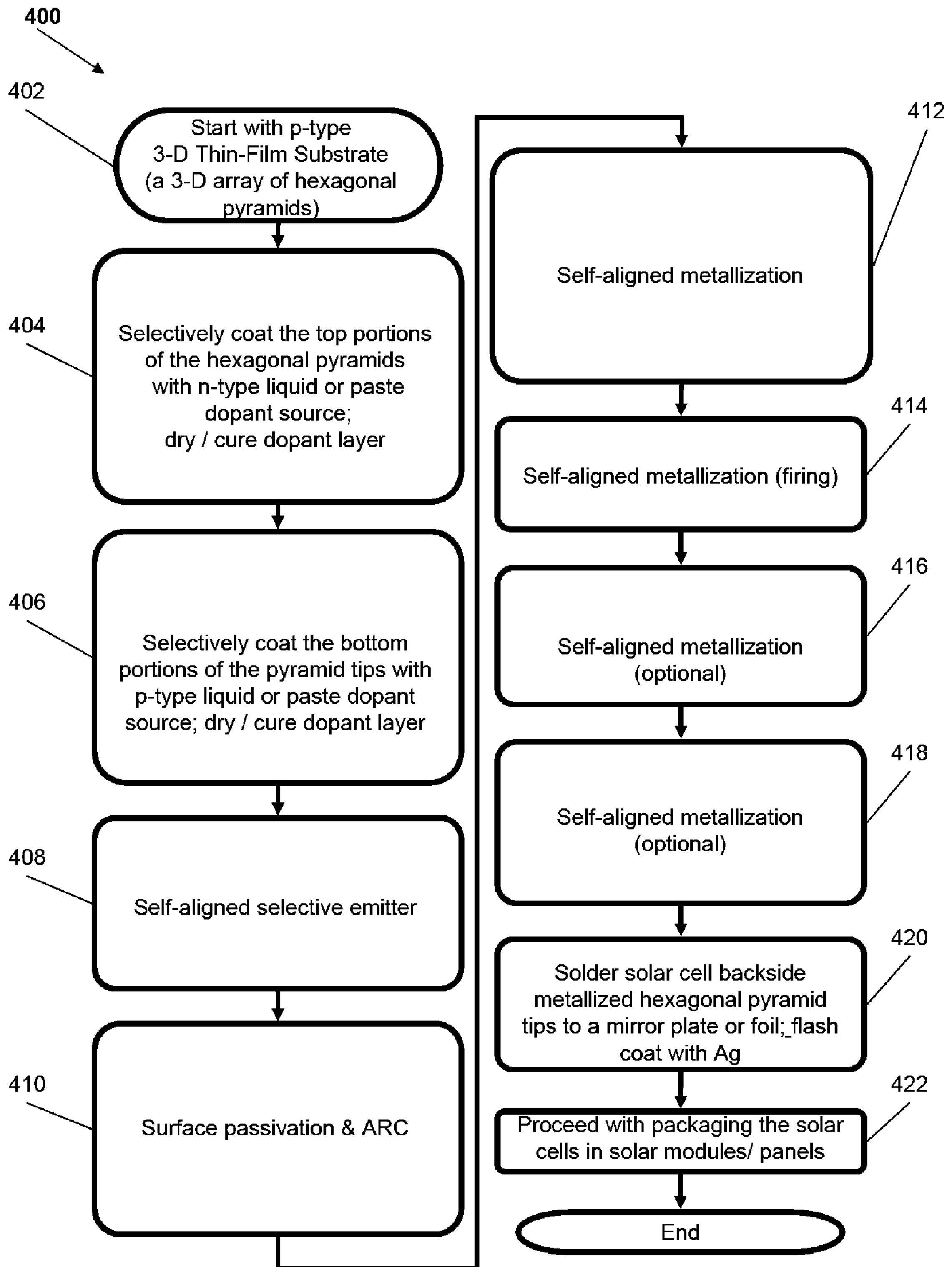

FIG. 28

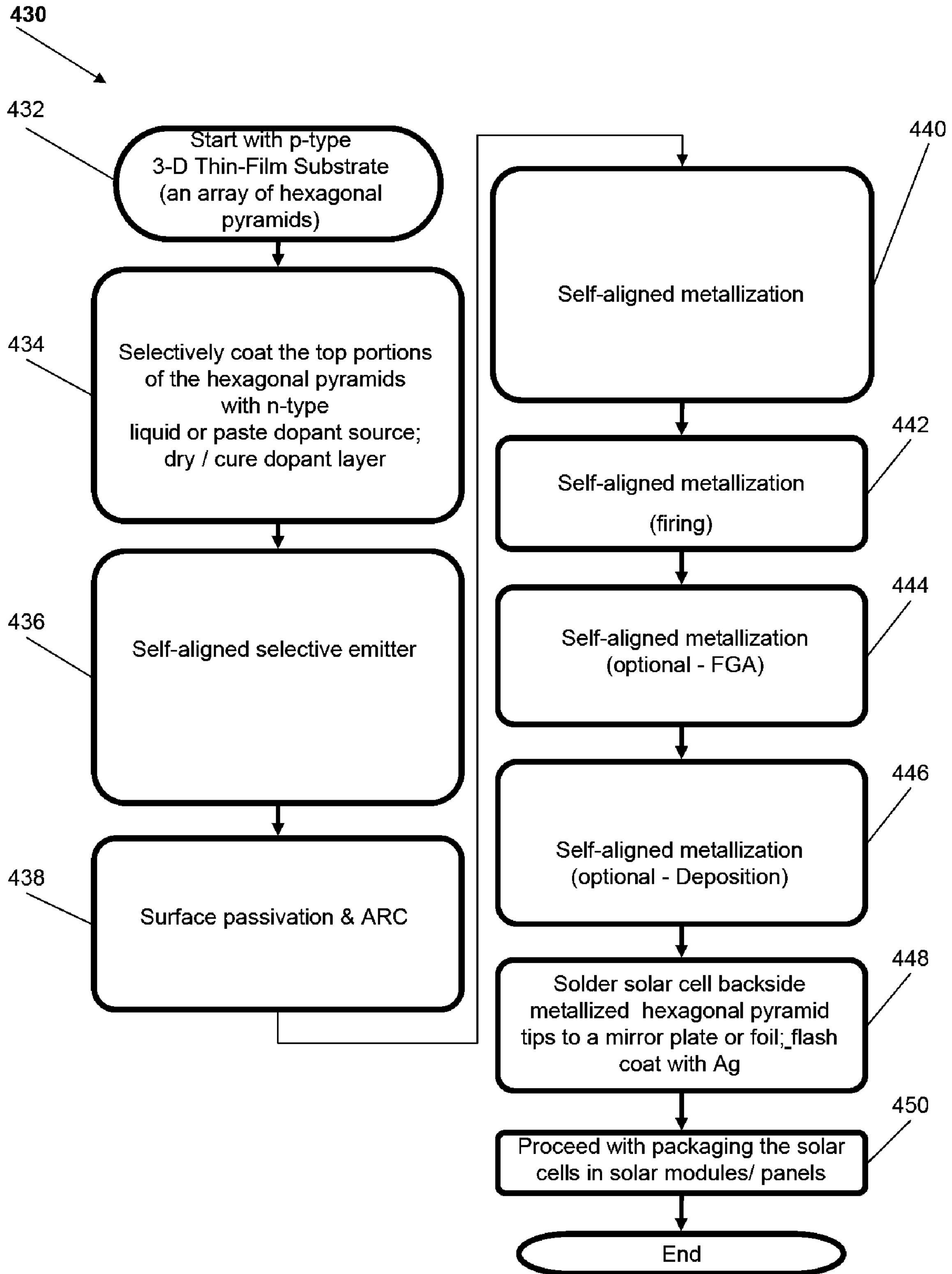

FIG. 29

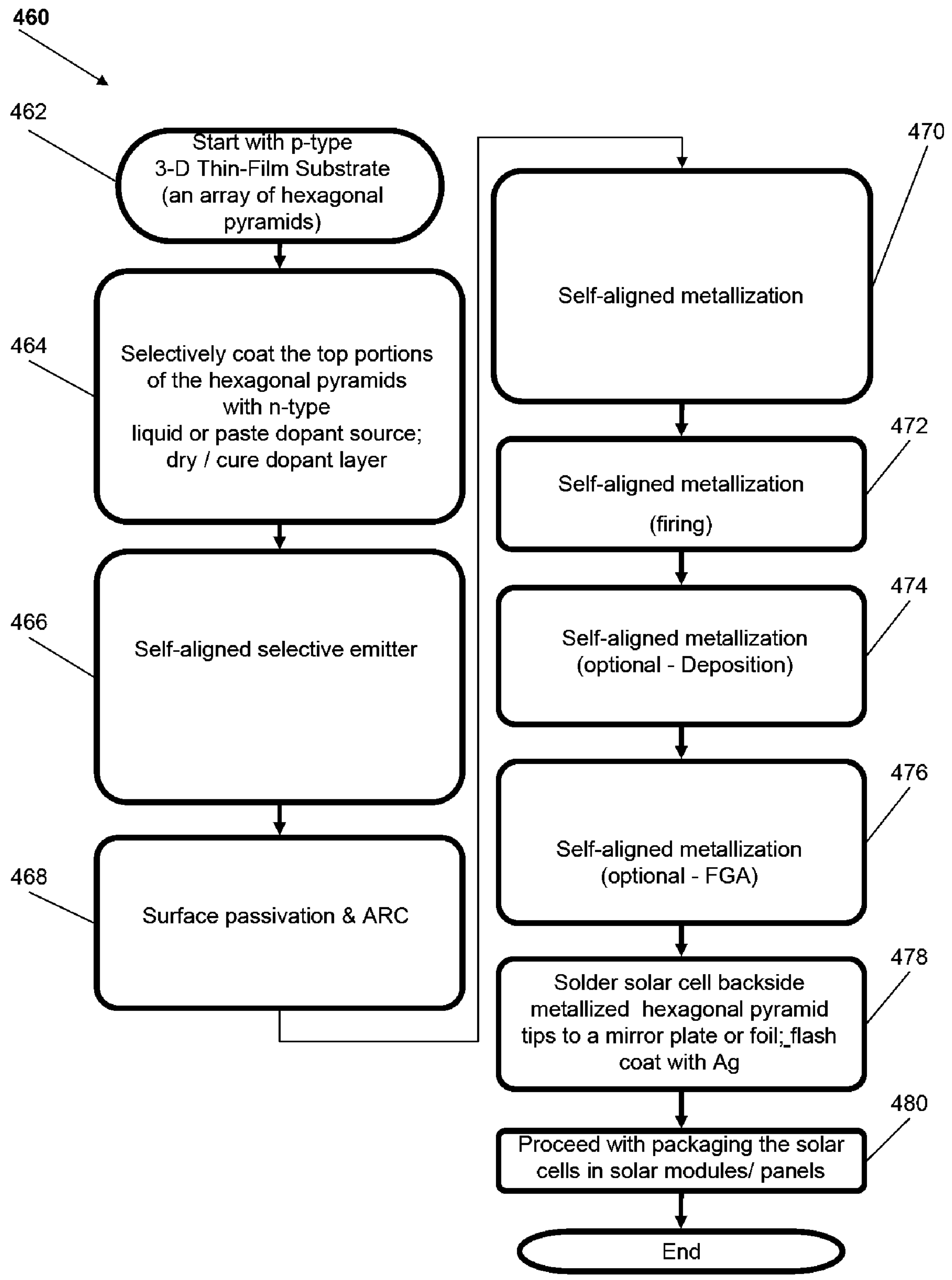

FIG. 30

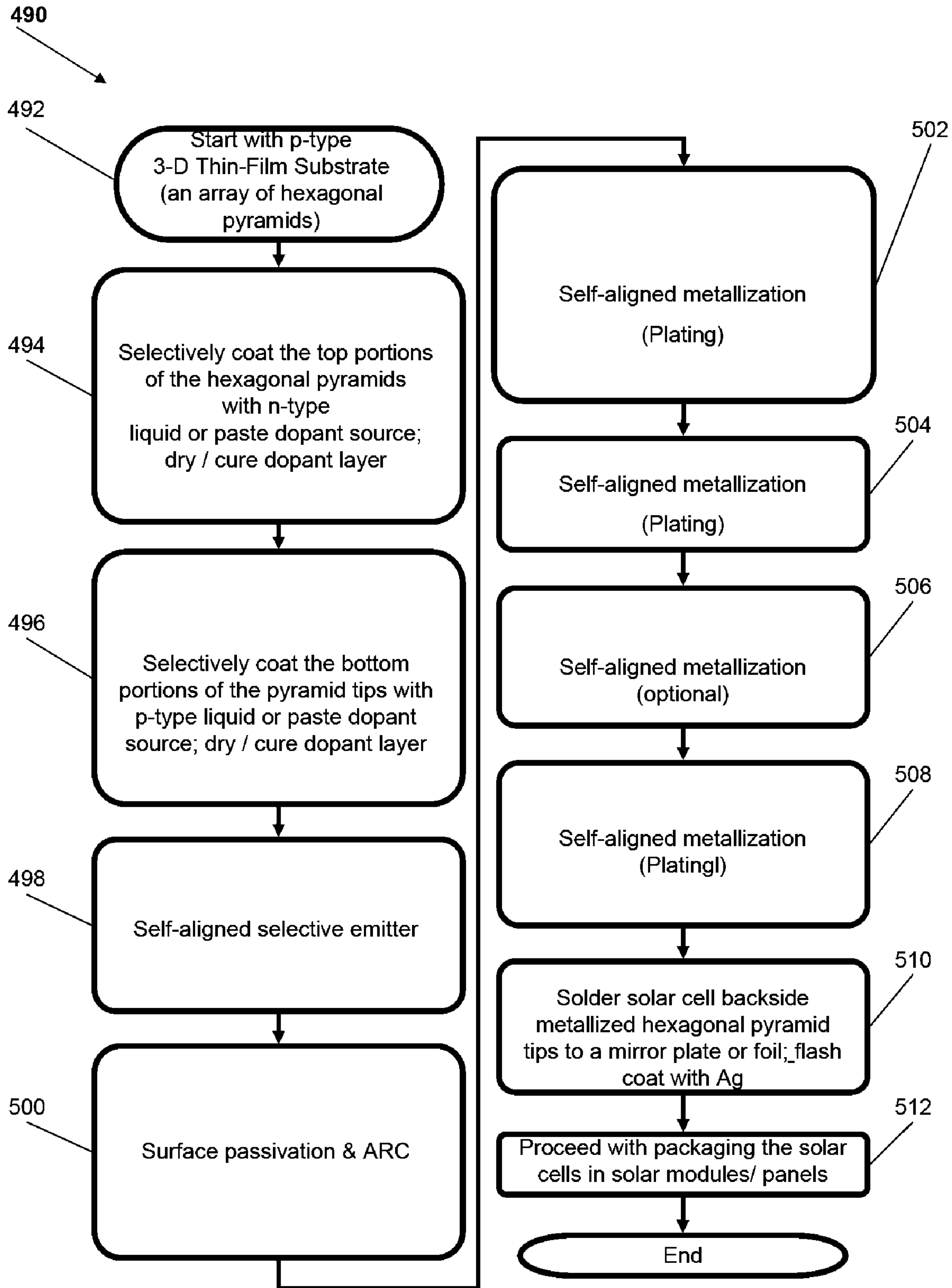

FIG. 31

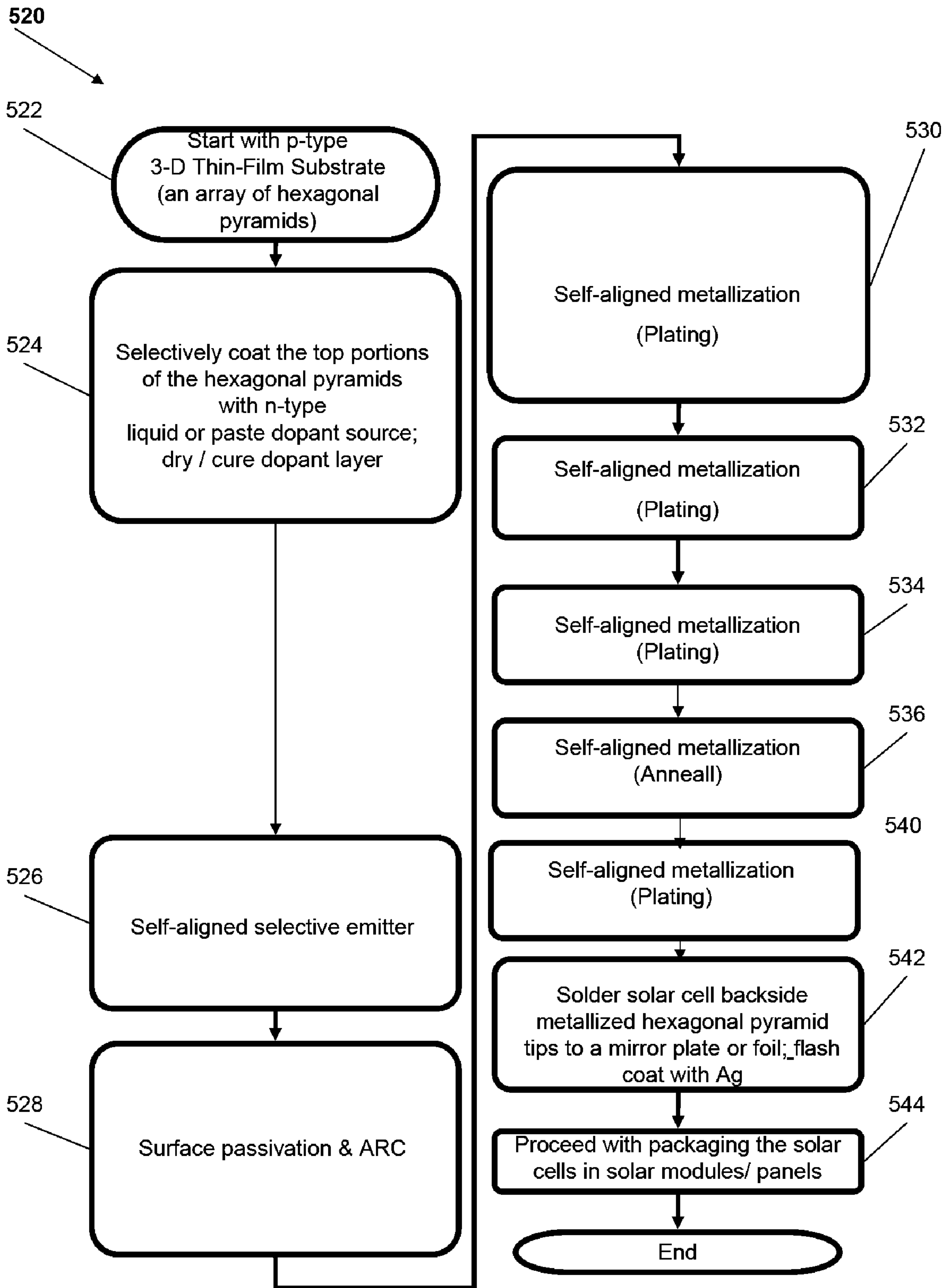

FIG. 32

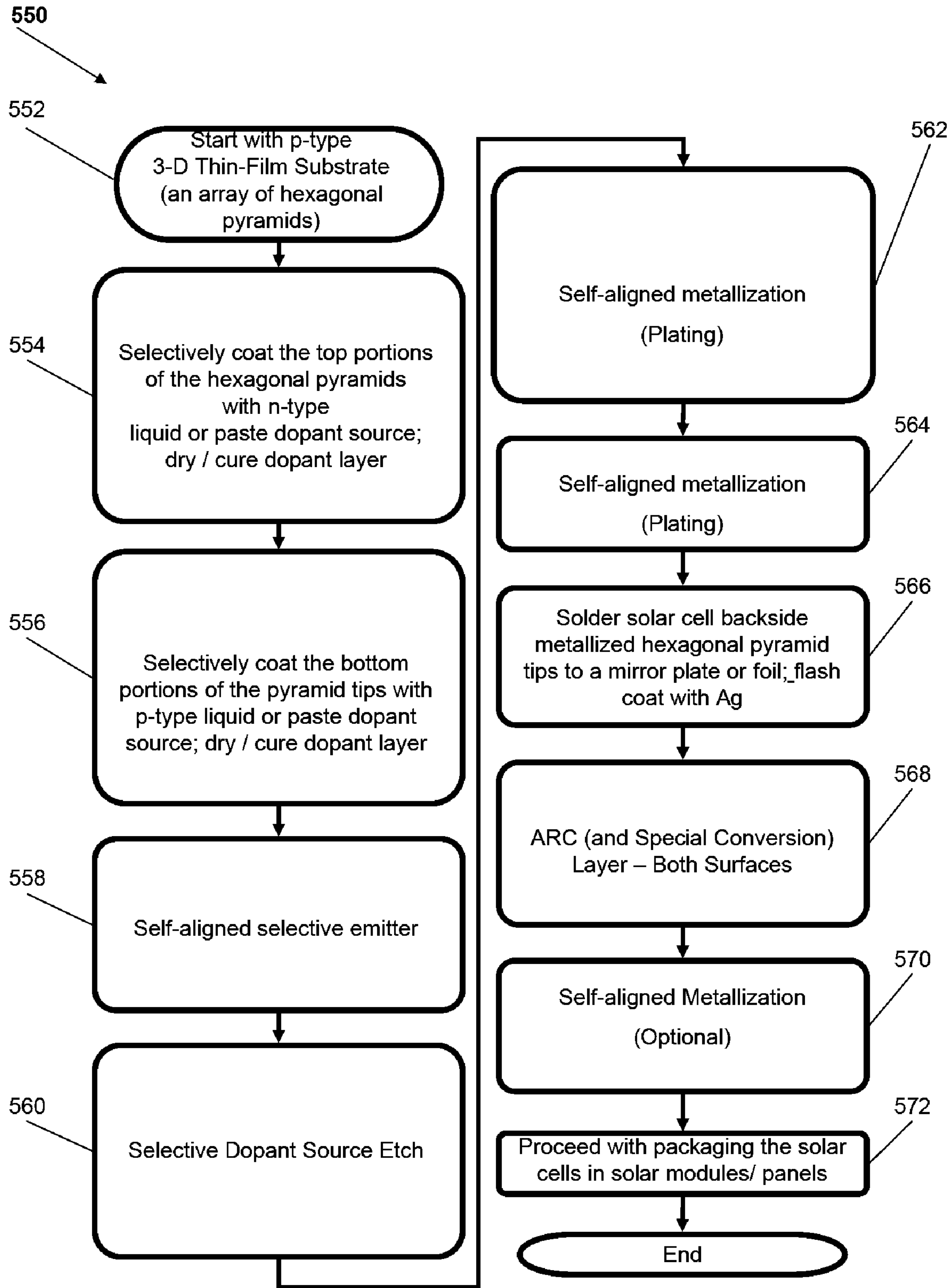

FIG. 33

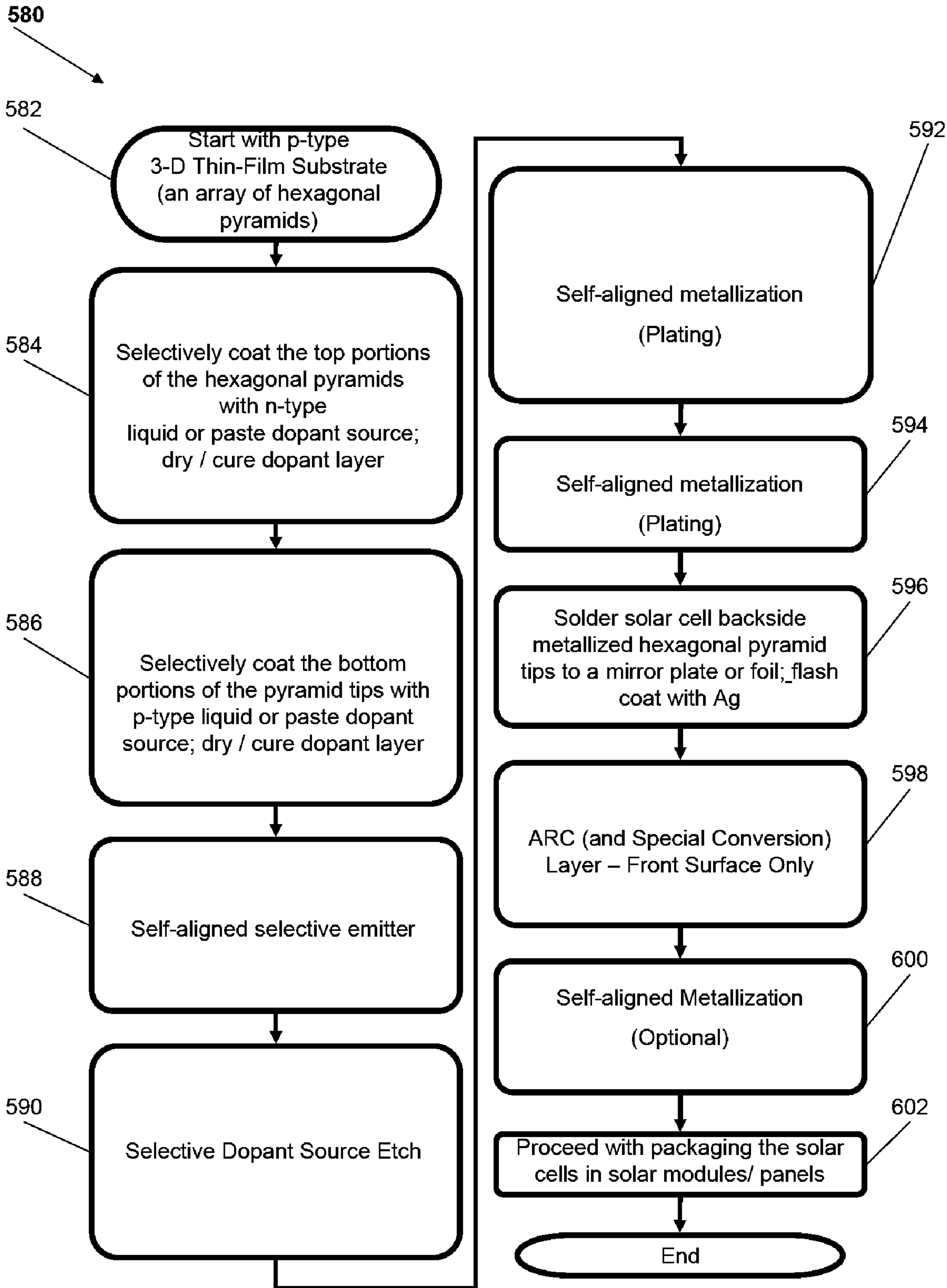

FIG. 34

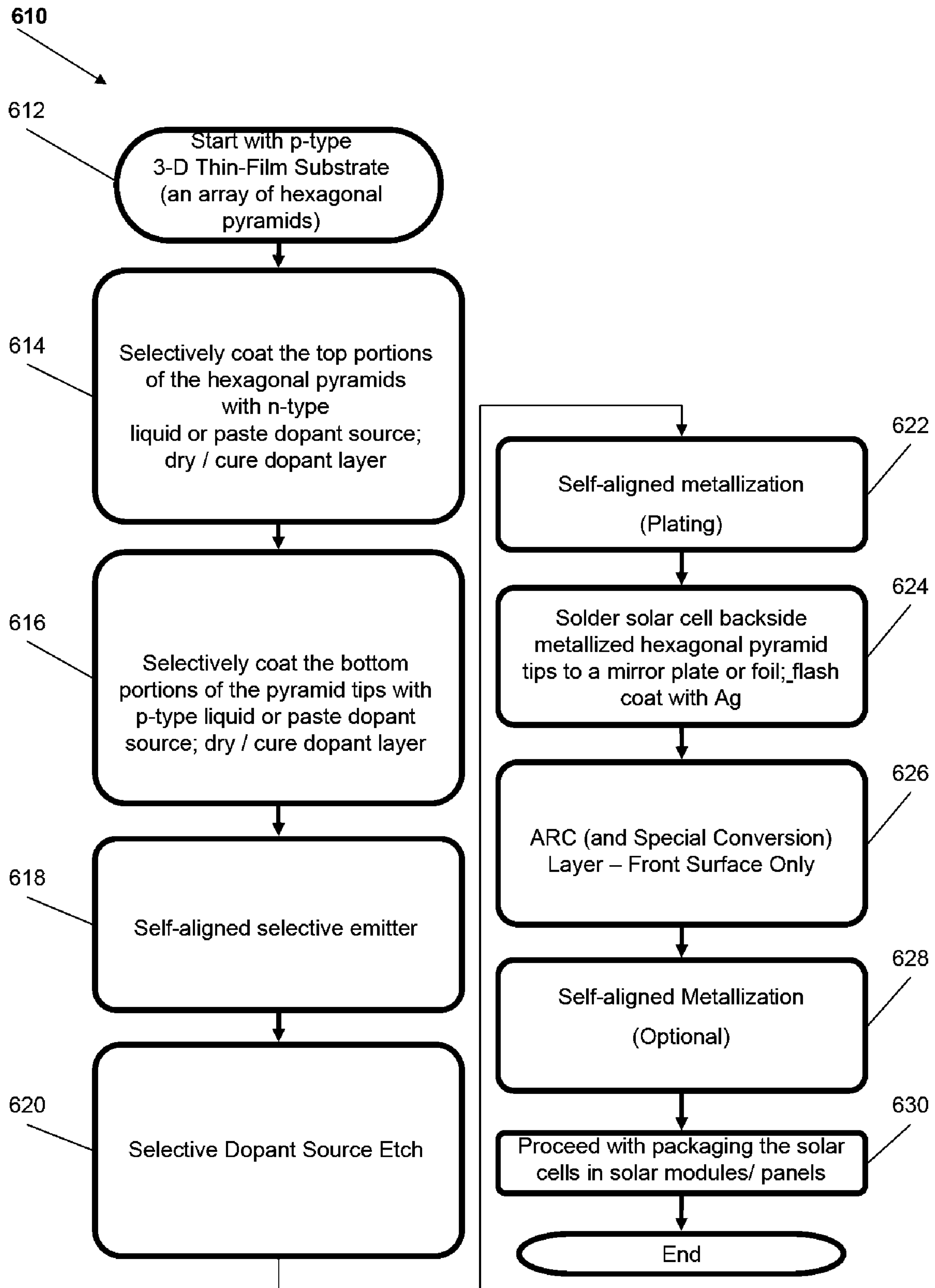

FIG. 35

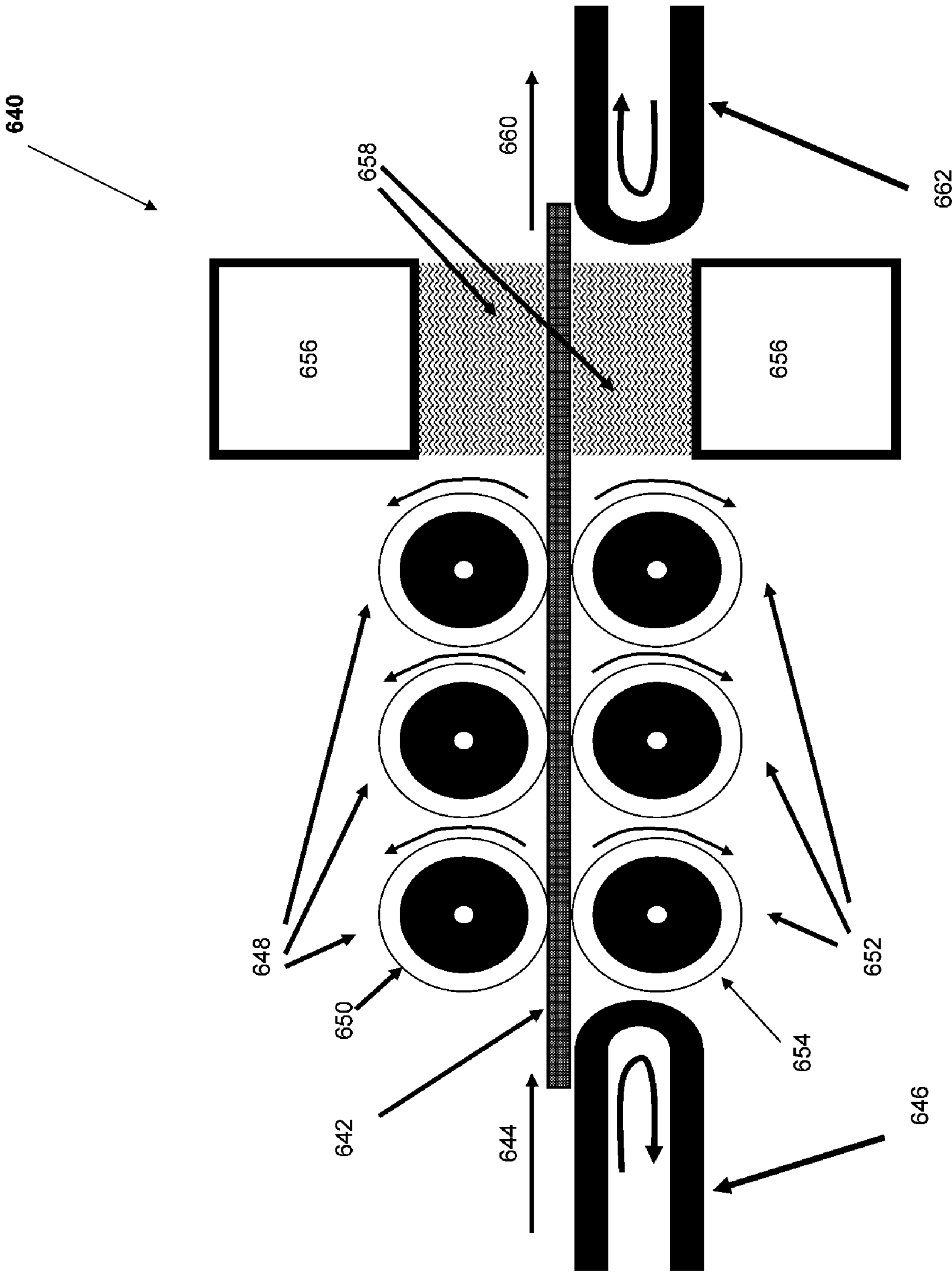

FIG. 36

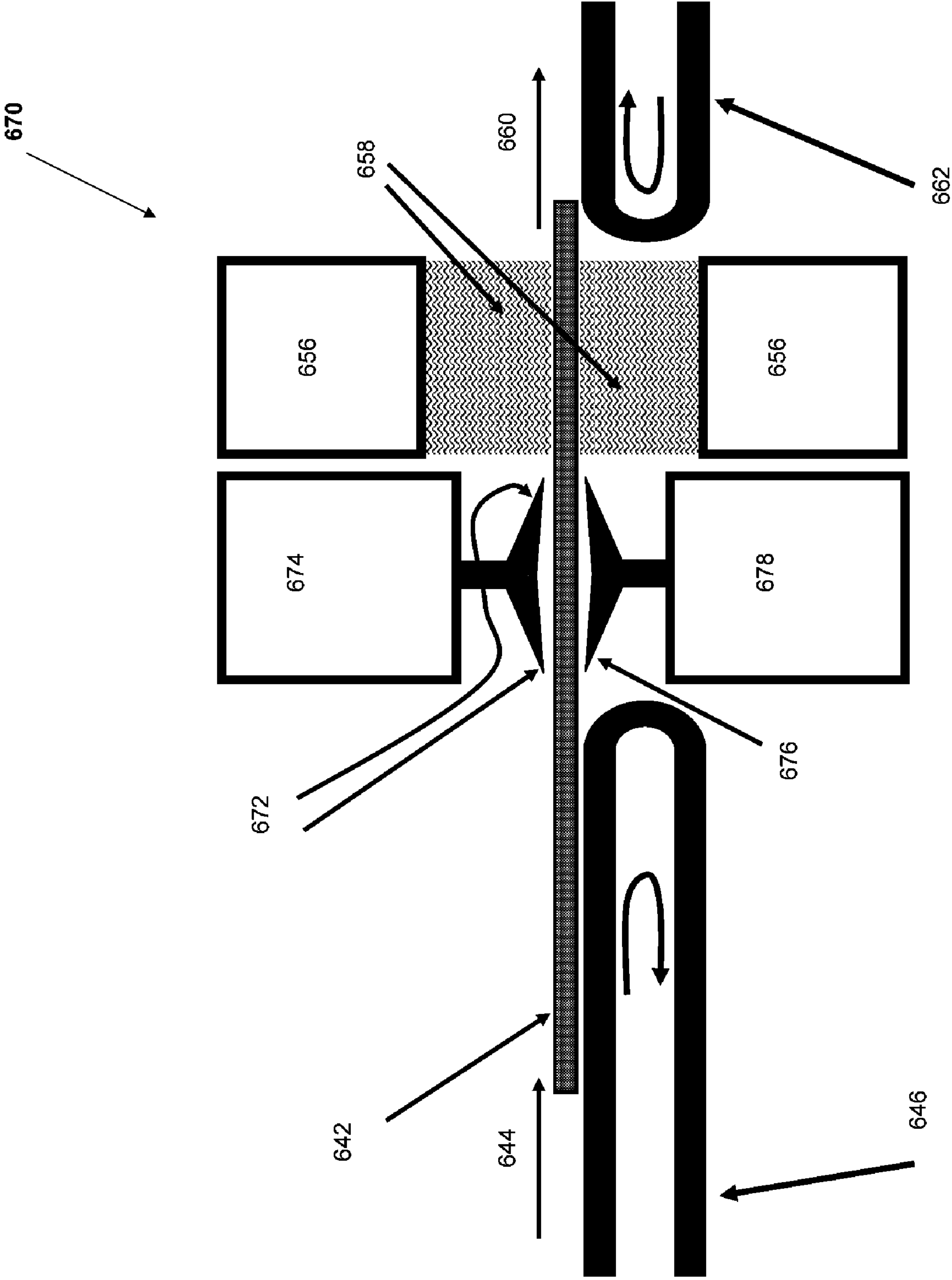

FIG. 37

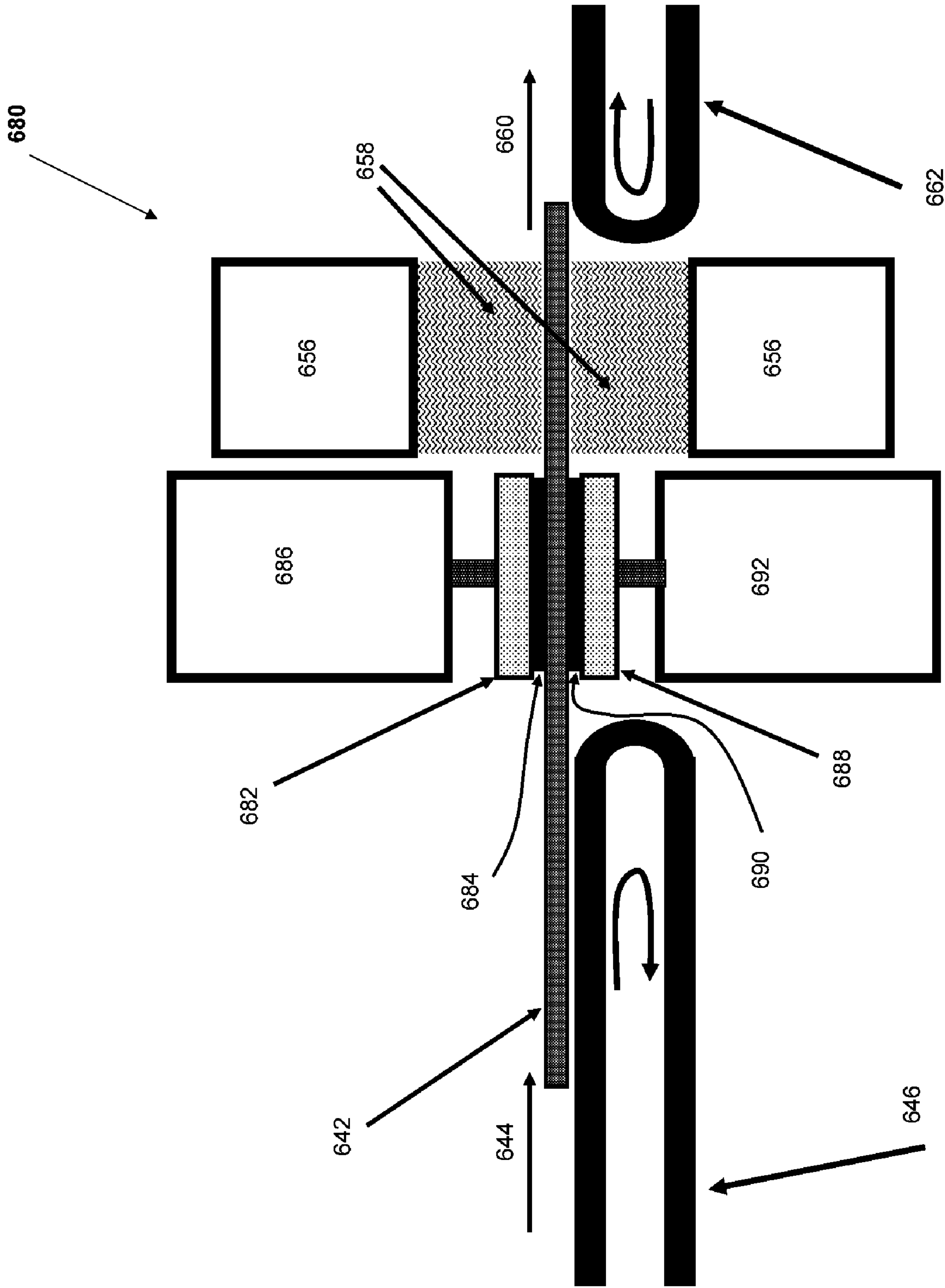

FIG. 38

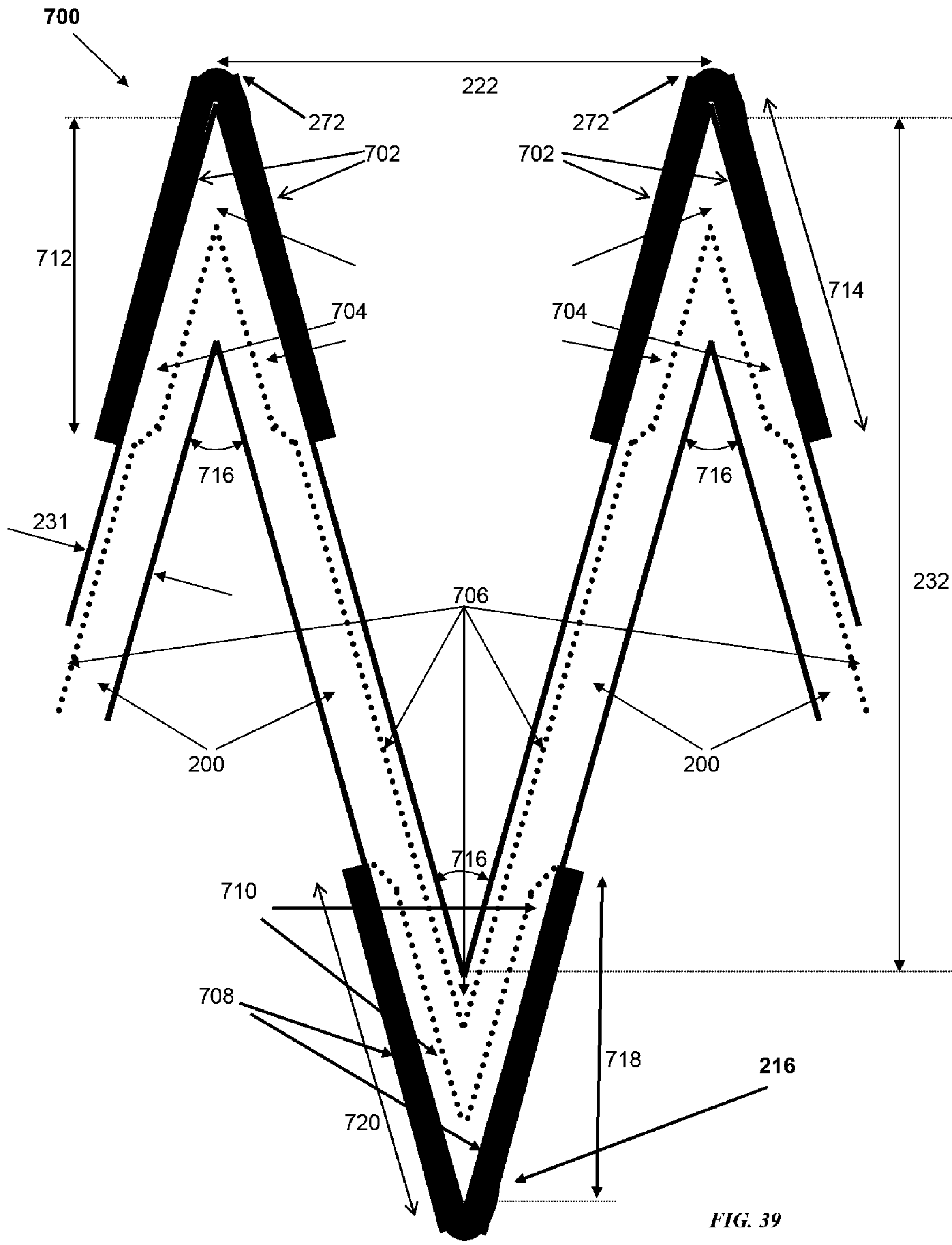

FIG. 39

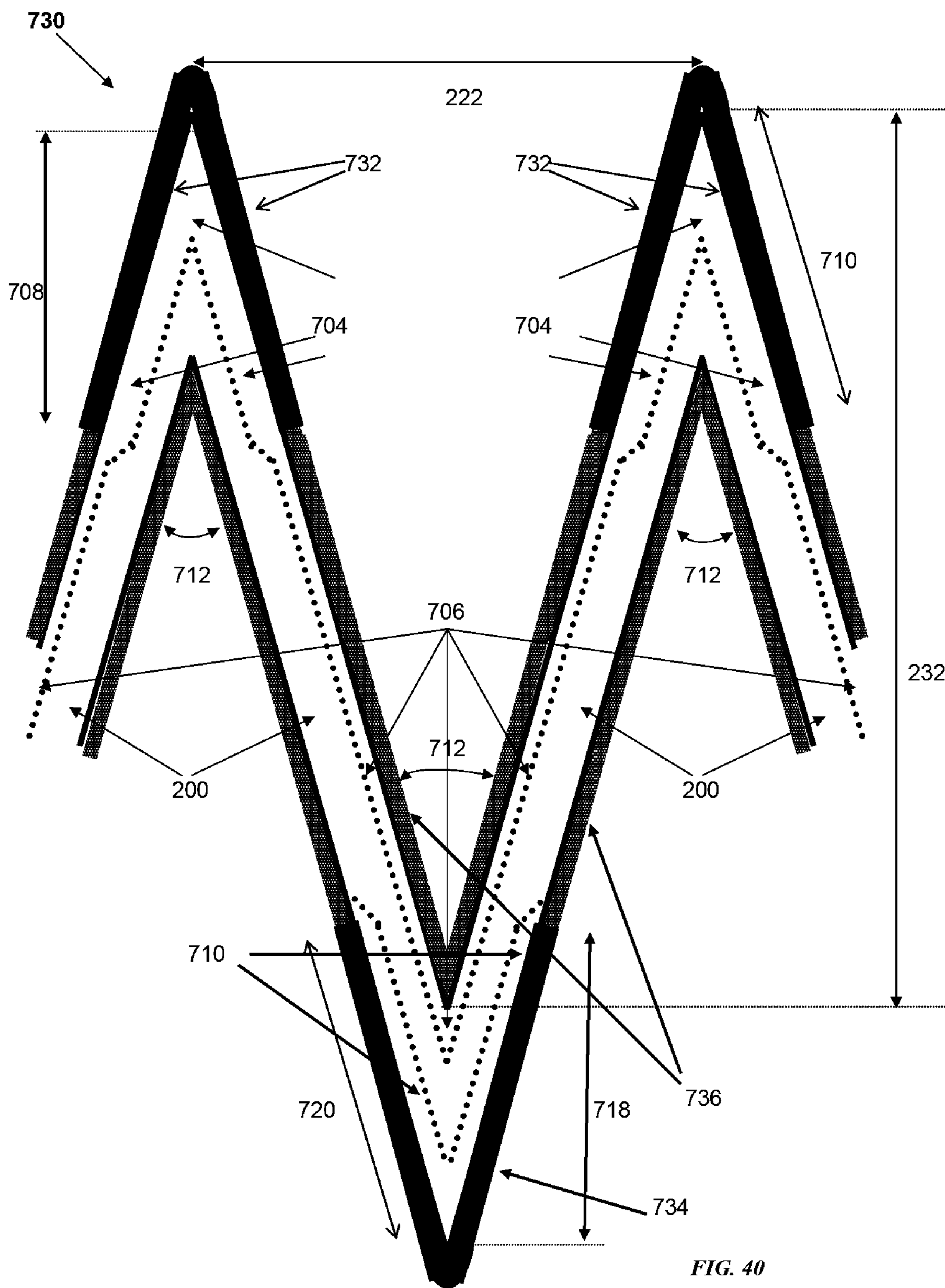

FIG. 40

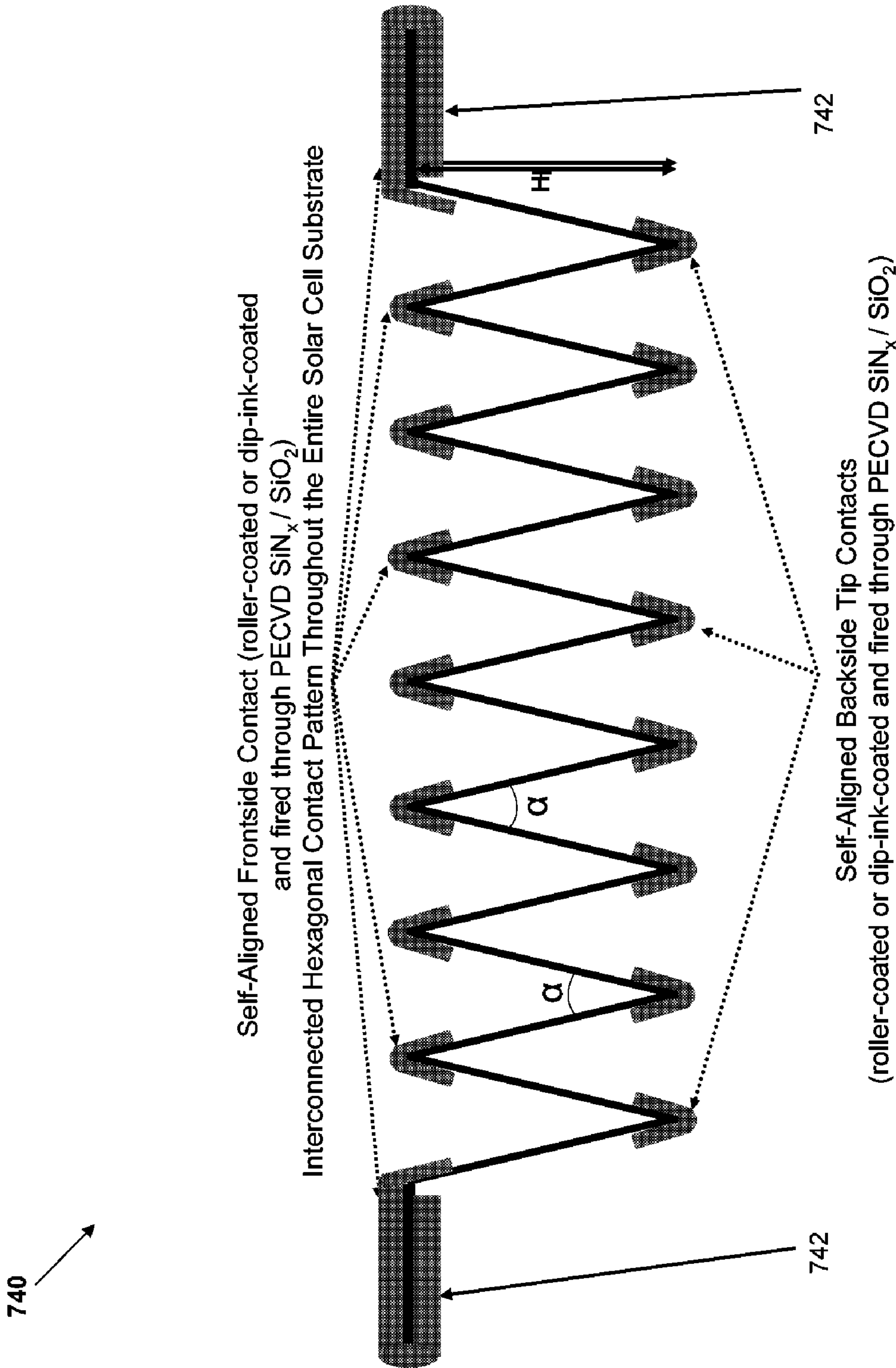

FIG. 41

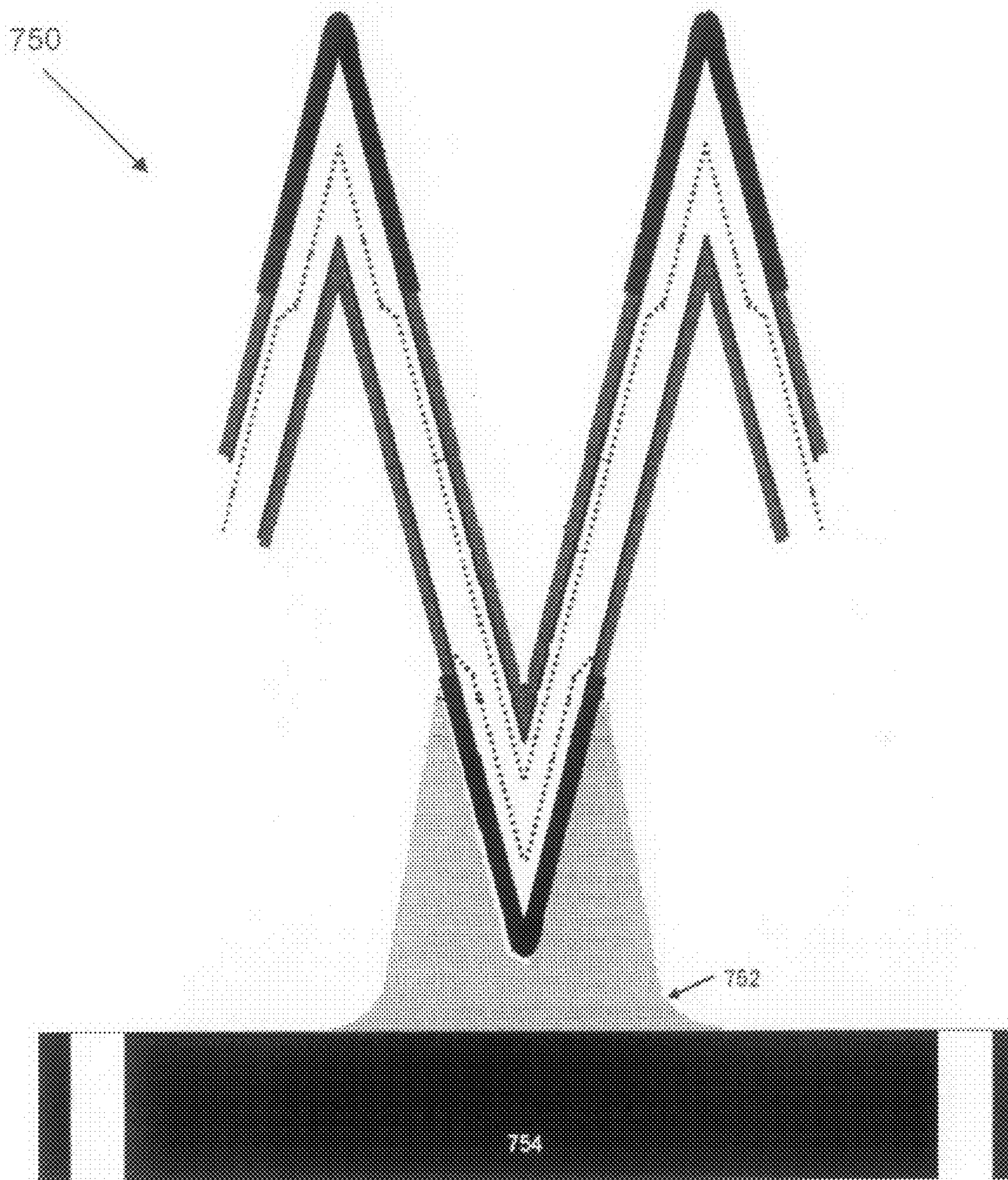

FIG. 42

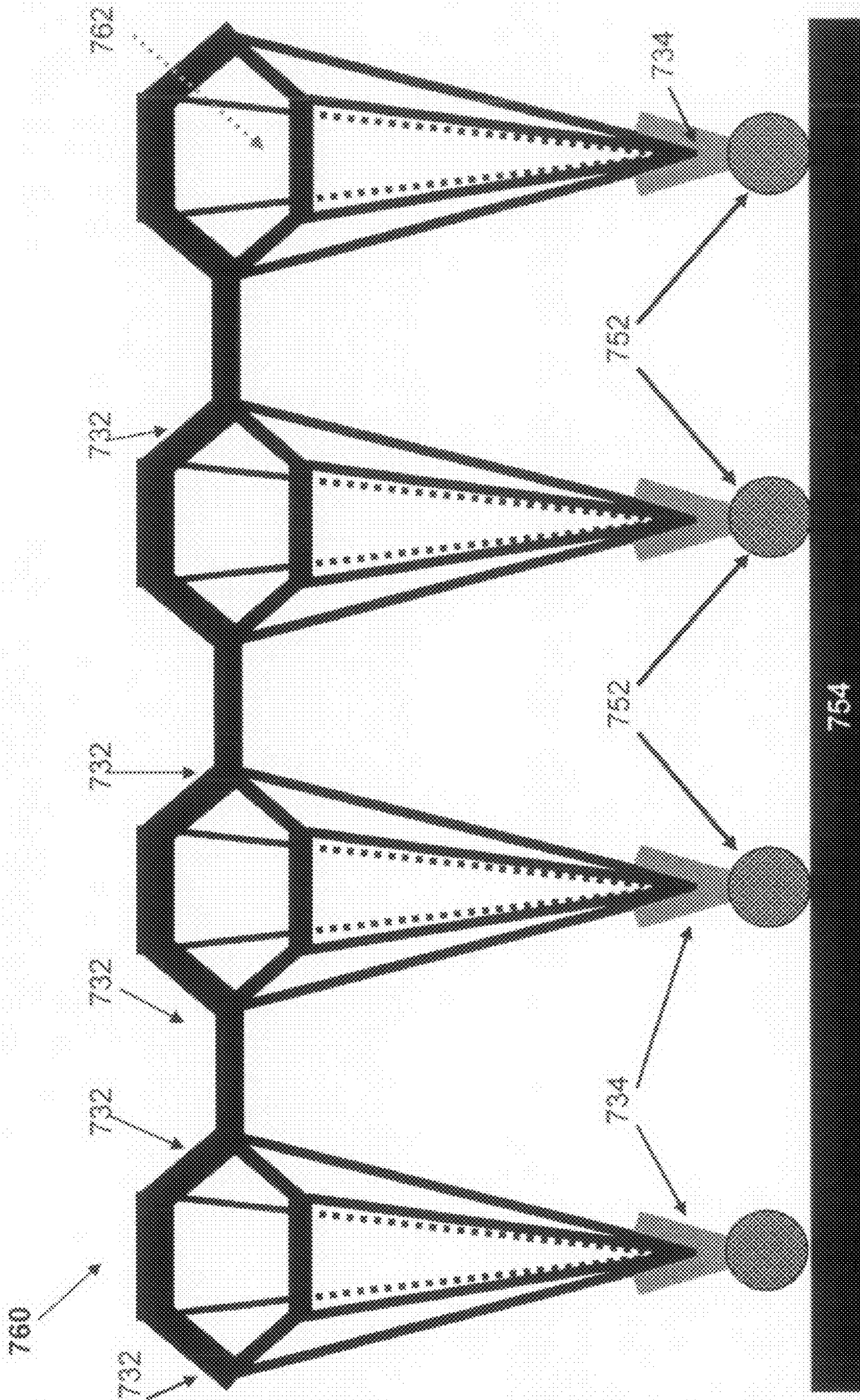

FIG. 43

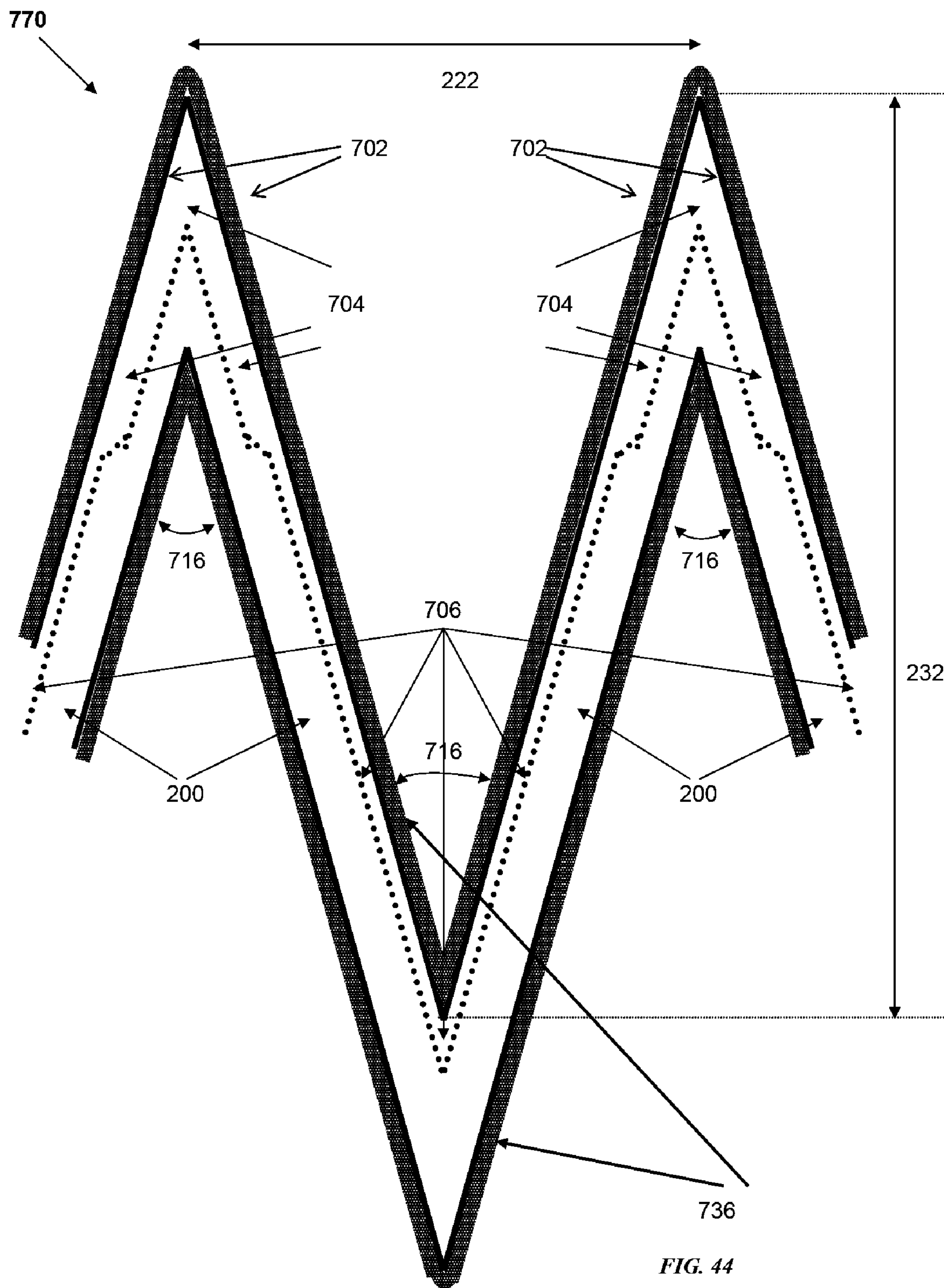

FIG. 44

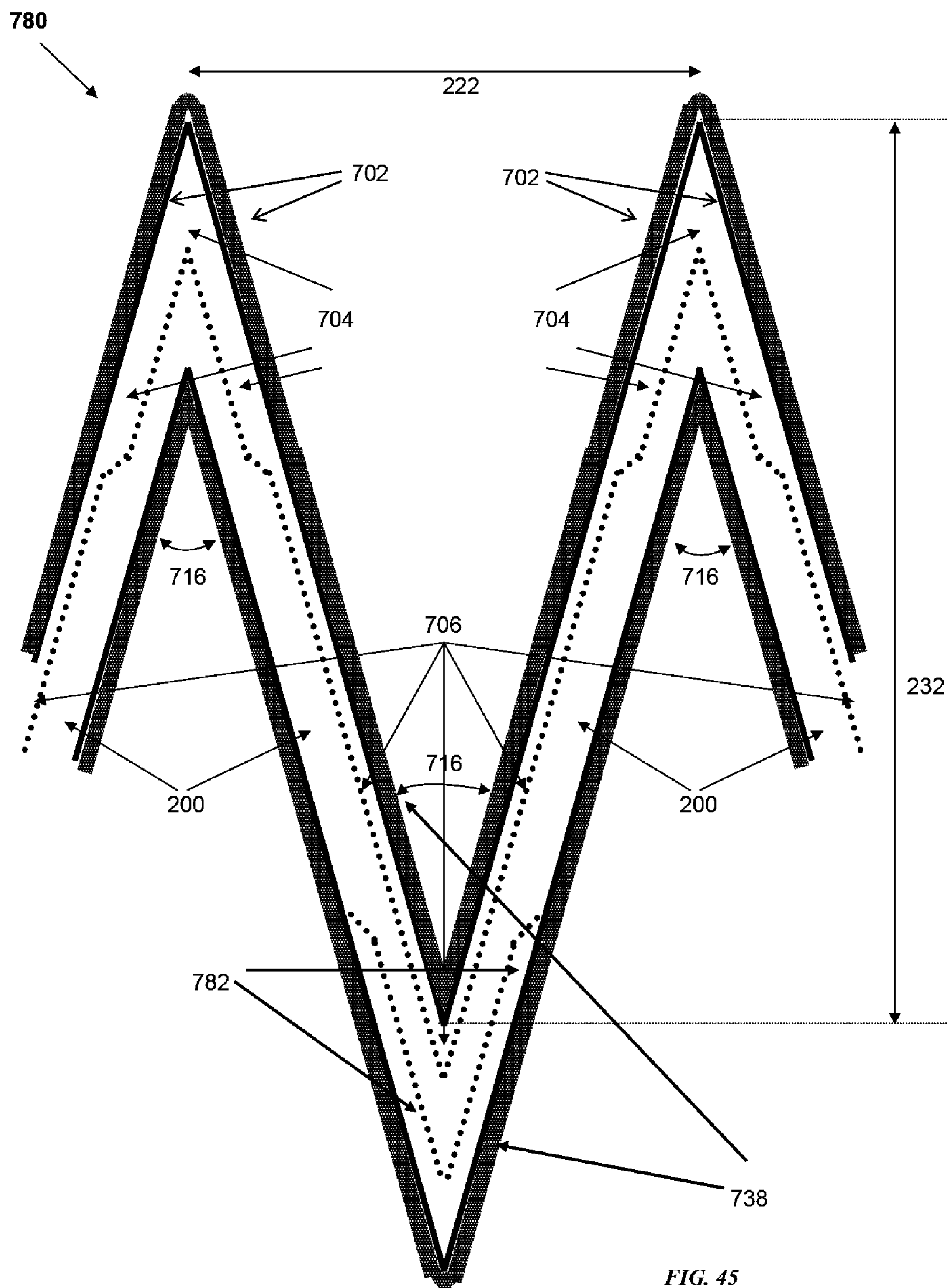

FIG. 45

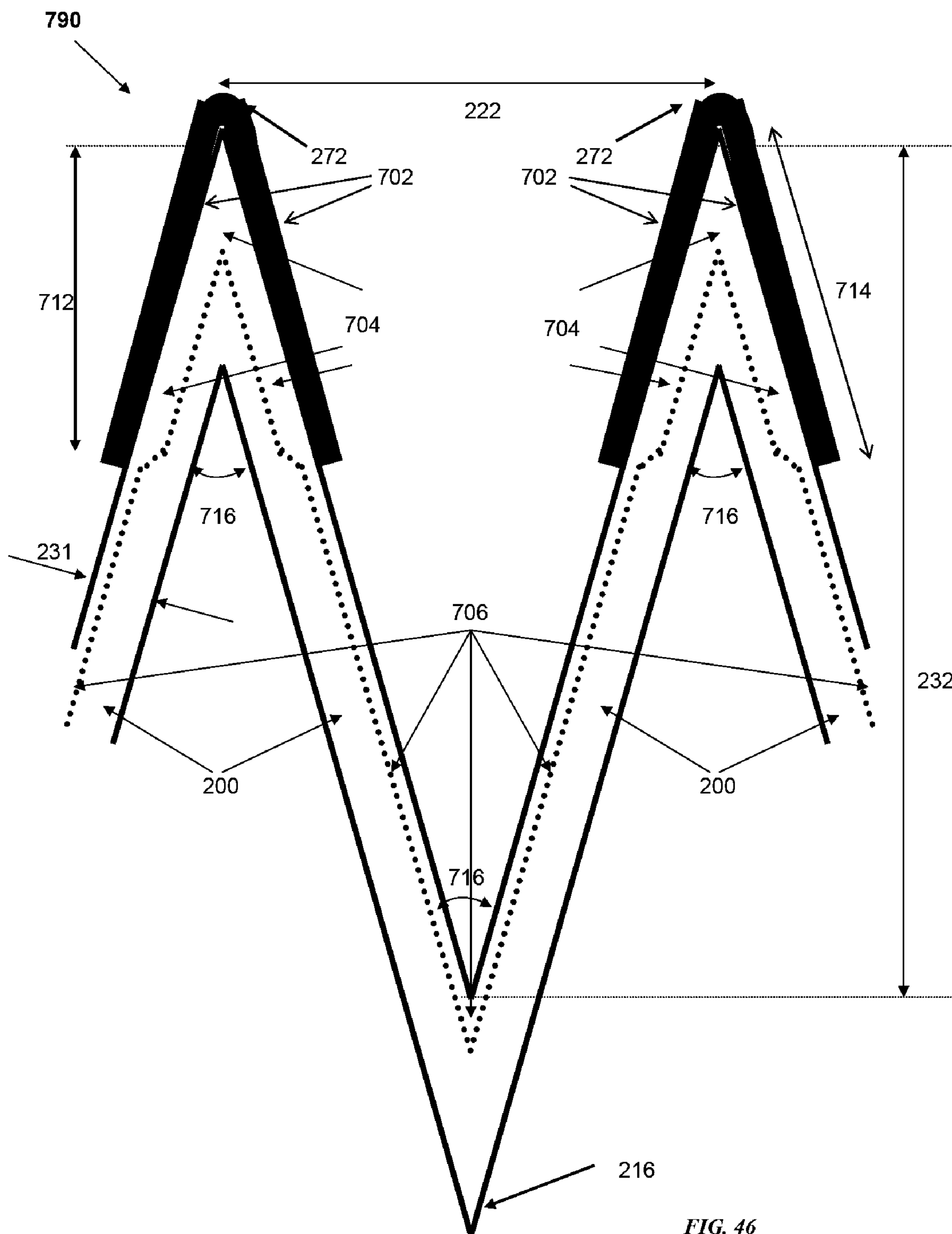

FIG. 46

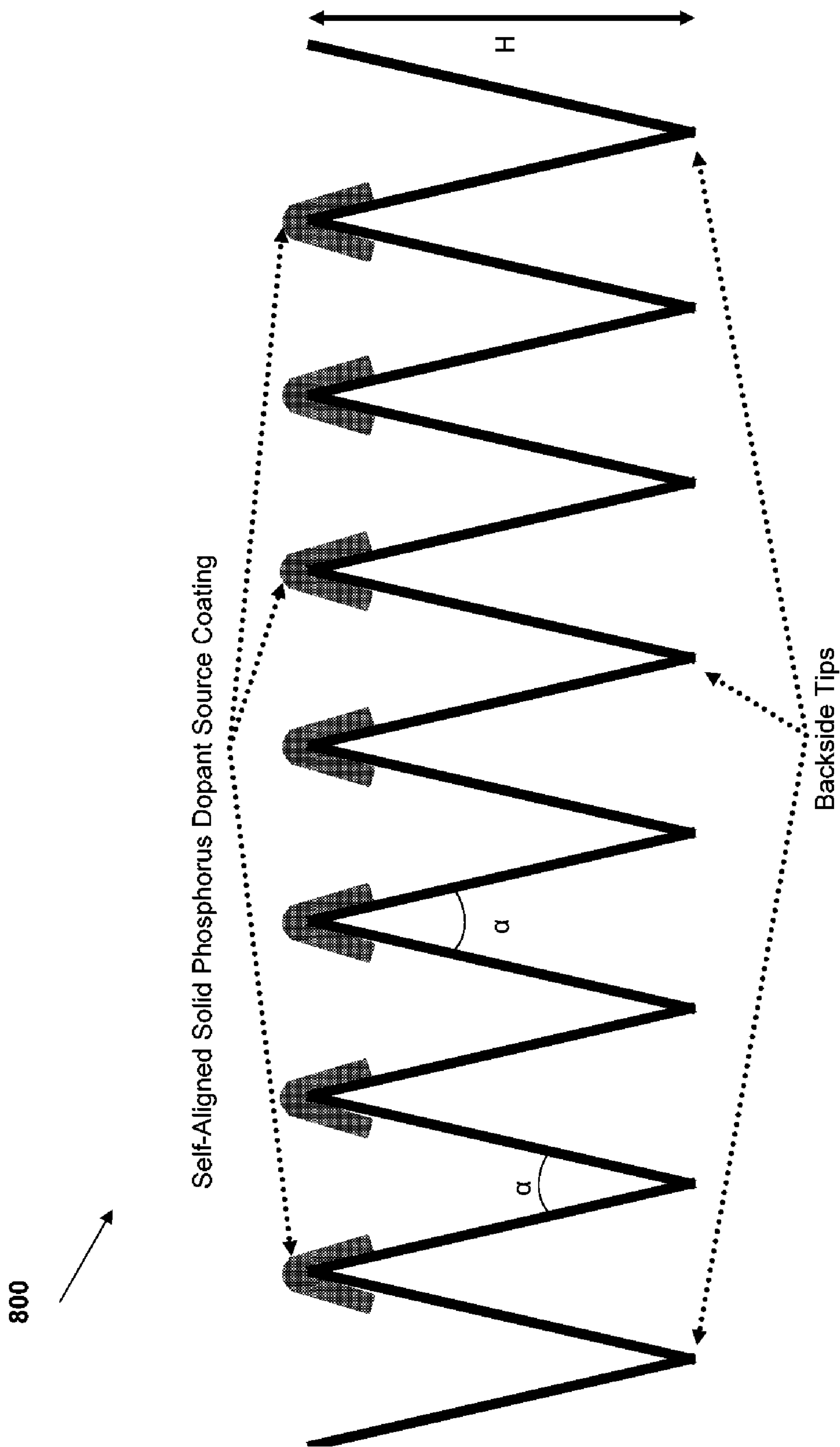

FIG. 47

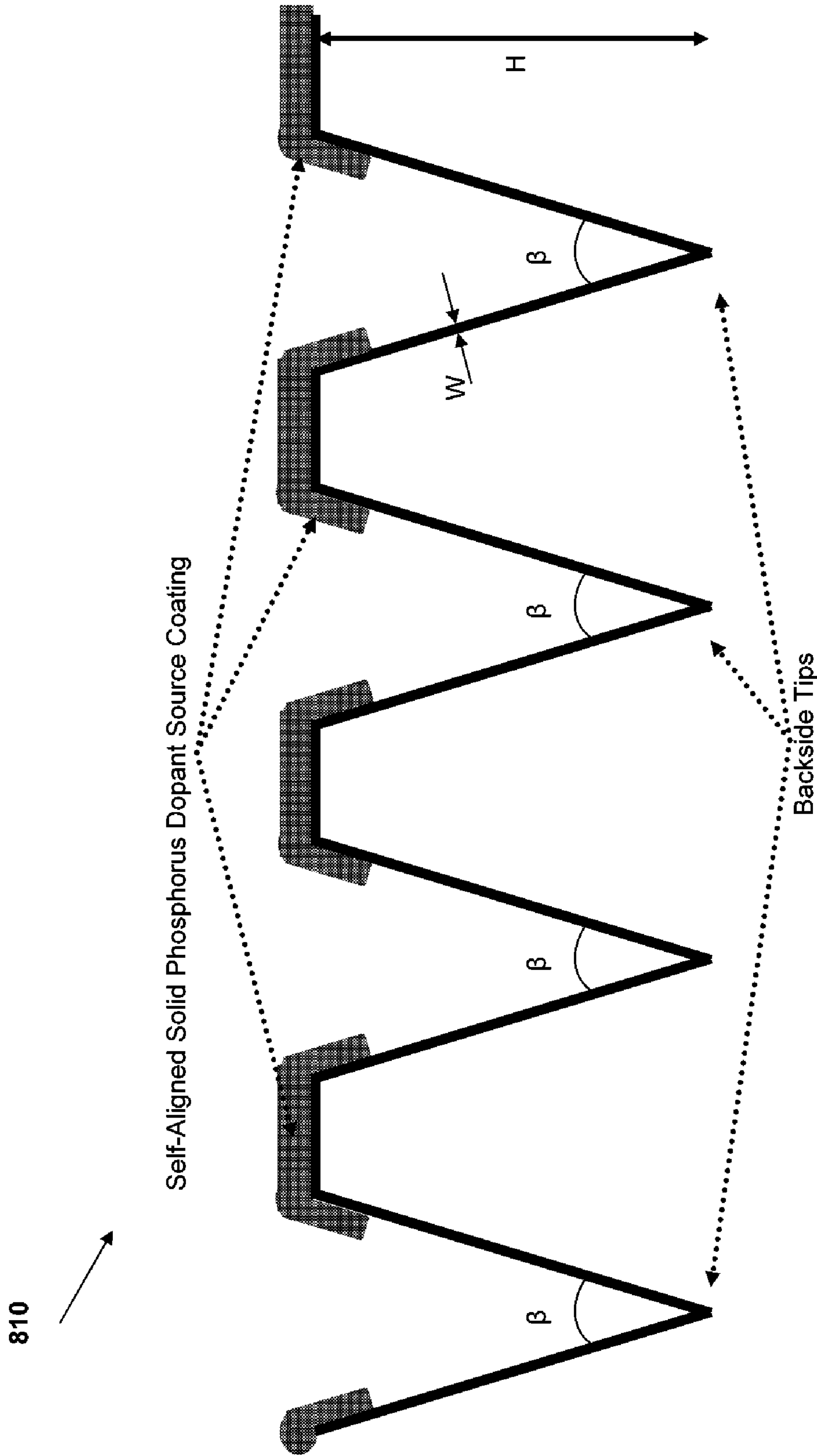

FIG. 48

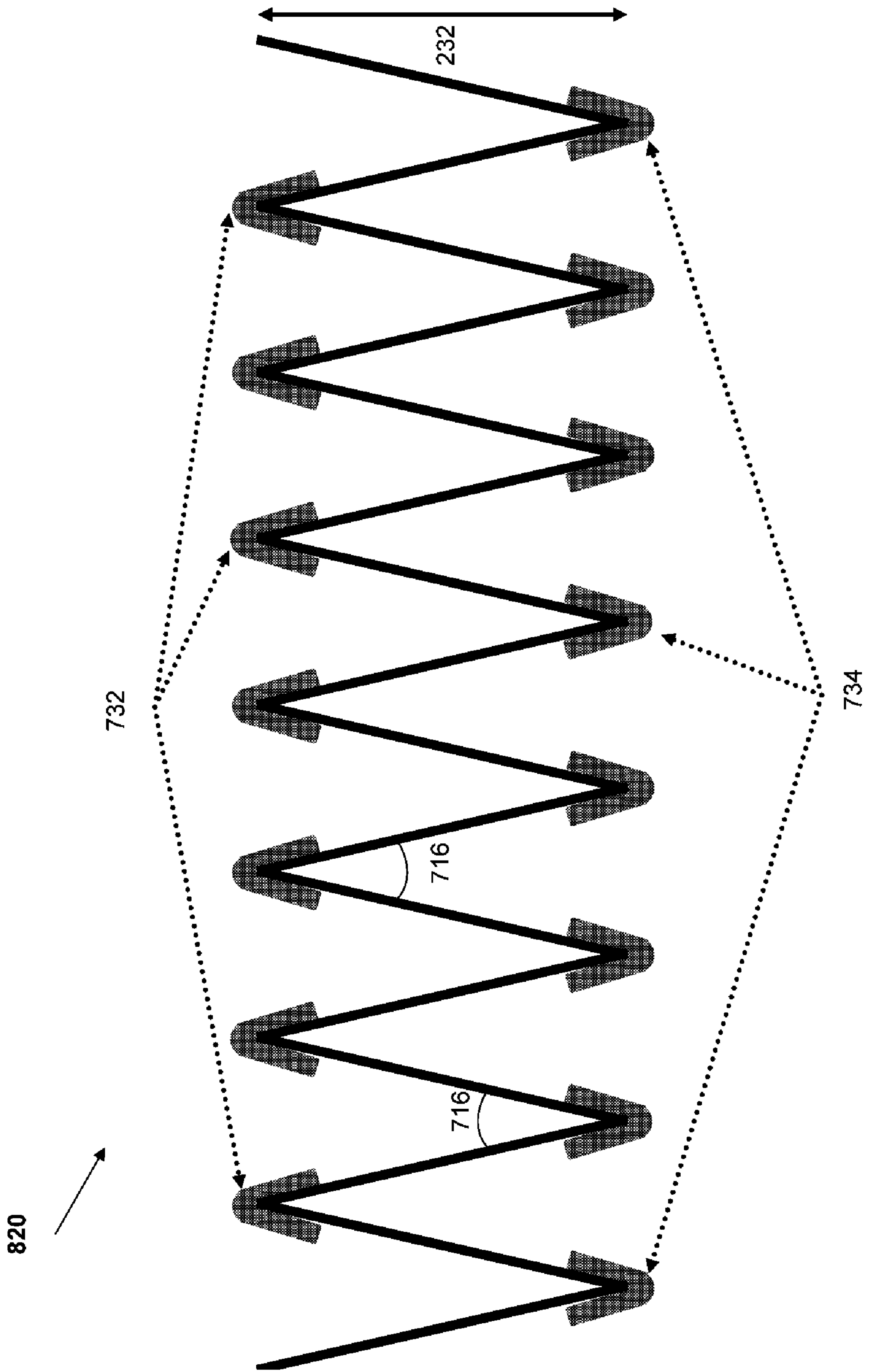

FIG. 49

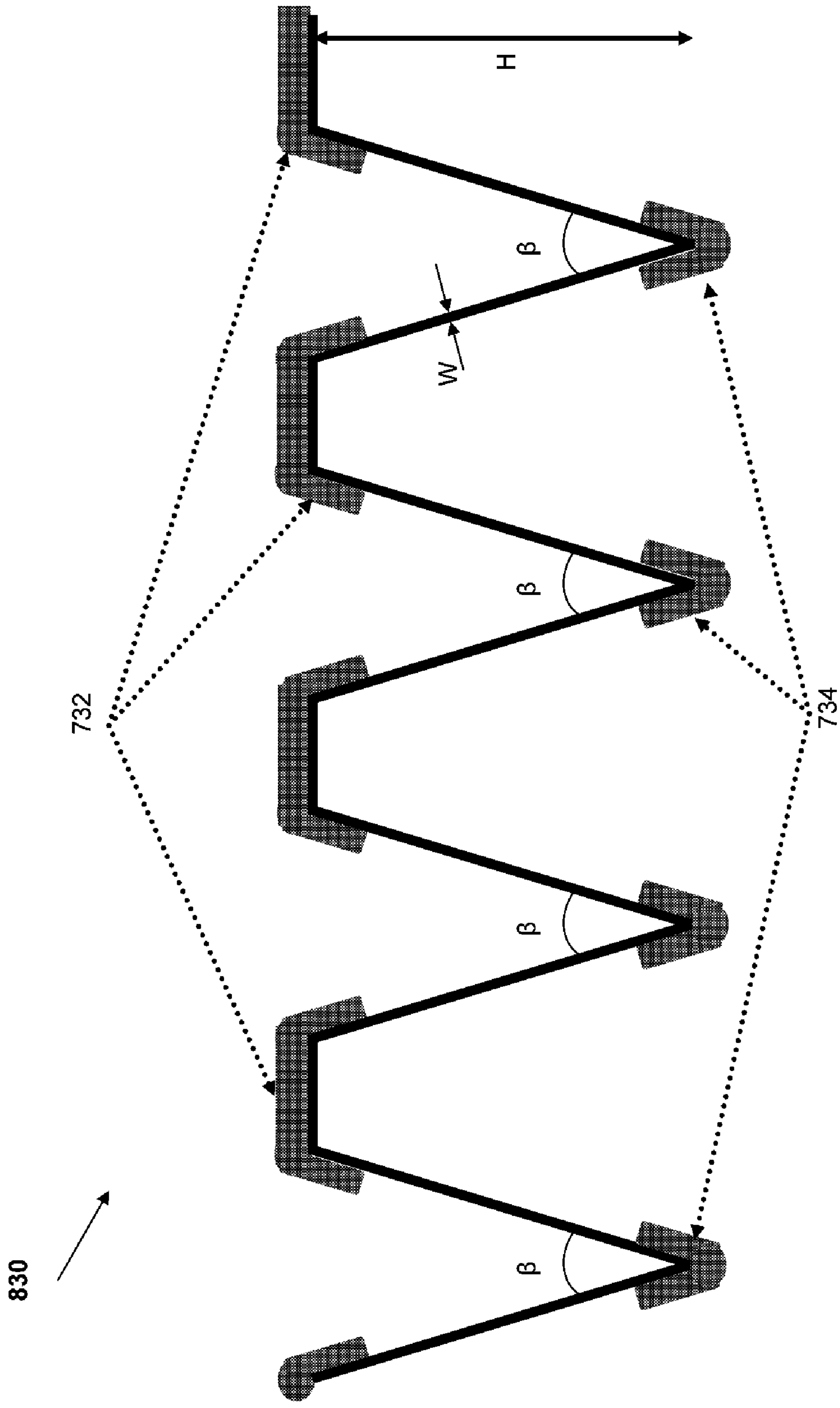

FIG. 50

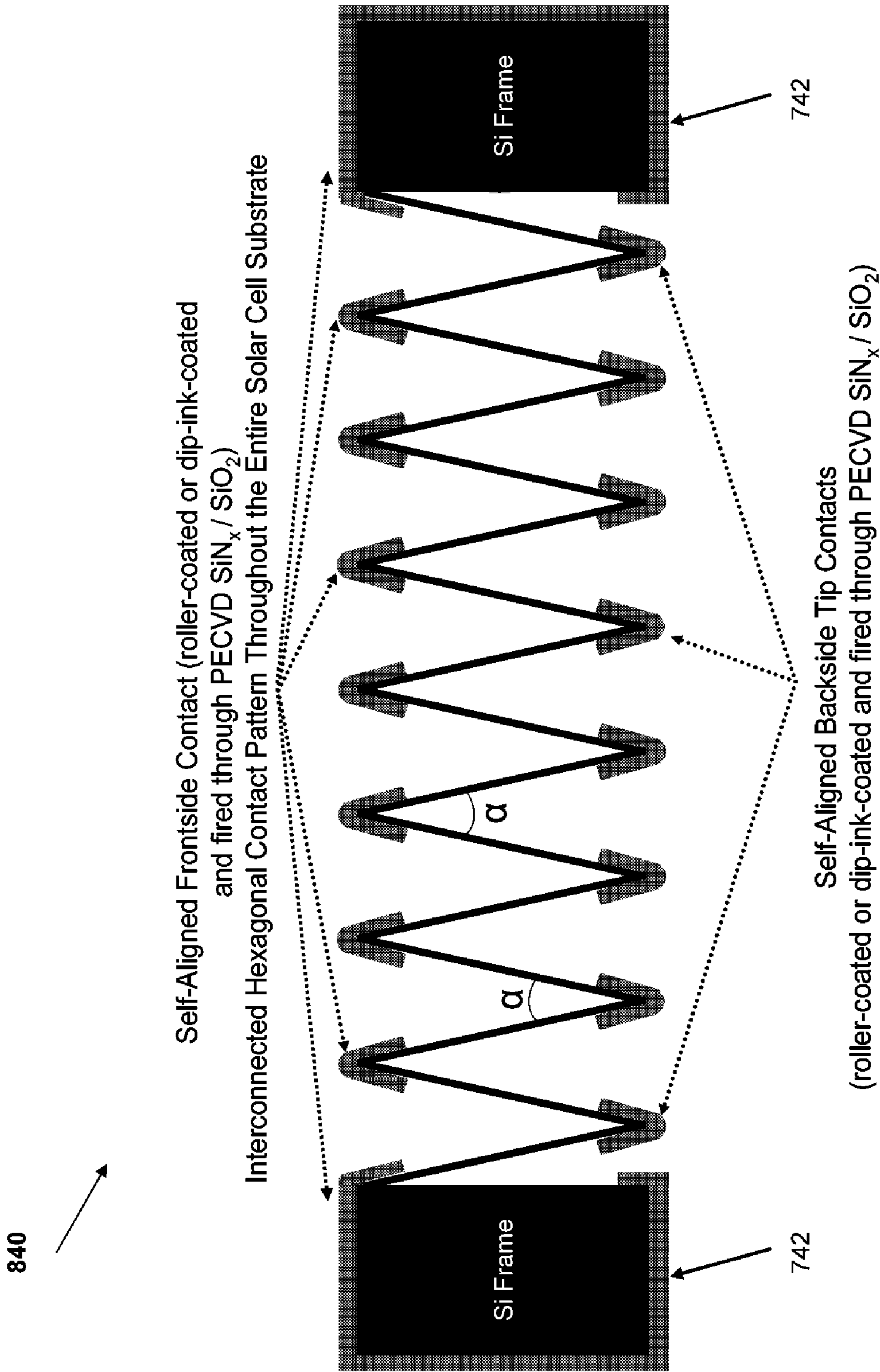

FIG. 51

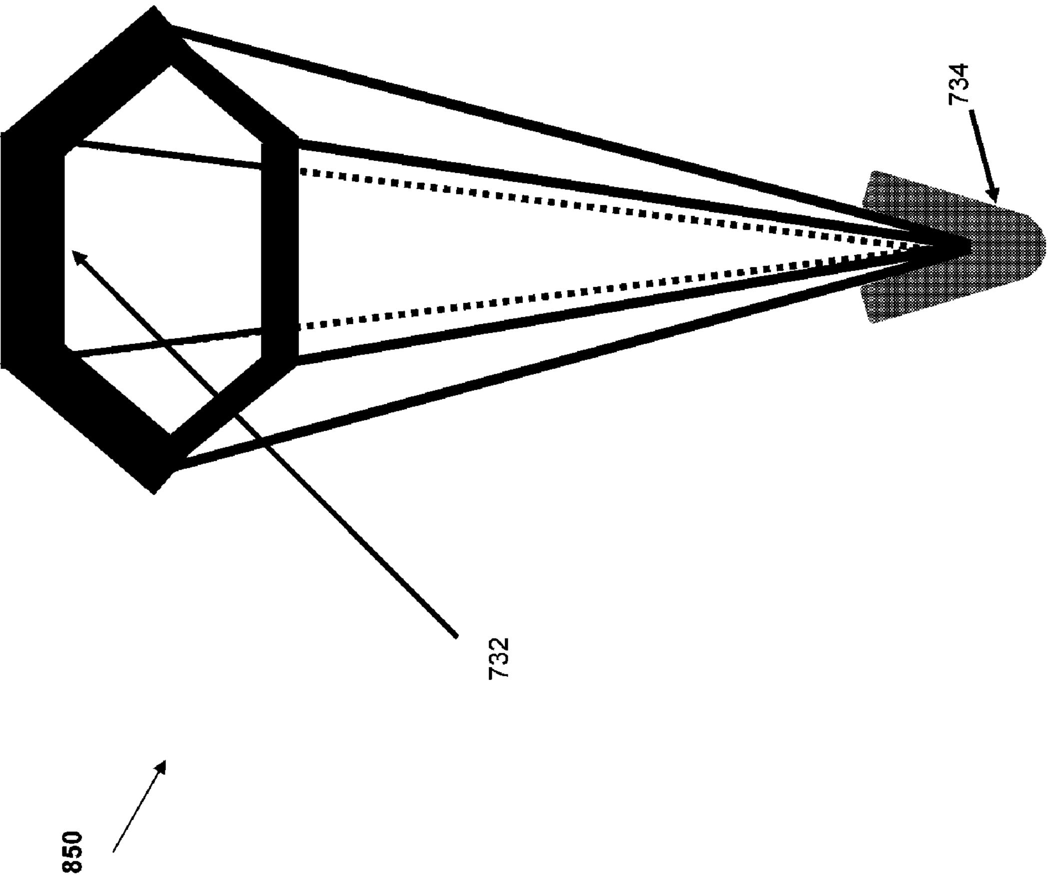

FIG. 52

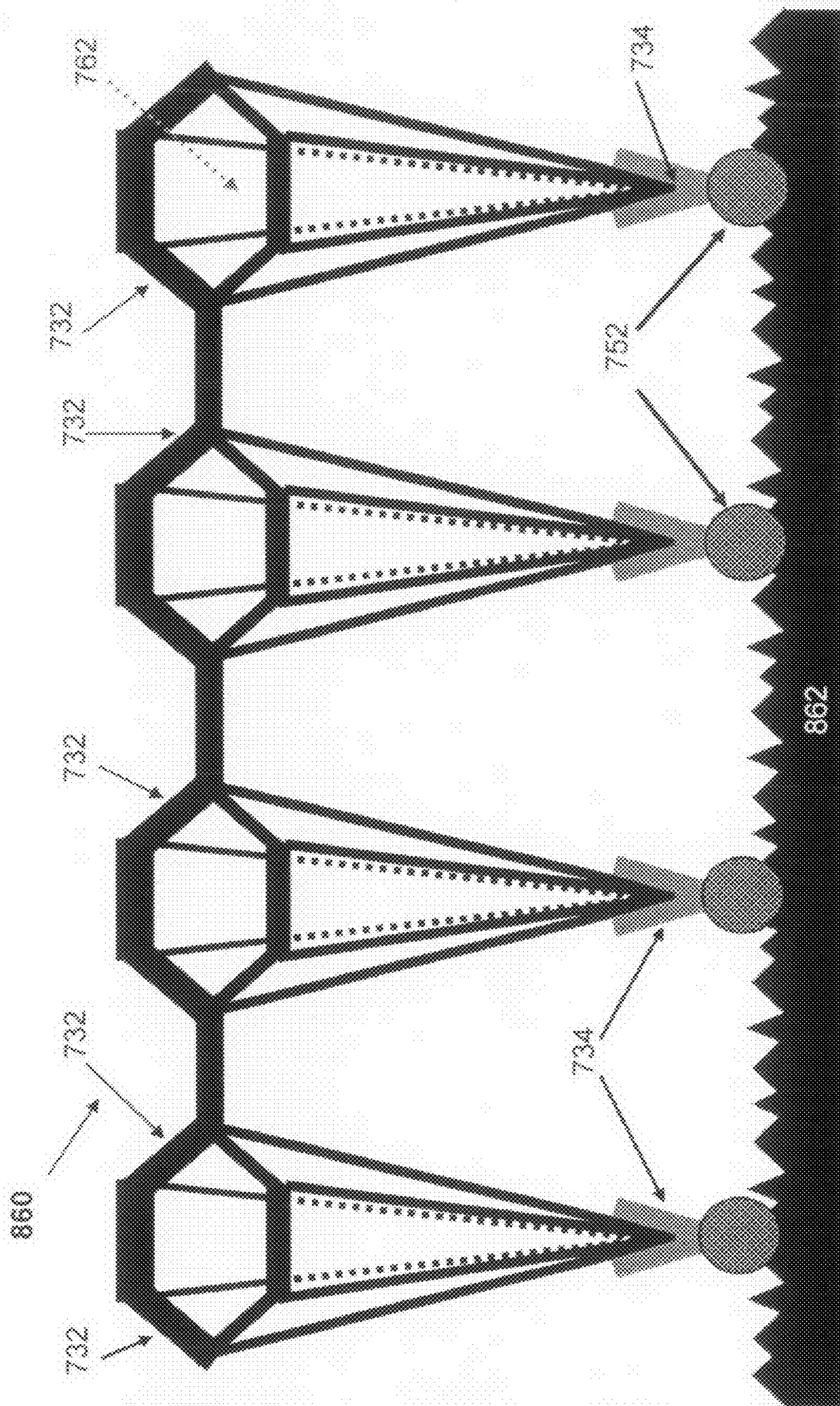

FIG. 53

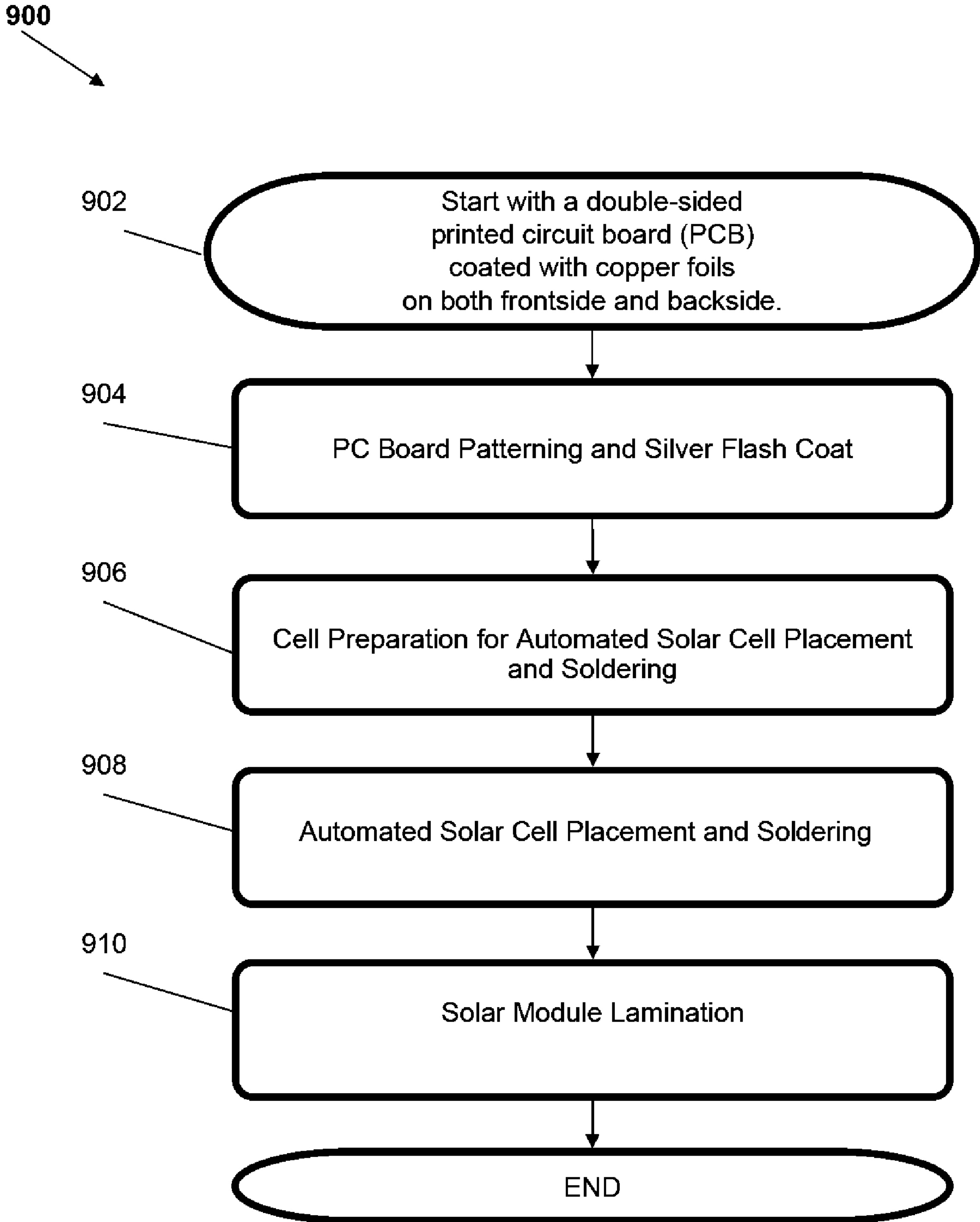

FIG. 54

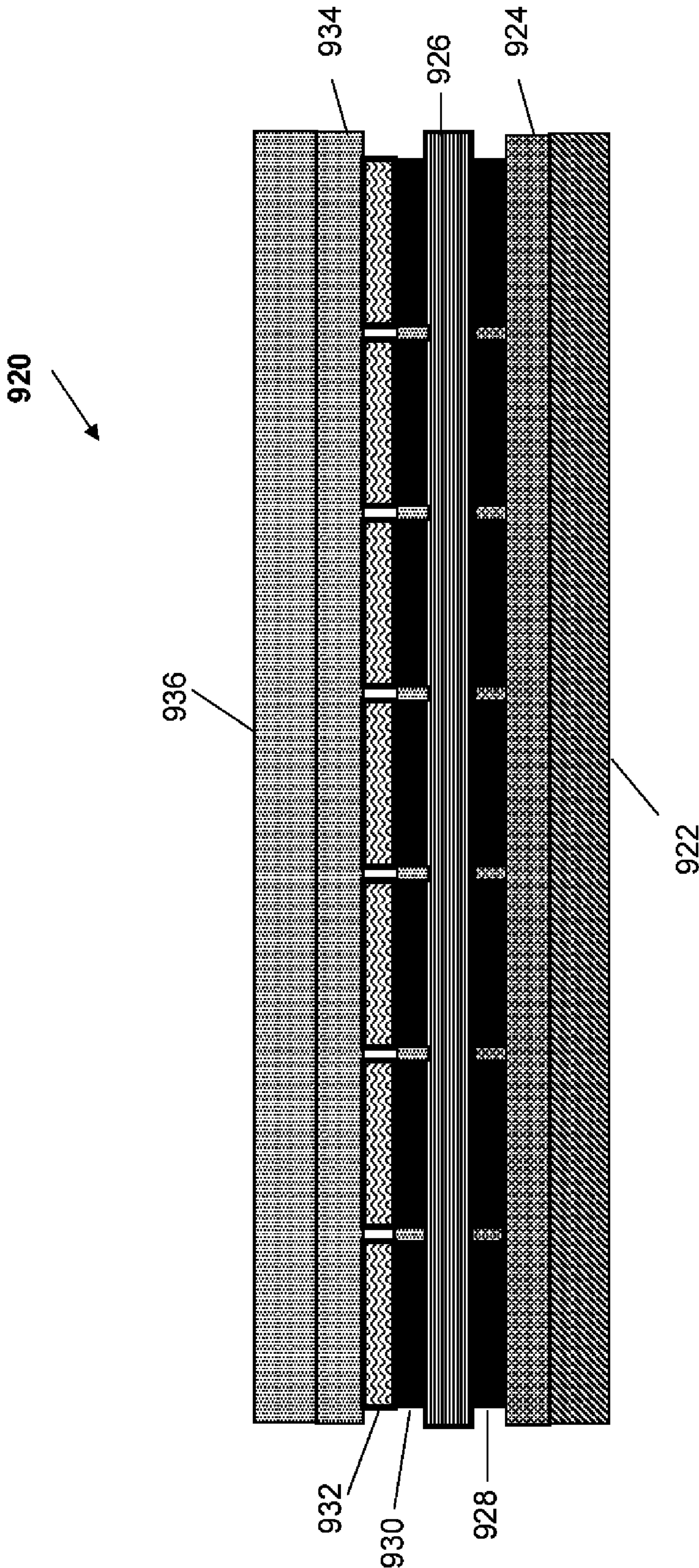

FIG. 55

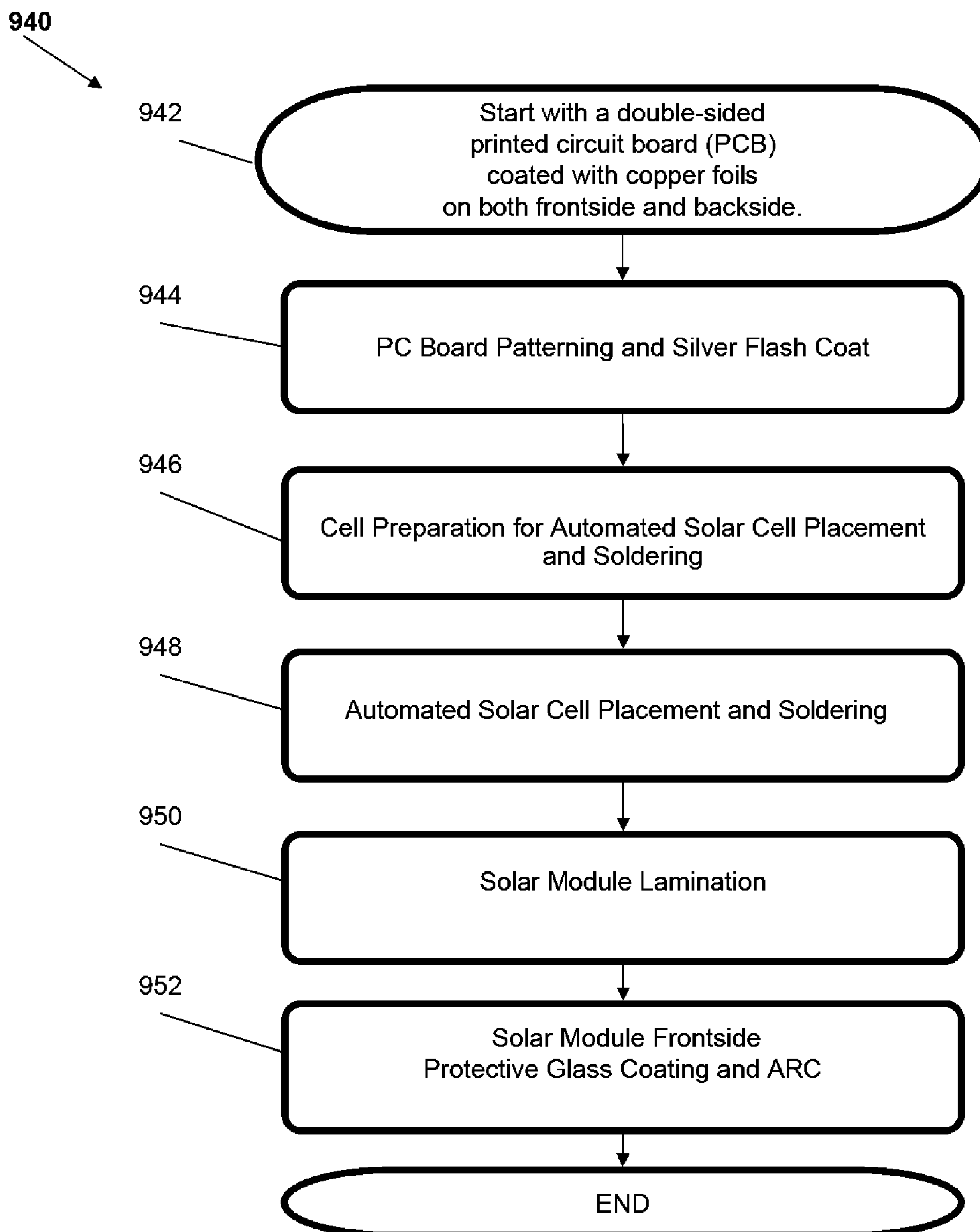

FIG. 56

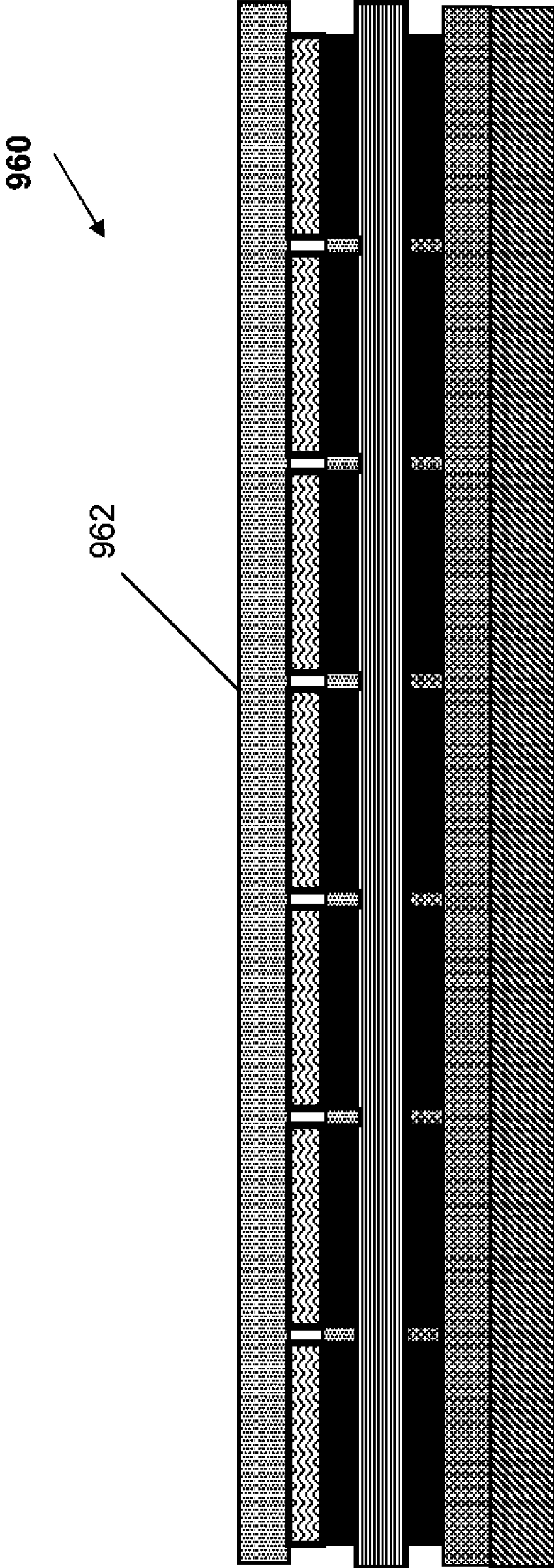

FIG. 57

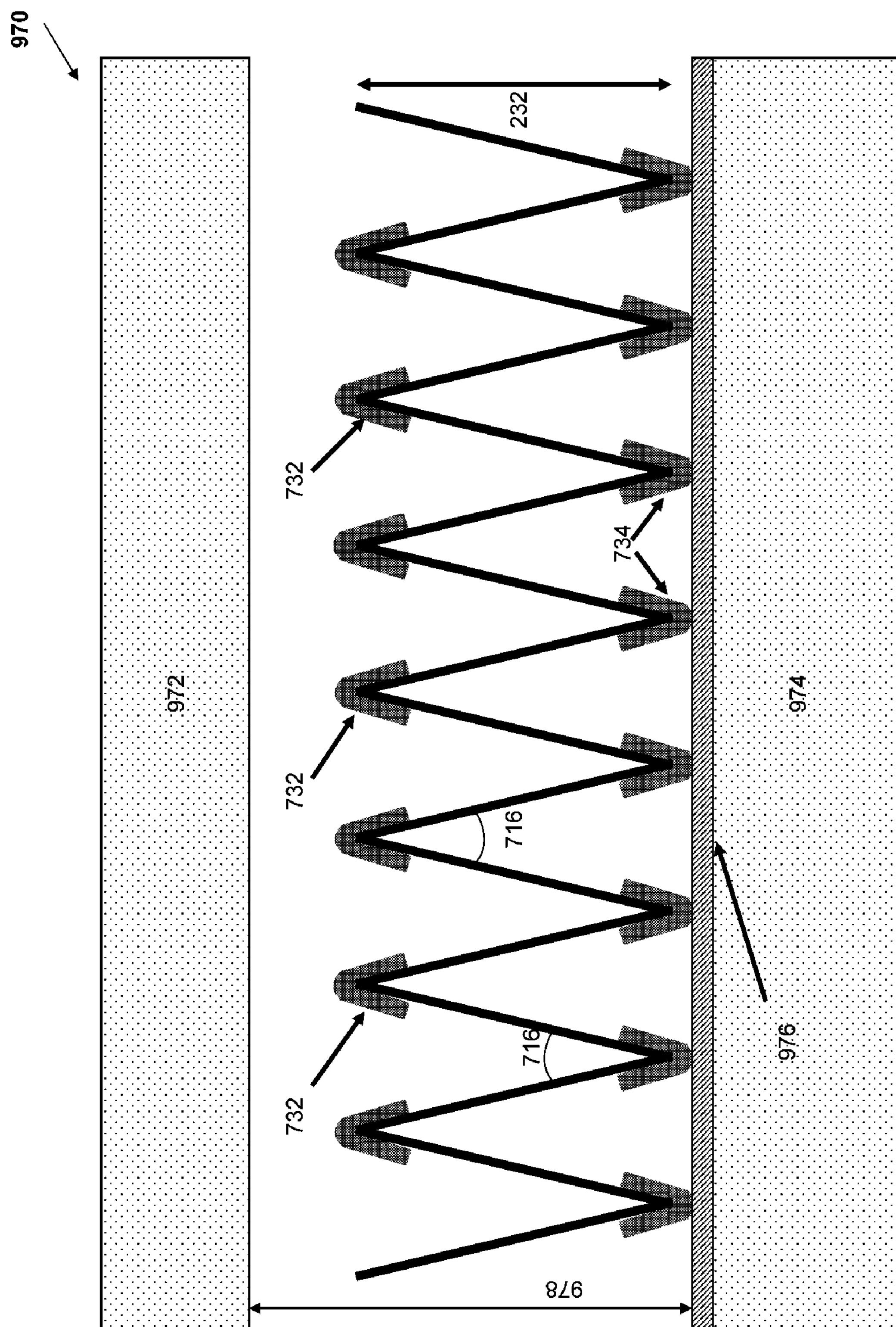

FIG. 58

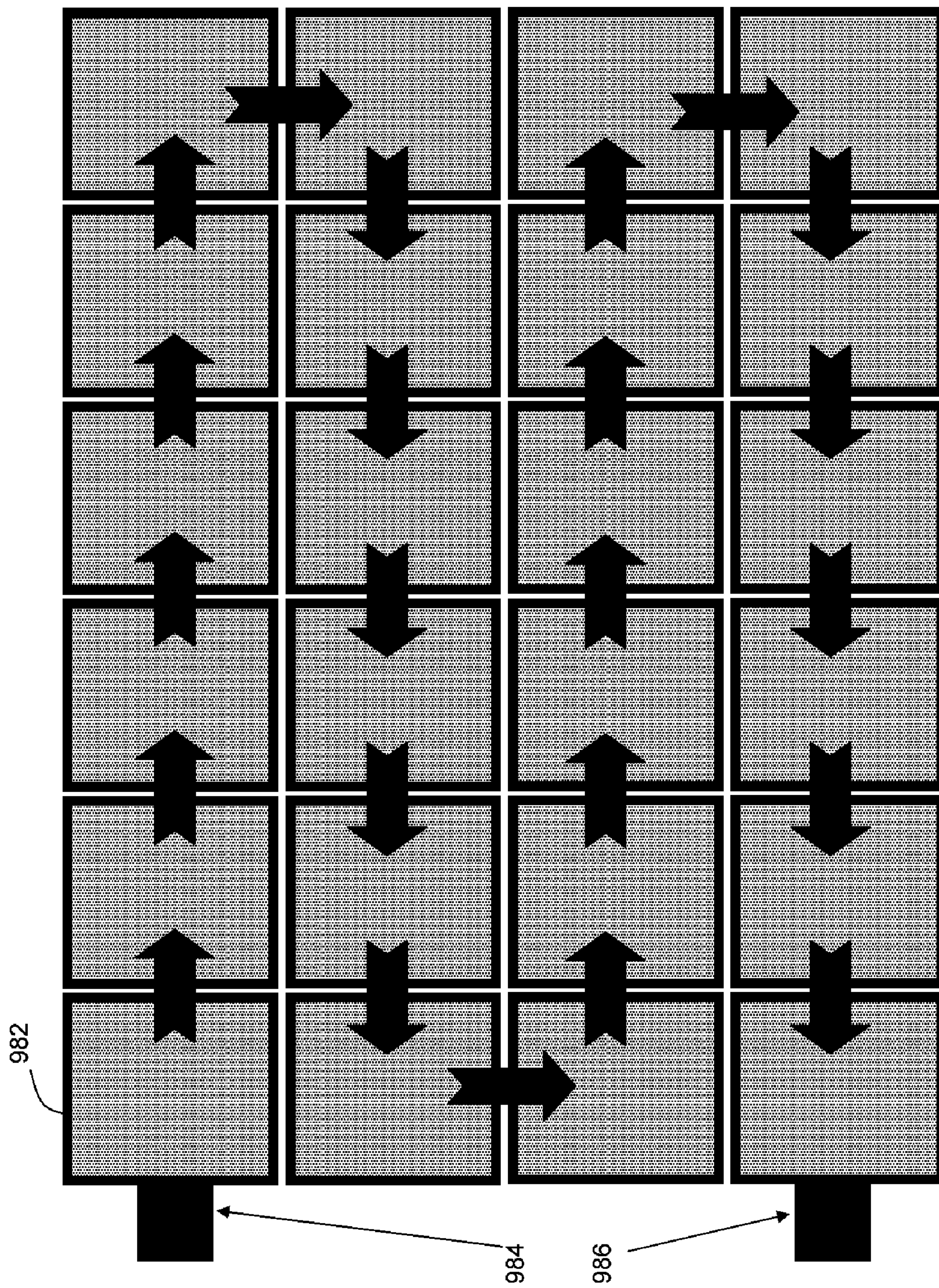

FIG. 59

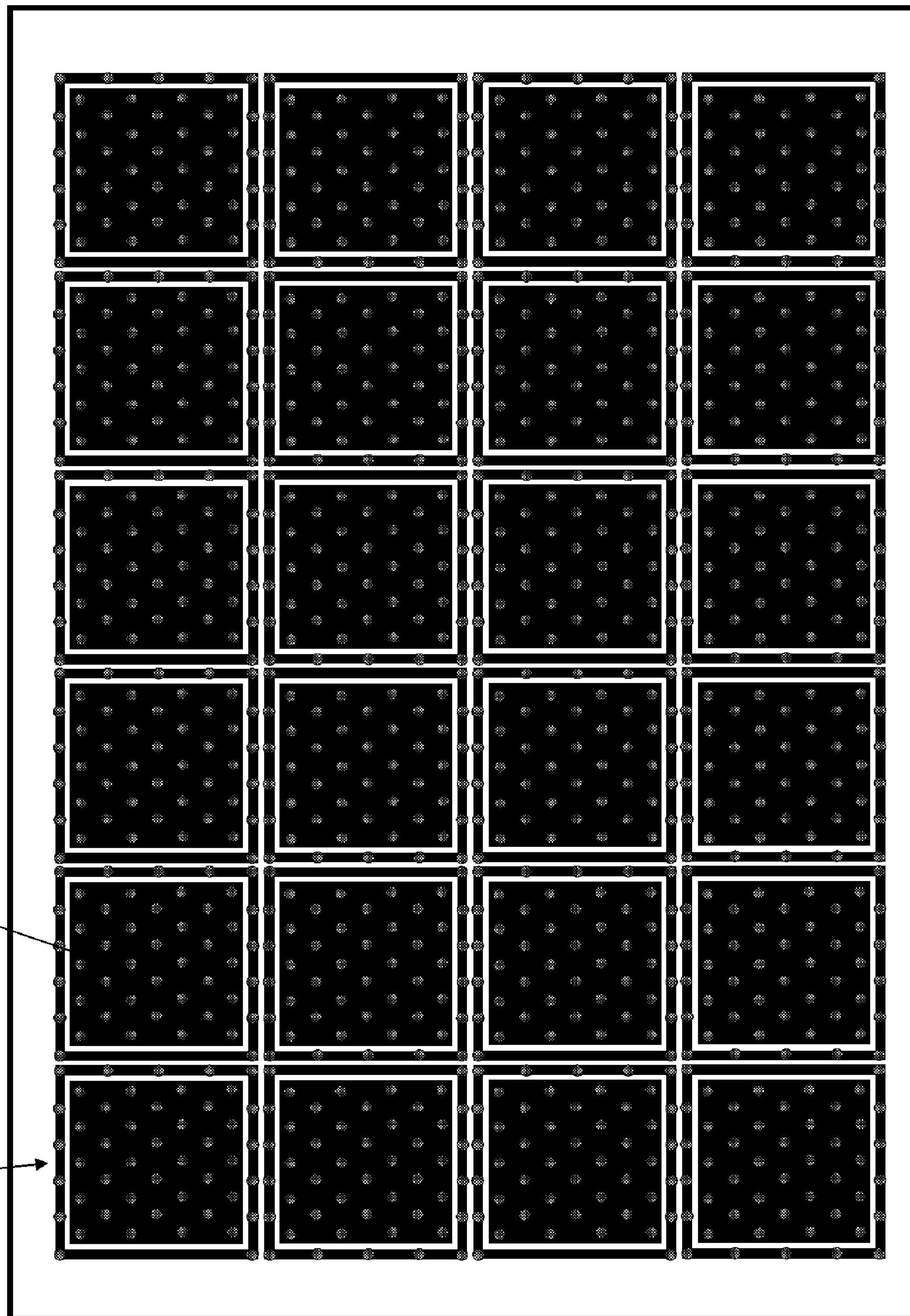

FIG. 60

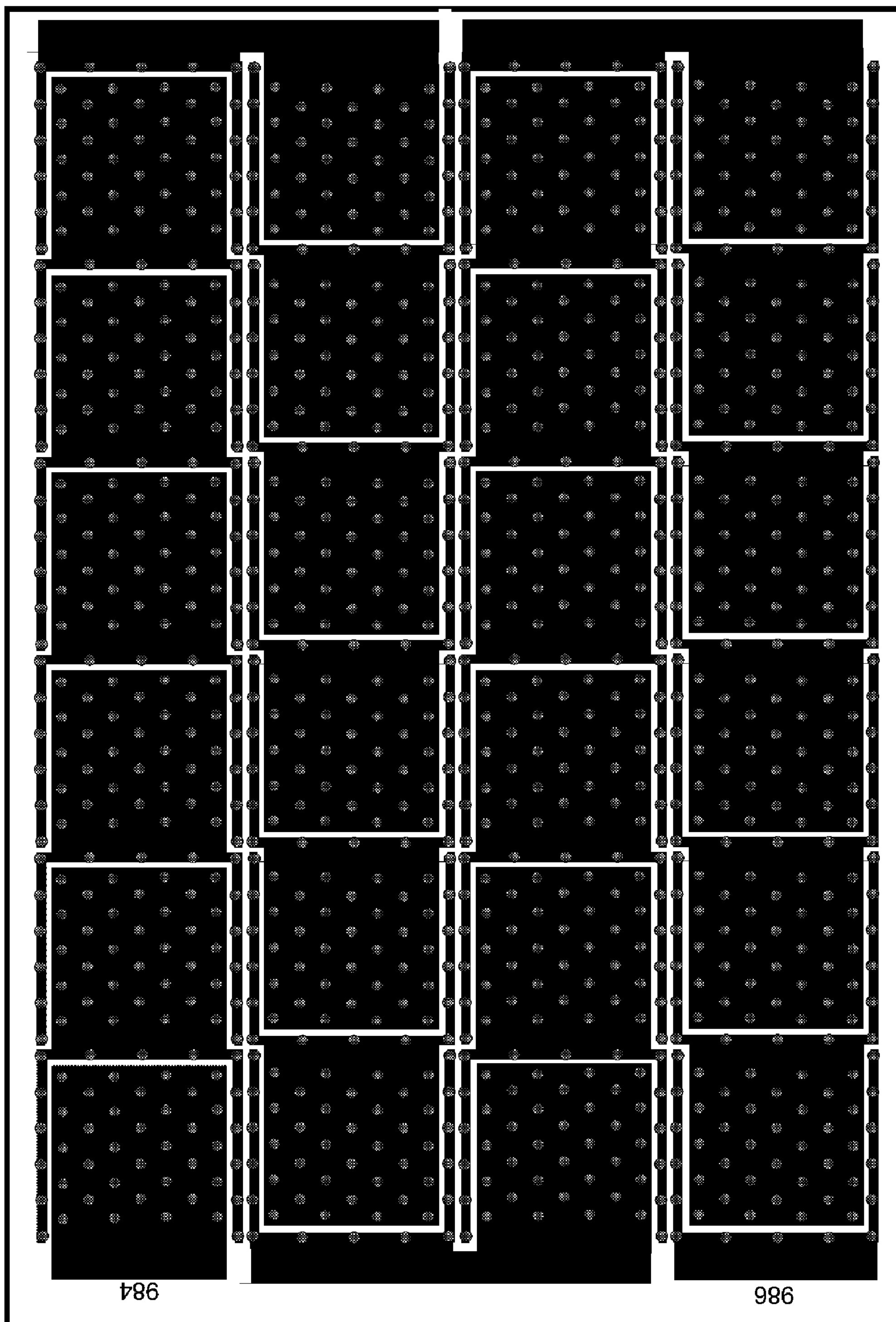

FIG. 61

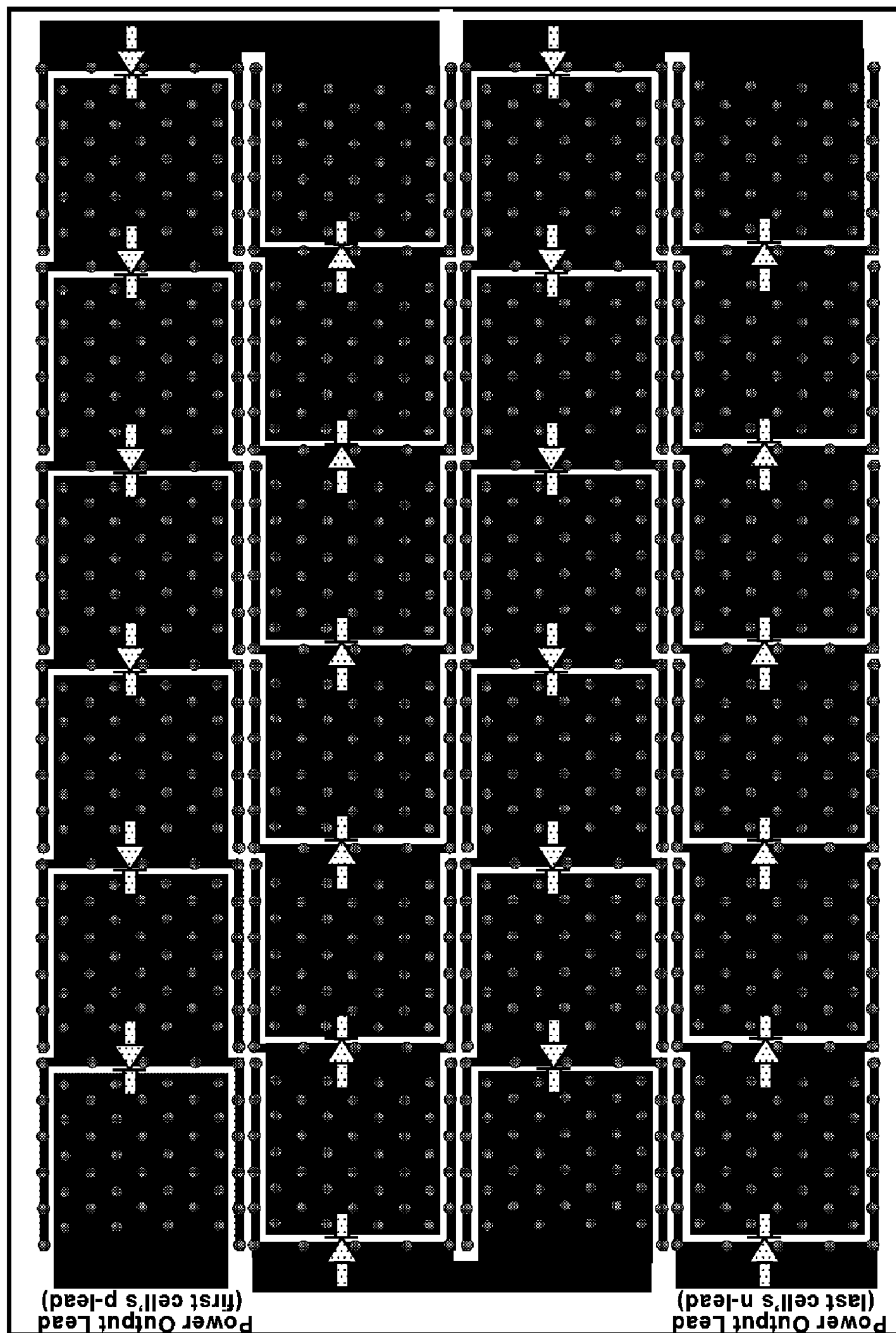

FIG. 62

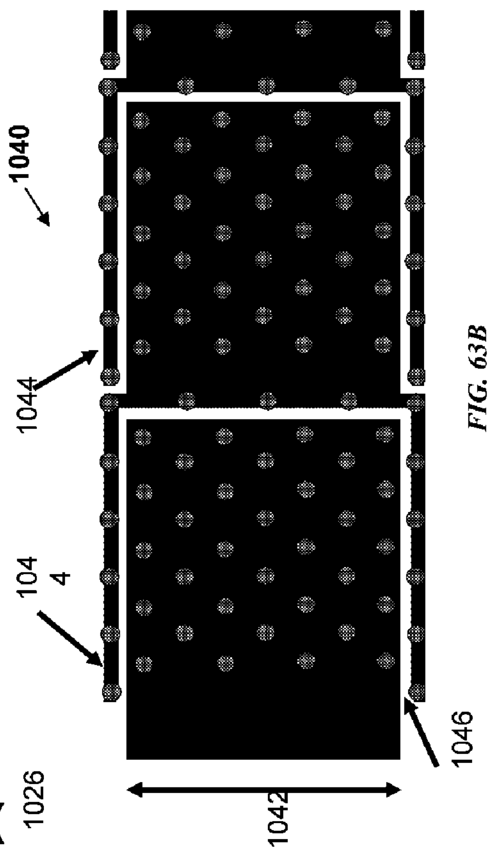

FIG. 63B

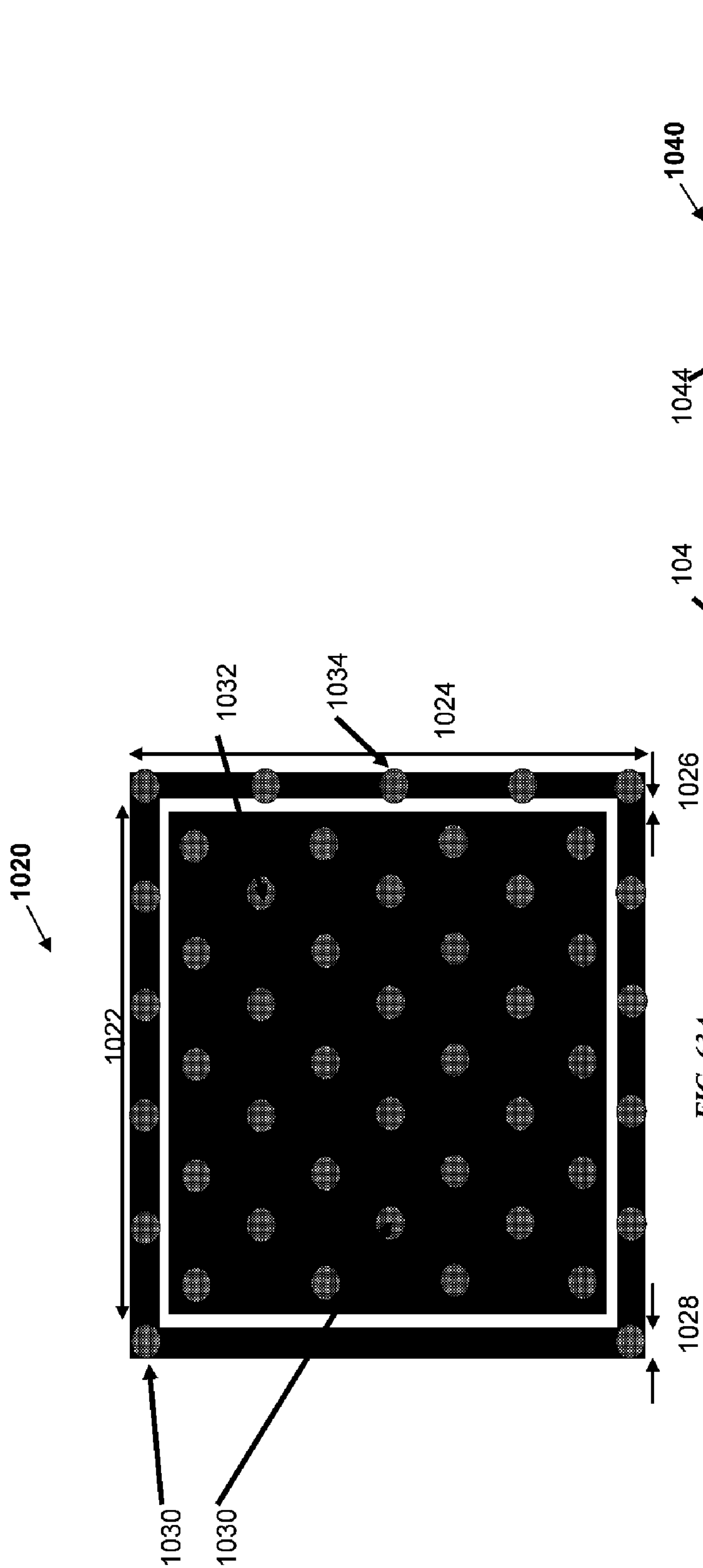

FIG. 63A

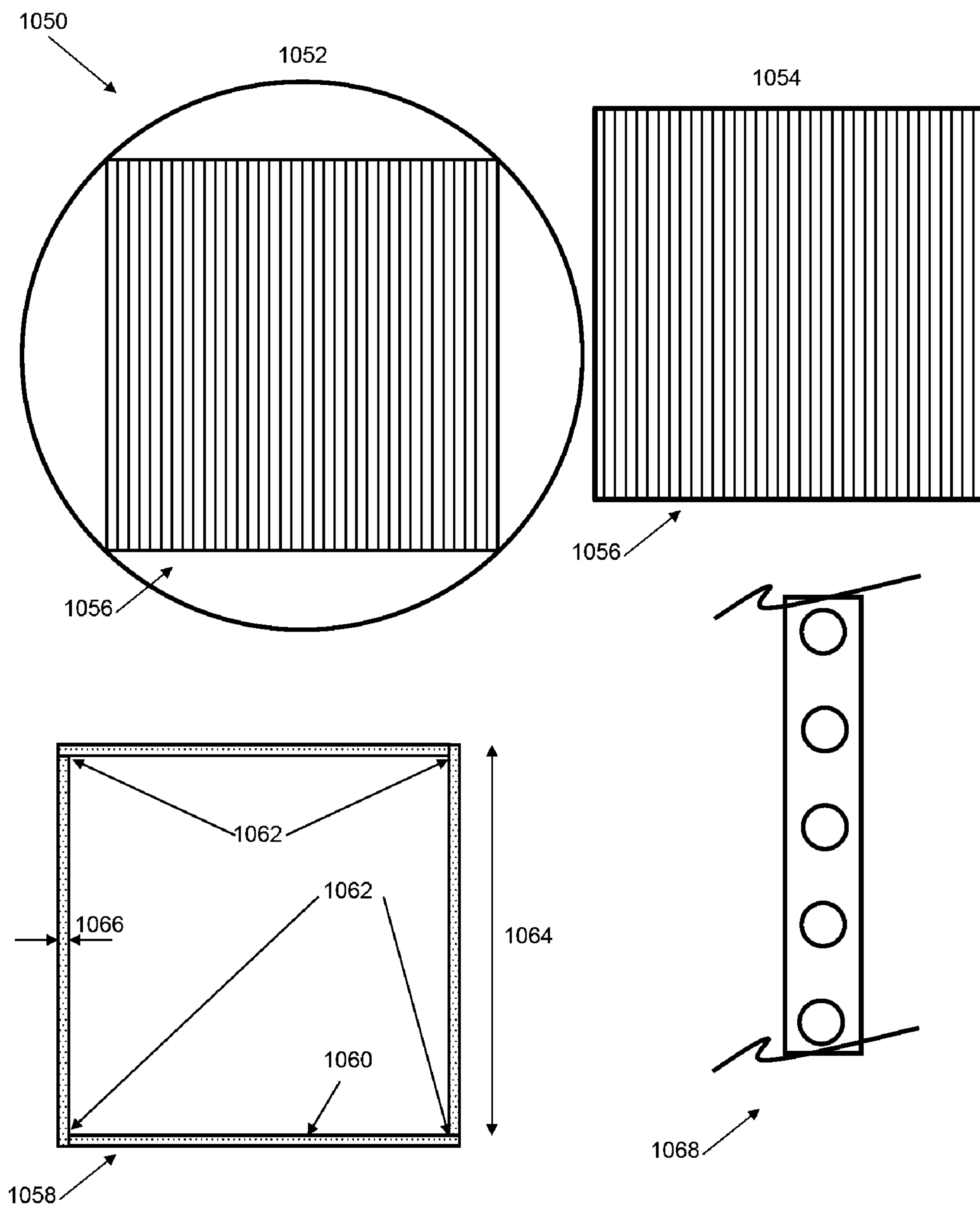

FIG. 64

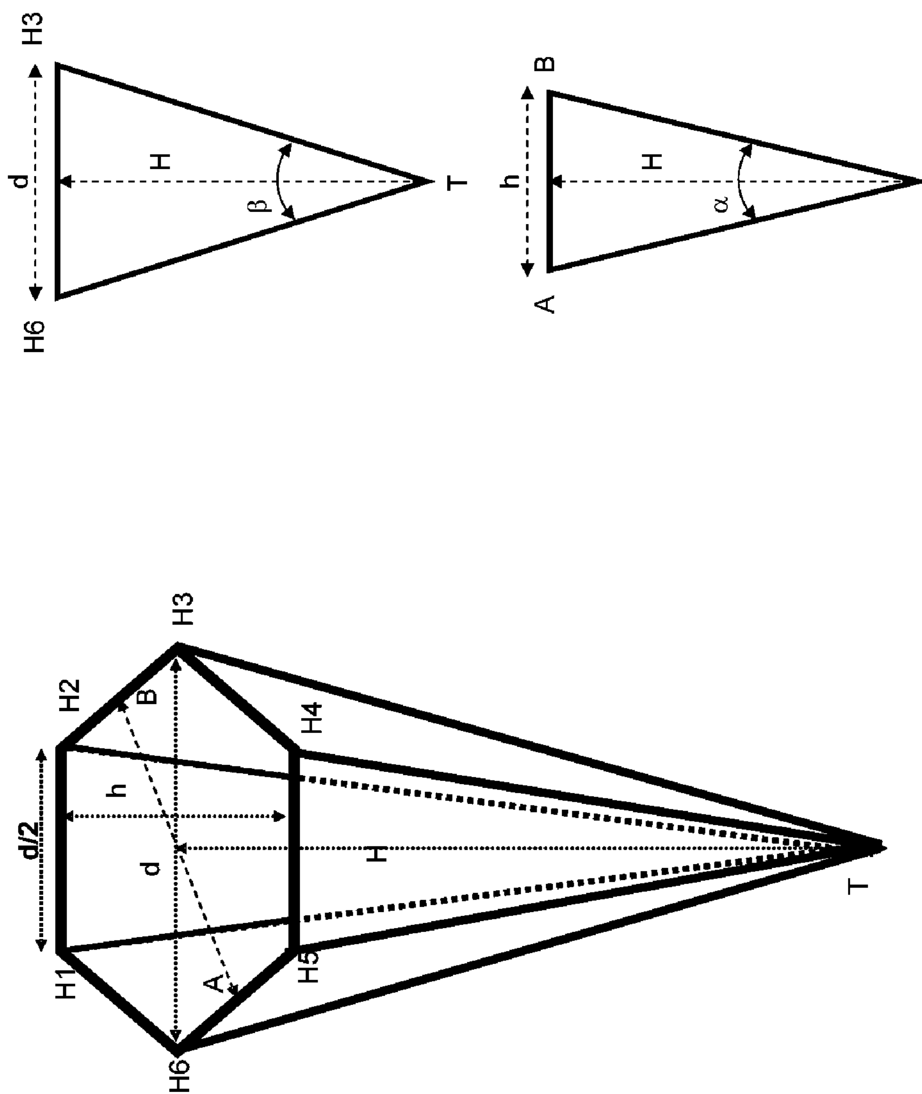

FIG. 65

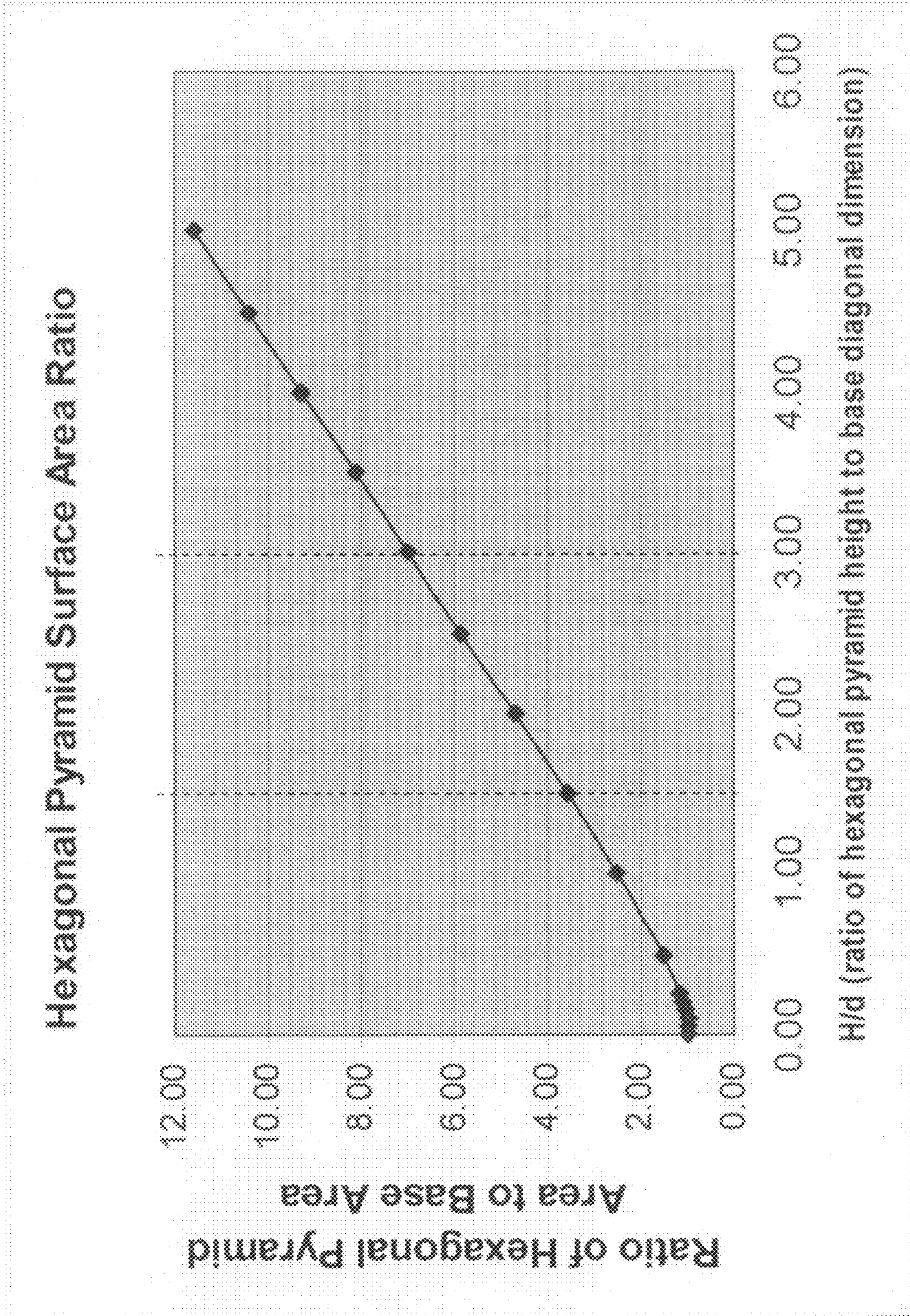

FIG. 66

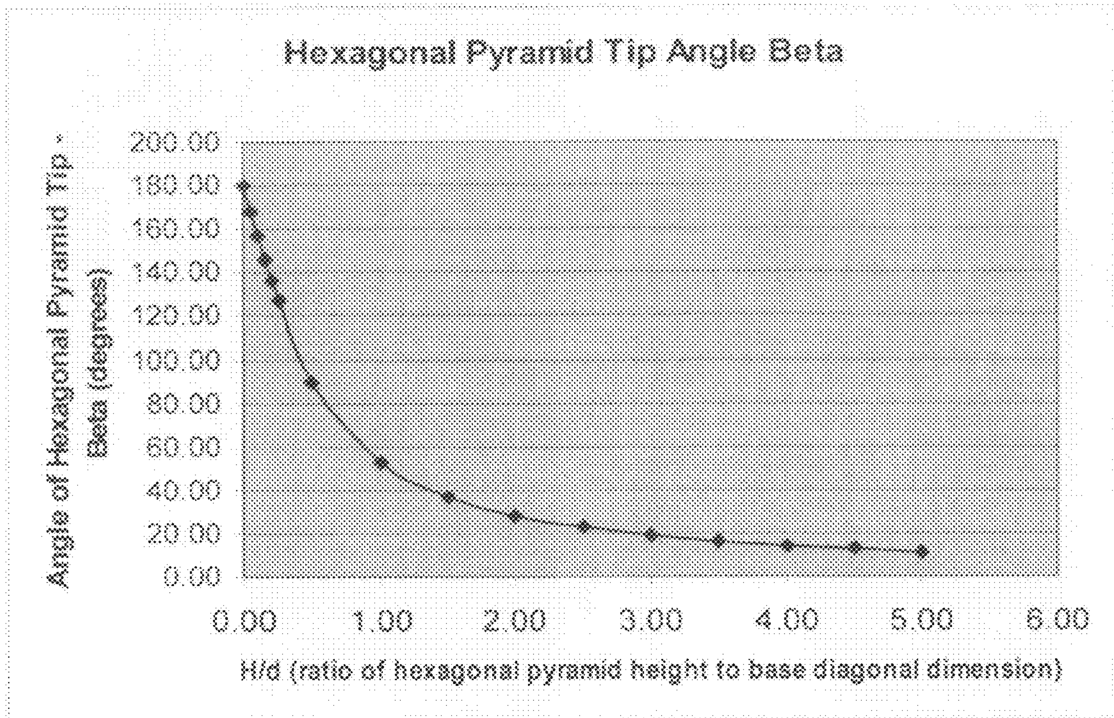

FIG. 67

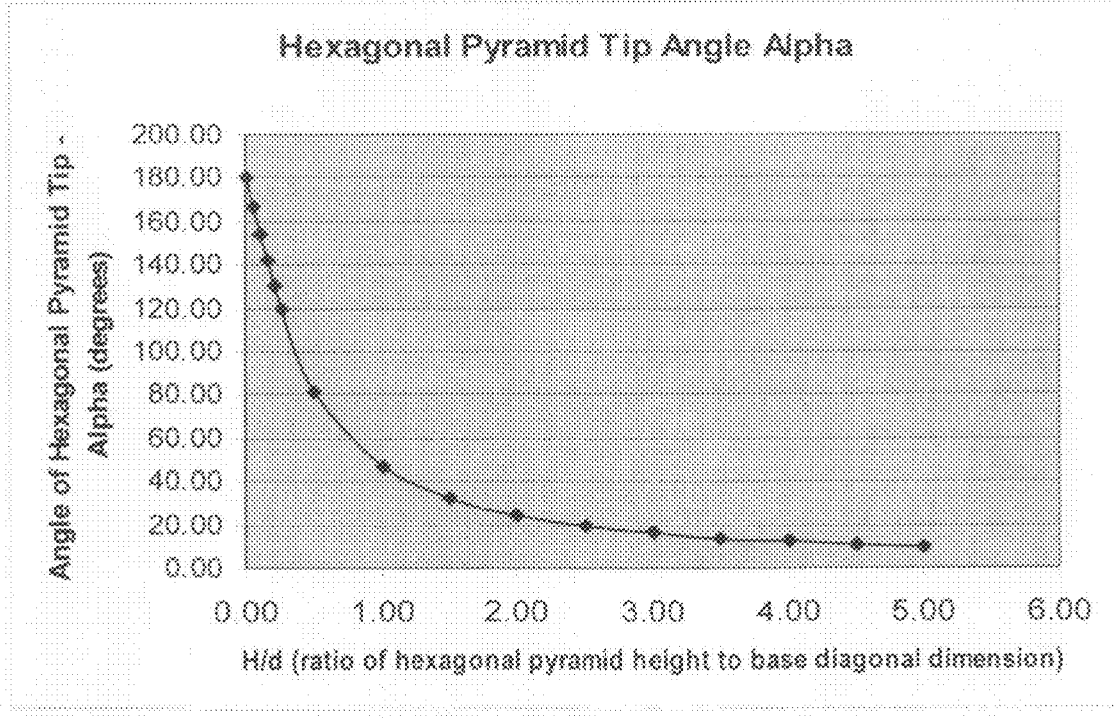

FIG. 68

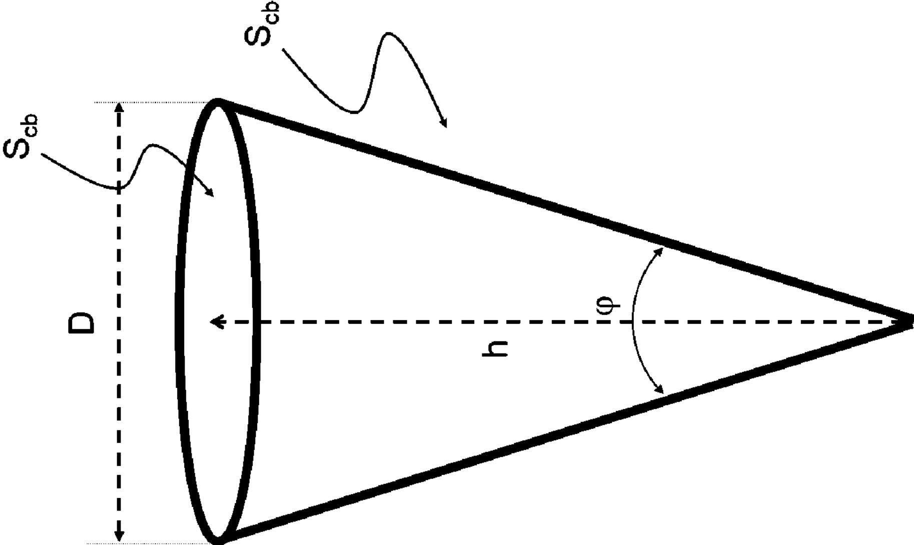

FIG. 69

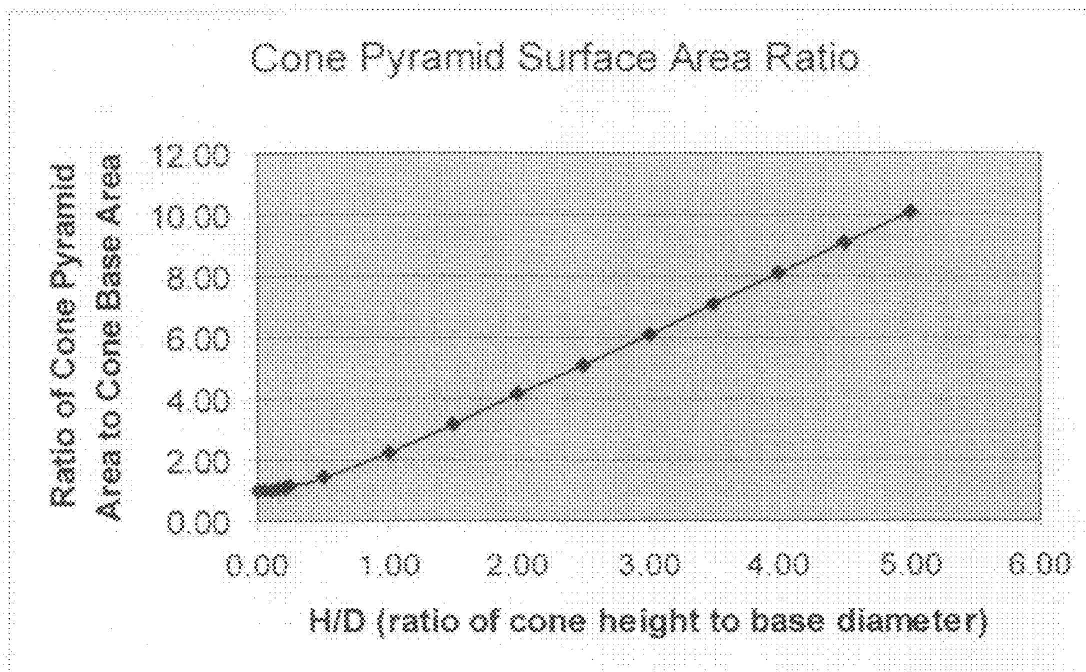

FIG. 70

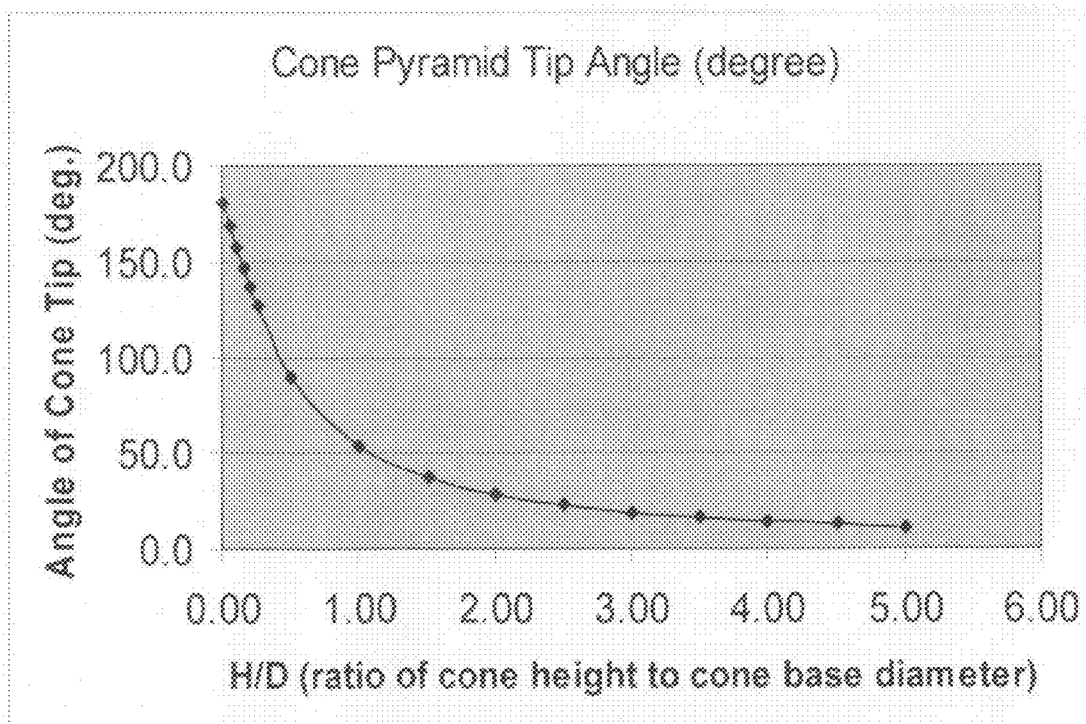

FIG. 71

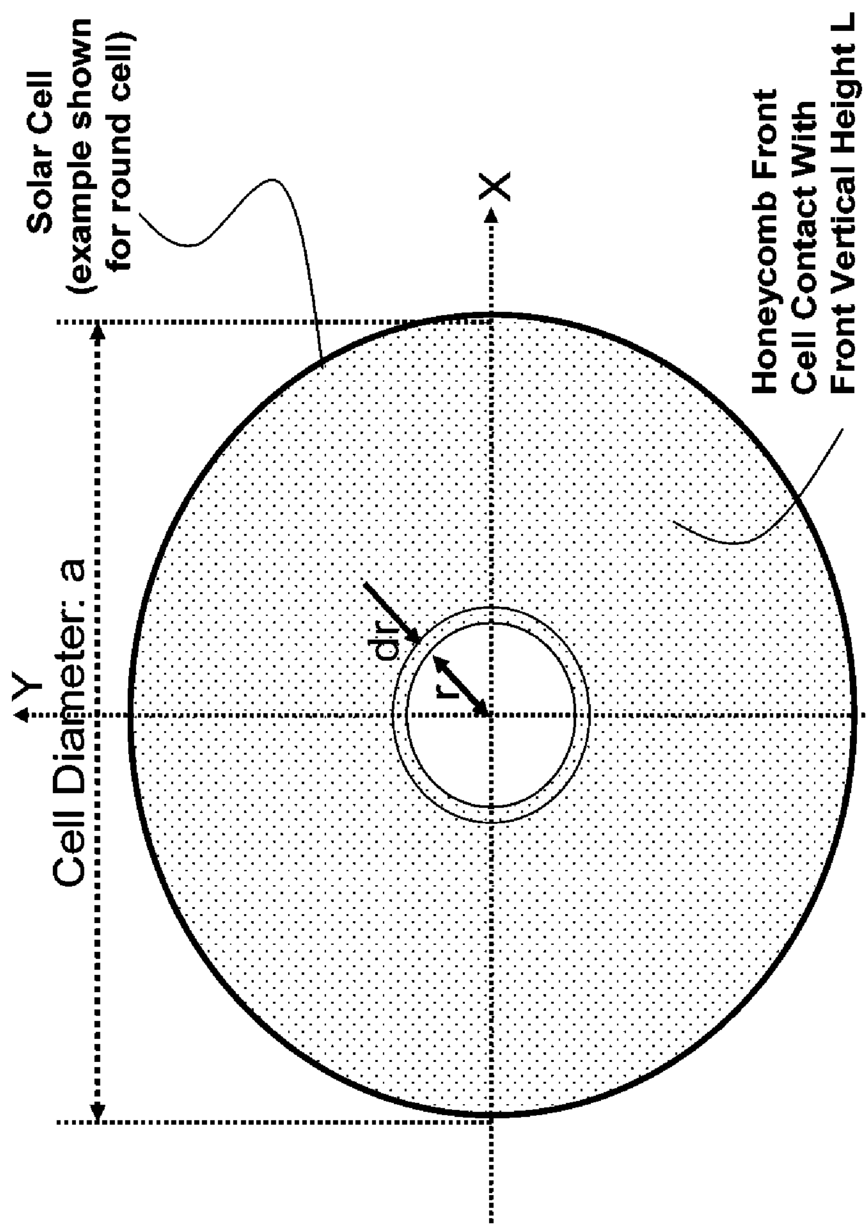

FIG. 72

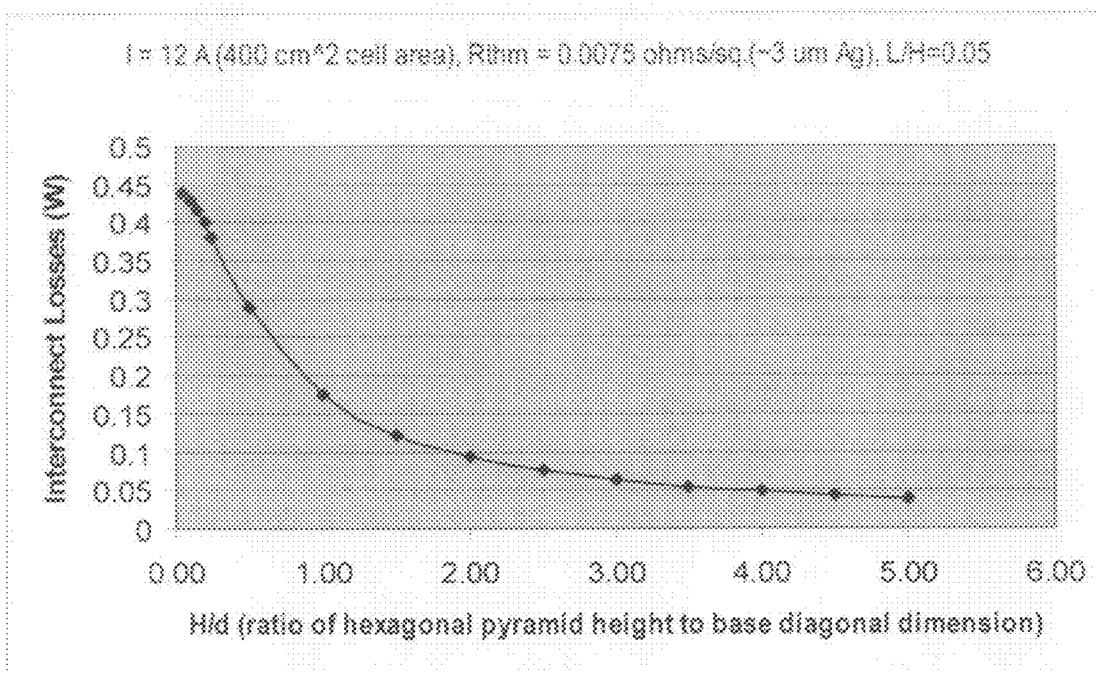

FIG. 73

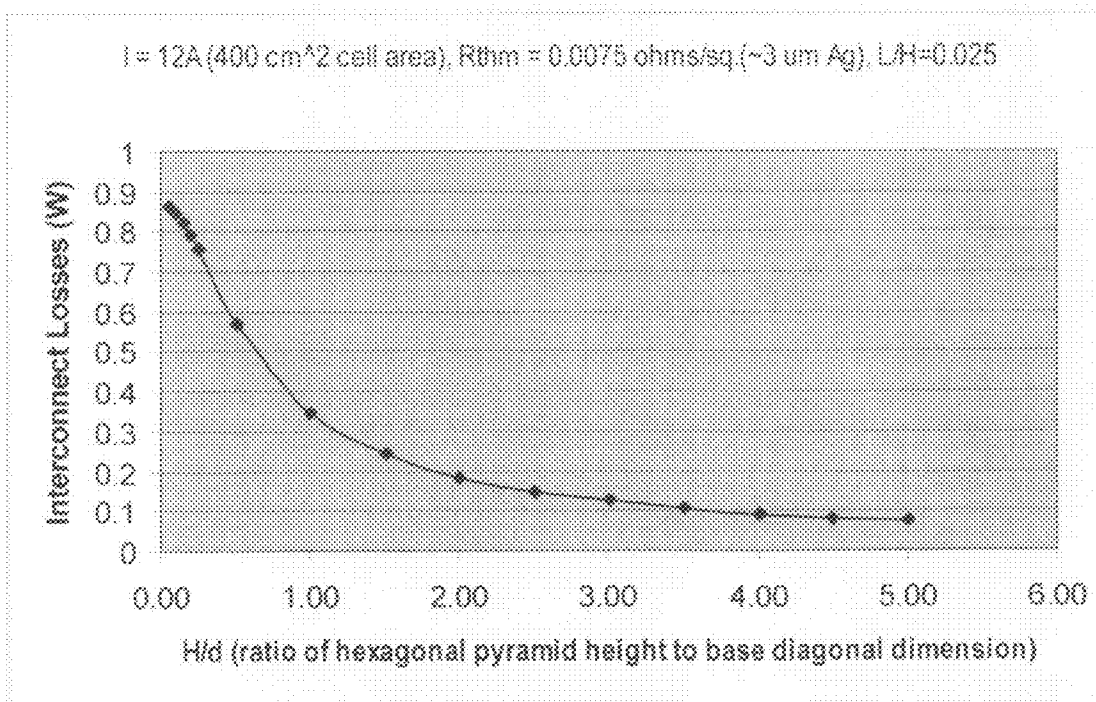

FIG. 74

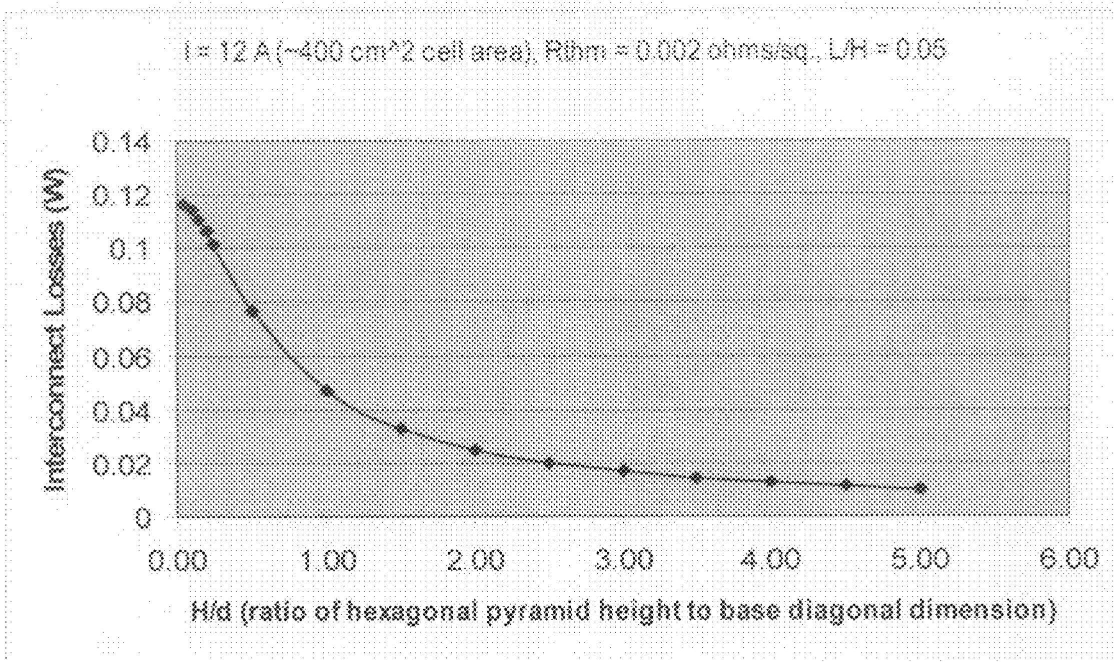

FIG. 75

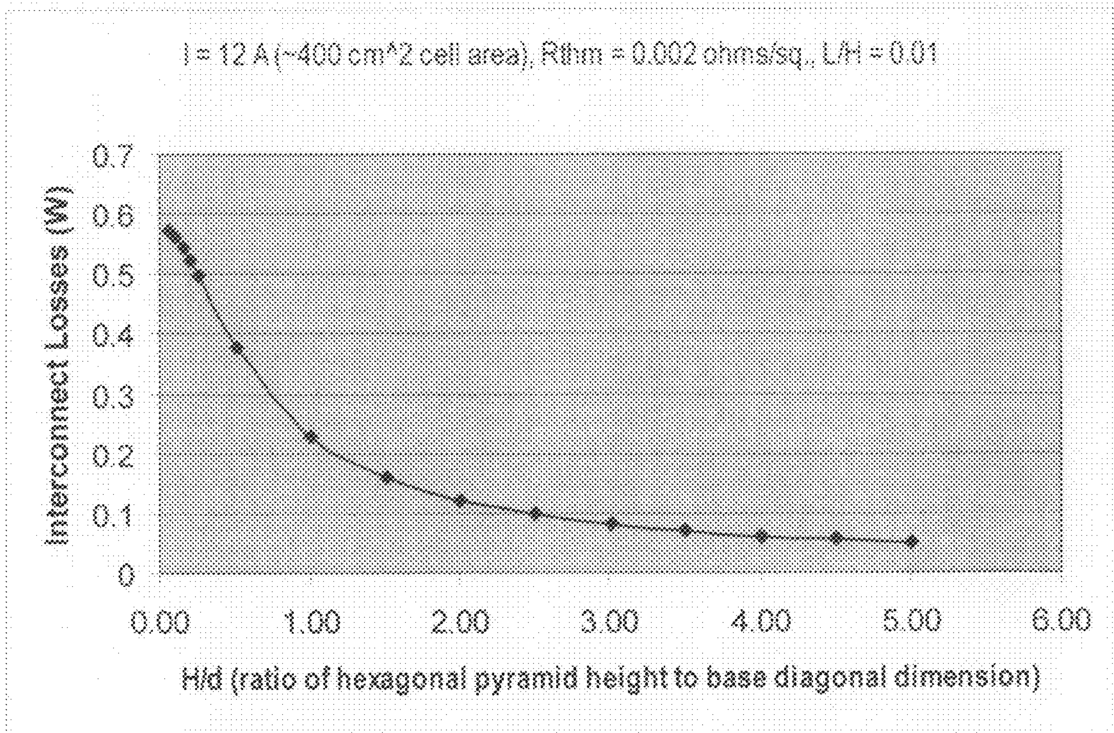

FIG. 76

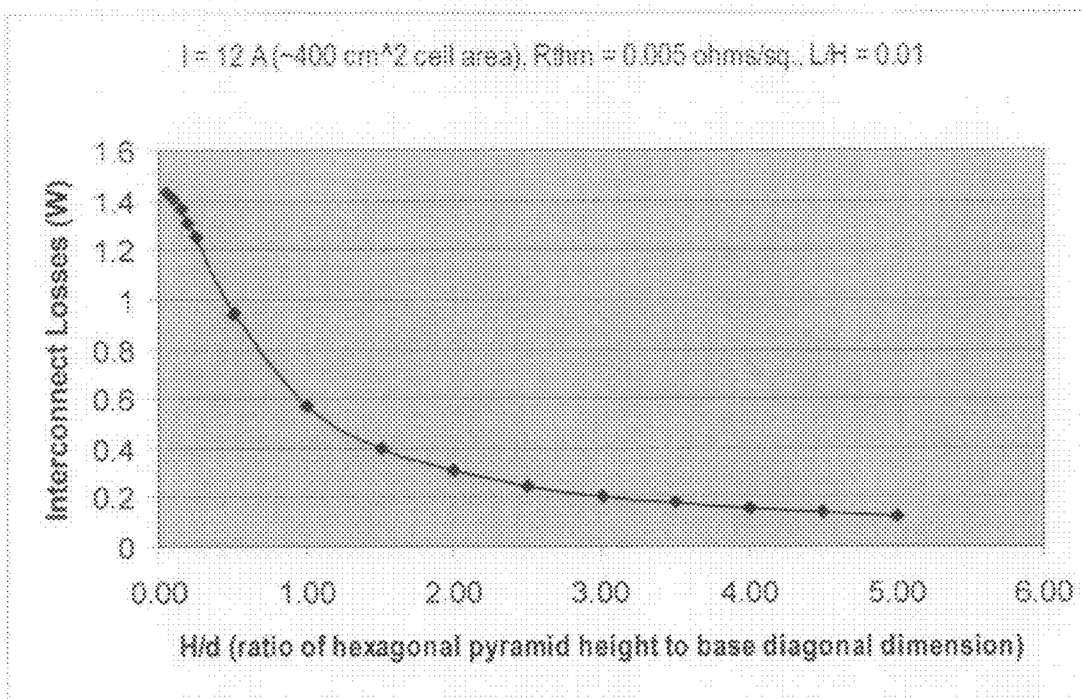

FIG. 77

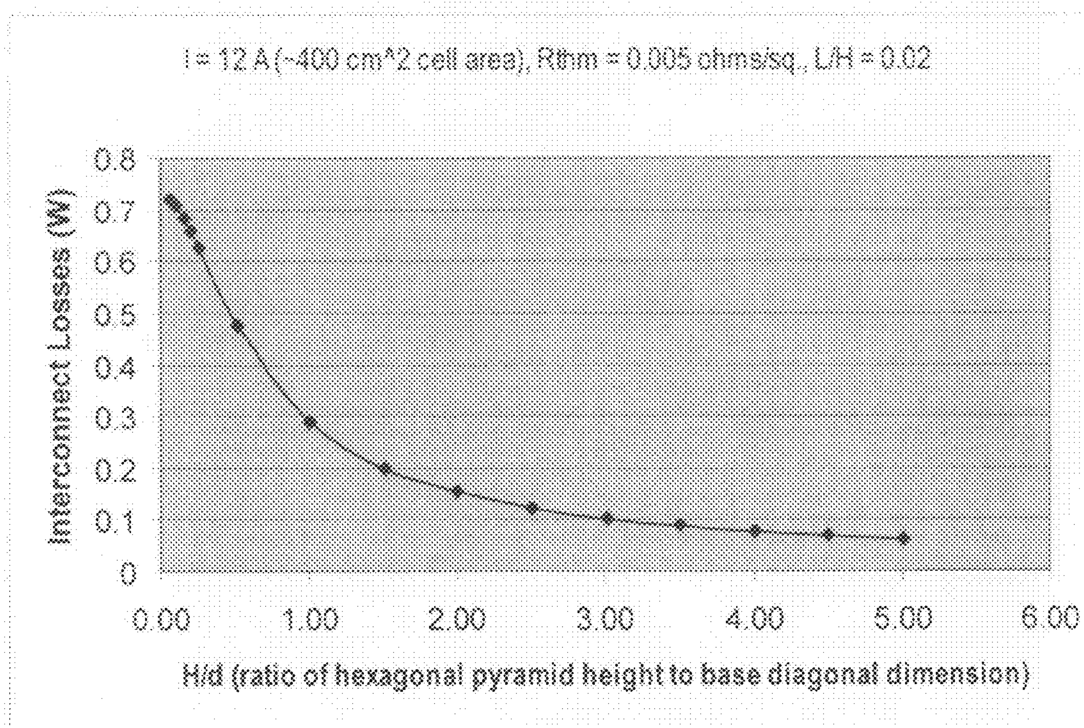

FIG. 78

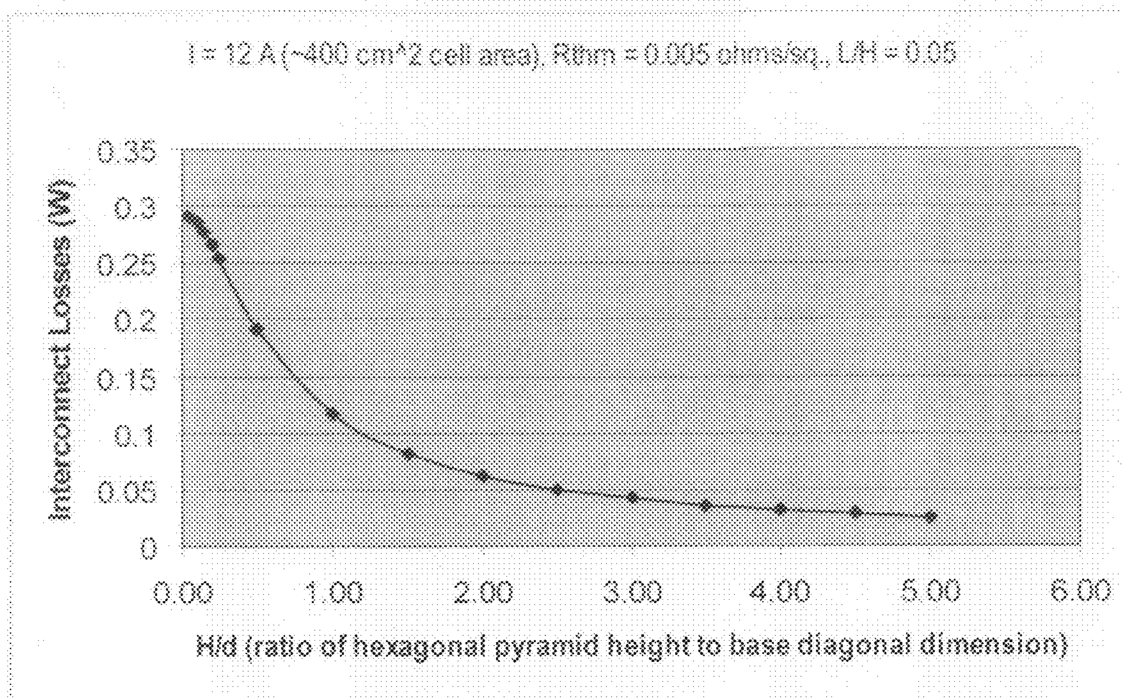

FIG. 79

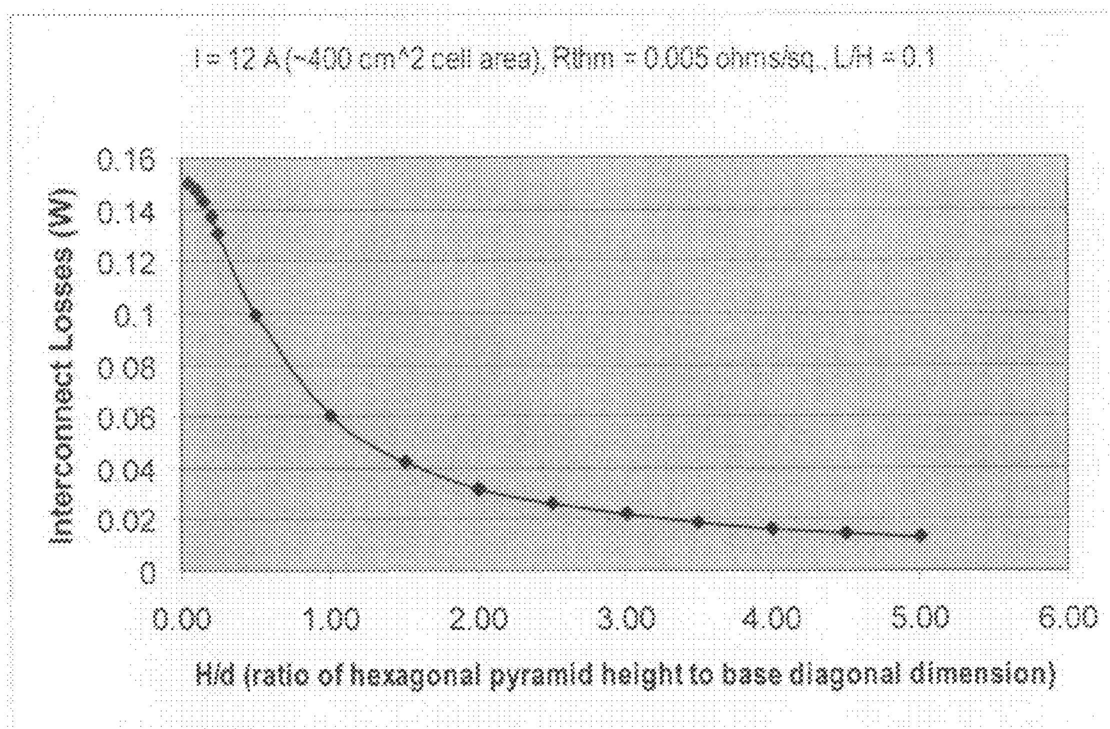

FIG. 80

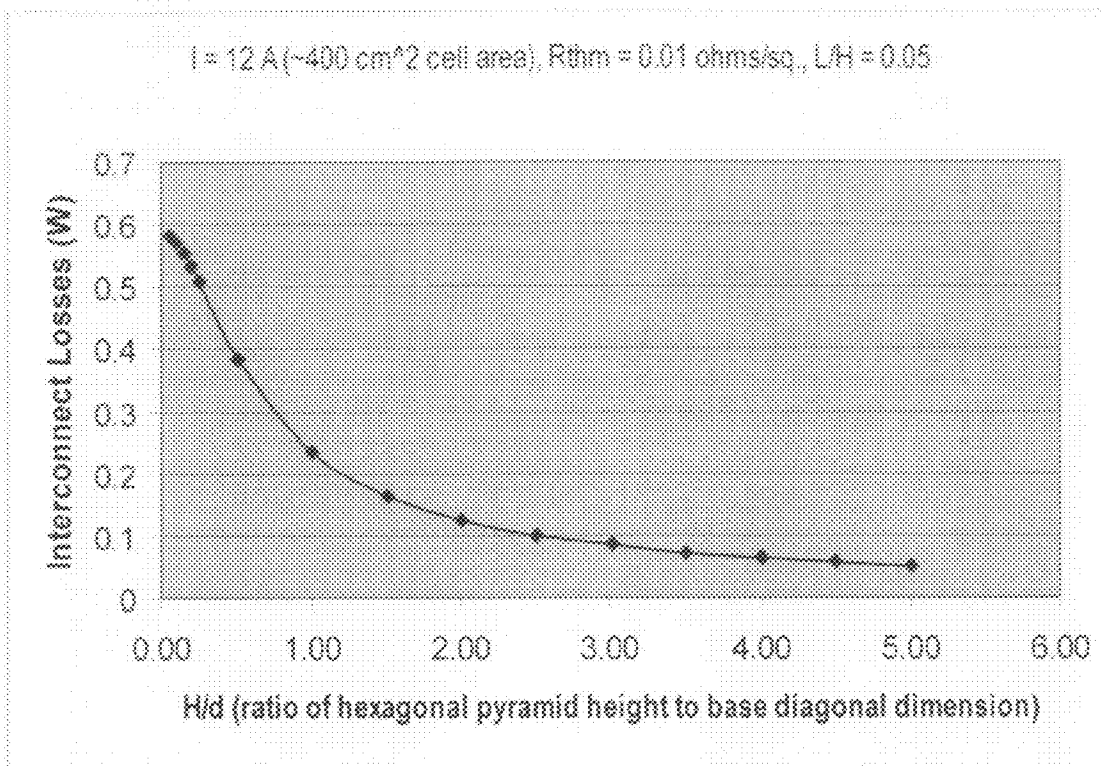

FIG. 81

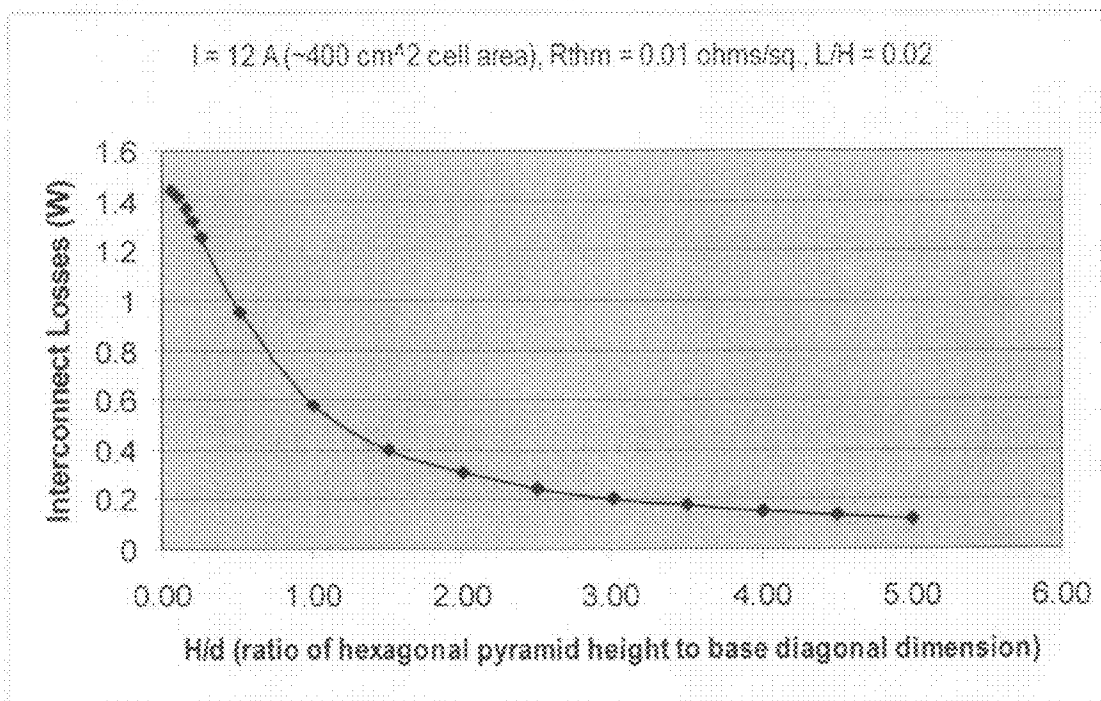

FIG. 82

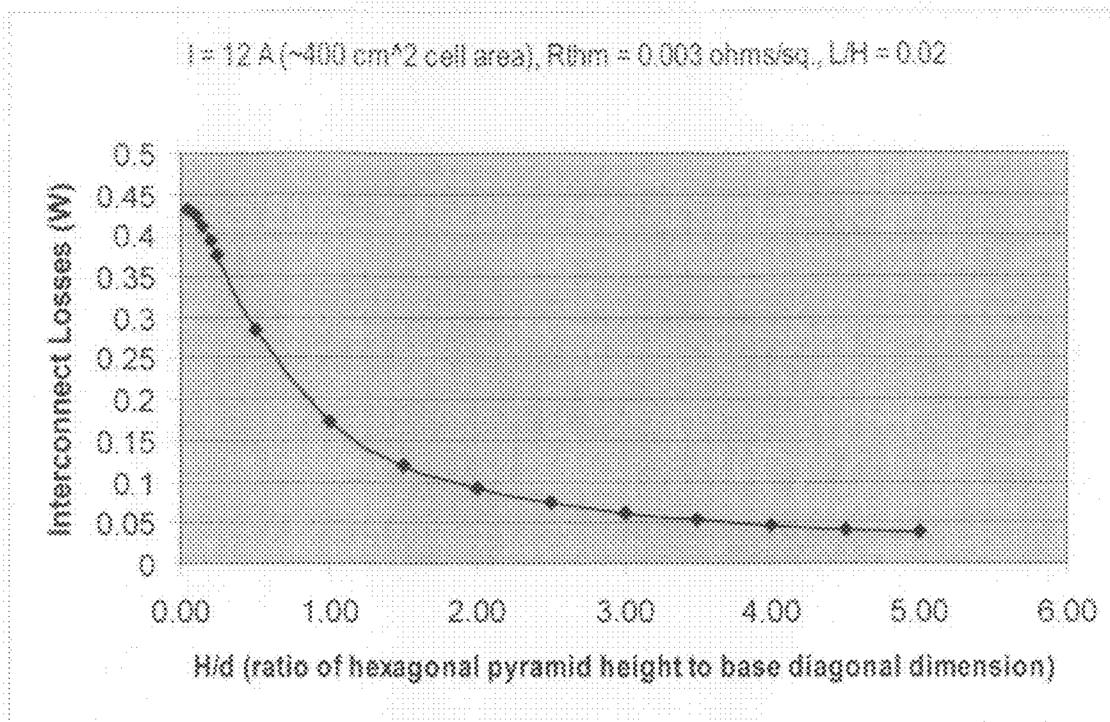

FIG. 83

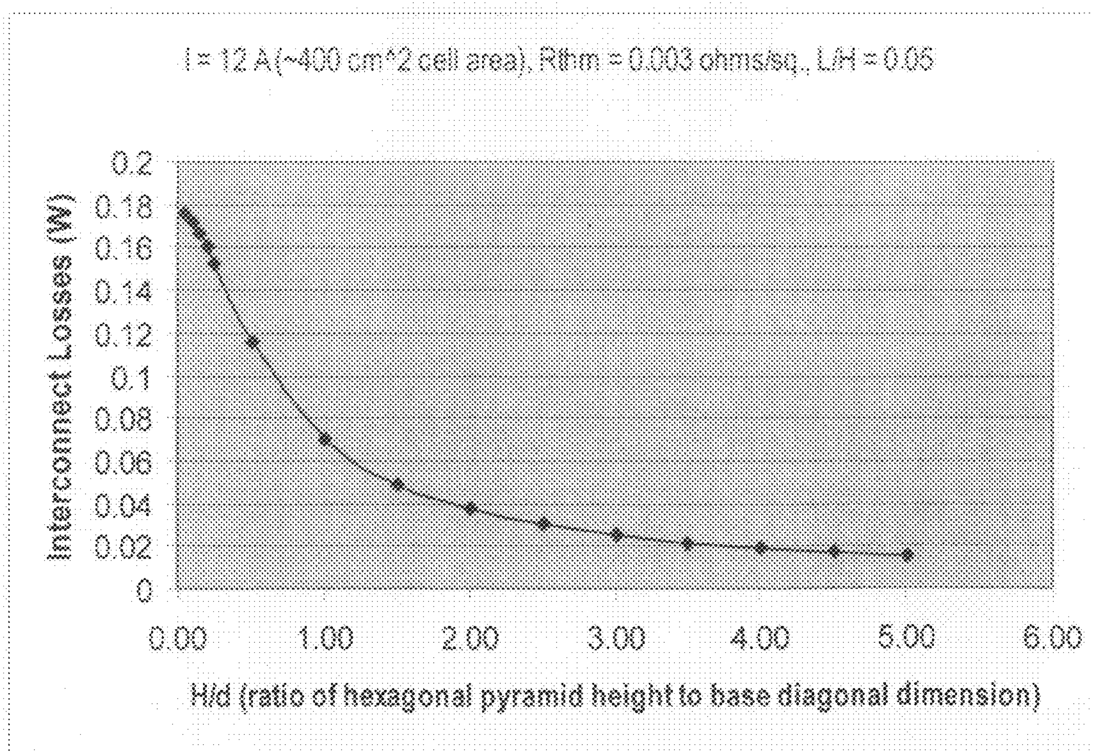

FIG. 84

TEMPLATE FOR PYRAMIDAL THREE-DIMENSIONAL THIN-FILM SOLAR CELL MANUFACTURING AND METHODS OF USE

[0001] This application claims the benefit of provisional patent applications 60/828,678 filed on Oct. 9, 2006 and 60/886,303 filed on Jan. 24, 2007, which are hereby incorporated by reference.

FIELD

[0002] This disclosure relates in general to the field of photovoltaics and solar cells, and more particularly to three-dimensional (3-D) Thin-Film Solar Cells (TFSCs) and methods for manufacturing same. Even more particularly, the presently disclosed subject matter relates to a template for pyramidal 3-D TFSC substrate manufacturing and methods for making and using the template.

DESCRIPTION OF THE RELATED ART

[0003] Renewable, high-efficiency, and cost-effective sources of energy are becoming a growing need on a global scale. Increasingly expensive, unreliable, and environmentally-risky fossil fuels and a rising global demand for energy, including electricity, have created the need for alternate, secure, clean, widely available, cost-effective, environmentally-friendly, and renewable forms of energy. Solar photovoltaic (PV) electricity generation using solar cells is uniquely suited to meet the needs of residential, commercial, industrial, and centralized utility applications. Key attributes that make solar energy attractive are the abundant, worldwide, point-of-use supply of sunlight, environmental friendliness, scalability (from milliwatts to megawatts), secure point-of-use generation of solar electricity, and excellent distributed energy economics. The sun provides more energy to the earth in one hour than the annual energy consumption of the entire world. Much of the earth's surface receives a significant amount of annual sun-hours which may be effectively harnessed for clean and secure electricity generation. A key driver for this market pull is a rising public awareness of environmentally-benign technologies. However, due to relatively low solar cell efficiencies (e.g., less than 12% for most thin-film technologies and roughly 12% to 18% for most crystalline silicon solar cell technologies), high costs of raw materials (e.g., silicon for crystalline silicon wafer solar cells) and manufacturing processes, limitations on cost-effective and efficient electrical storage, and a general lack of infrastructure to support solar cell proliferation, to date there has been limited use of this energy solution (currently, electricity generation by solar photovoltaics accounts for less than 0.1% of total worldwide electricity generation).

[0004] For commercial applications, cost of energy to the end-user (e.g., in cents/kWh for electricity) should be sufficiently low and comparable to or even better than that from utility grids using conventional electricity generation sources. The solar photovoltaic electricity generation, which currently accounts for less than 0.1% of the global electricity generation, may be substantially expanded if it achieves cost parity with conventional grid electricity. As the costs of solar cells and modules (typically expressed as $\$/W_p$) are reduced, grid-tied solar photovoltaic applications are gaining acceptance at an accelerated pace, making them an attractive option for significant proliferation in electricity generation.

[0005] In the price-sensitive solar cell market, two principal technology options exist. On the one hand, crystalline silicon (c-Si) wafers may serve as the basis for solar cell formation (currently accounting for more than 90% of the solar PV market). On the other hand, thin-film (amorphous and polycrystalline) technologies using silicon and other semiconductor absorber materials (such as amorphous silicon, CdTe, or CIGS) may offer significant cost advantages compared to crystalline silicon wafer-based solar cells. These different approaches are at opposite ends of the price-performance scale. Crystalline silicon wafers offer higher performance, but at higher costs (due to the relatively high cost of starting monocrystalline and multicrystalline silicon wafers). Thin-film technologies may offer lower manufacturing costs, but typically at lower performance levels (i.e., lower efficiencies). For both approaches, the price-per-watt typically increases as cell efficiencies rise (due to higher material and/or manufacturing costs).

[0006] Due to a rapid annual growth rate of more than 40% during the past ten years and the concurrent demands for silicon material by both semiconductor microelectronics and solar PV industries, the solar PV industry has been experiencing a shortage of polysilicon feedstock supply. The polysilicon feedstock shortage has significantly constrained the solar PV industry growth, particularly during the past several years. In fact, the solar cell industry currently consumes over half of the worldwide production of high-purity polysilicon feedstock. Within the last few years, the contract price of polysilicon has increased from roughly $30/kg to roughly $85/kg, with spot prices exceeding $250/kg. This has led to large increases in the price of monocrystalline and multicrystalline silicon wafers, which now account for roughly half of the total solar module manufacturing cost.

[0007] The trend in the mainstream crystalline silicon (c-Si) wafer solar cell industry has been to scale down wafer thicknesses to below 200 microns (in order to reduce the amount of silicon material in grams used per watt of solar cell rated peak power). For example, monocrystalline silicon wafer solar cells are projected to scale down to a thickness of roughly 120 microns by 2012, from a current wafer thickness of roughly 200 microns. Multicrystalline silicon wafer solar cells are projected to scale down to a thickness of roughly 180 microns by 2012, from a current average wafer thickness of roughly 260 microns. This wafer thickness reduction, however, presents additional challenges related to mechanical rigidity, manufacturing yield, and solar cell efficiency. Despite its high cost, crystalline silicon (c-Si) technology still dominates the solar cell market, mainly due to higher efficiencies and synergies with the established microelectronics industry and supply chain. Currently, c-Si accounts for slightly over 90% of the solar cell market (95% when ribbon silicon is included).

[0008] Historically, crystalline silicon solar cells have achieved a 20% cost reduction for each doubling of cumulative global cell production (measured in megawatts or MW_p and gigawatts or GW_p). It is projected that through innovative cost reduction and efficiency enhancement methods, the cost of electricity derived from grid-connected rooftop solar photovoltaic modules may become comparable to the cost of electricity purchased from the utility grid in five to ten years. A 2005 survey of the commercially available monocrystalline silicon and multicrystalline silicon solar modules reports the

solar module efficiencies then in the range of 9.1% to 16.1%, with a median efficiency value of about 12.5%. Commercial crystalline silicon modules usually show a rapid initial efficiency degradation of 1% to 3% (relative) due to various effects, including photodegradation effects in wafered solar cells (e.g., wafer minority carrier lifetime degradation). Monocrystalline silicon wafer solar cell efficiencies are projected to increase to roughly 20.5% by 2012, from a current efficiency of roughly 16.5% (leading-edge commercially available monocrystalline silicon solar cell and solar module efficiencies are currently about 21.5% and 18%, respectively). Multicrystalline silicon wafer solar cell efficiencies are projected to increase to roughly 18% by 2012, from a current efficiency level of roughly 15.5%.

[0009] State-of-the-art crystalline silicon solar cell manufacturing currently uses about 10 grams of high-purity polysilicon feedstock per peak watt (g/W_p), resulting in a polysilicon feedstock material cost of about $\$0.85/W_p$ (assuming a polysilicon price of $85/kg). Over the next five years, the projected trends of solar cell wafer thickness reduction (e.g., to less than 200 micron wafers) and a long-term assumed price of about $20/kg for solar-grade polysilicon may reduce the polysilicon feedstock cost (in g/W_p) by about a factor of four to eight to about $\$0.10/W_p$ to $\$0.20/W_p$. Thus, any competing solar cell technologies should benchmark their manufacturing cost goals against this reduced raw material cost number. For a given cell efficiency, silicon wafer thickness reduction presents a prime opportunity for solar cell cost reduction by reducing the amount of polysilicon feedstock consumed per watt of peak solar power.

[0010] The cost associated with wire saws, amounting to about $\$0.25/W_p$ for current silicon solar cells provides another wafer-related cost component for silicon wafer solar cells. Innovative and cost-effective technologies that eliminate the kerf losses associated with sawing and slicing should further facilitate silicon solar cell cost reductions. It is projected that the wafer-based crystalline silicon solar module manufacturing cost (which is currently on the order of $2.10 per watt to more than $2.70 per watt) may be reduced to the range of roughly $\$1.50/W_p$ to $\$1.80/W_p$ by the year 2012, in part due to wafer sawing kerf loss reduction to roughly 130 microns by 2012 from the current value of roughly 200 microns. The overall cost reductions for wafer-based crystalline silicon solar cells may come from various sources including: lower cost polysilicon feedstock, thinner wafers, higher cell-level efficiencies, reduced wafer sawing kerf losses, and increased economy of scale or manufacturing volume.

[0011] State-of-the-art silicon wafer solar cell fabrication facilities ("solar fabs") typically produce 125 mm×125 mm up to 156 mm×156 mm solar cells today. The trend in crystalline silicon wafer solar cells is toward thinner and larger wafers. The monocrystalline and cast (as well as ribbon) multicrystalline silicon solar cell wafer thicknesses in leading-edge solar cells used for power generation modules are projected to be reduced to around 150 and 200 microns, respectively, by around 2009-2010. Any cost-effective, high-efficiency, innovative silicon solar cell technology which enables a substantial reduction of the silicon material consumption (e.g., wafer or film thickness) per W_p of cell power compared to the above-mentioned current and projected 2009-2010 numbers may offer significant promise as a viable commercial solar cell technology for solar photovoltaic applications (e.g., residential, commercial, and industrial rooftop as well as large-scale centralized utilities electrical power generation applications).

[0012] Higher solar cell efficiencies have favorable effects on the entire solar cell value chain and levelized cost of energy (LCOE in $/kWh) due to reduced material consumption and cost as well as reduced balance-of-system (BOS) costs (e.g., area-related solar module installation and inverter costs). The current mainstream commercial crystalline solar cells provide efficiencies on the order of 14% to 17%. It is expected that the projected crystalline silicon solar cell efficiencies in commercial solar cells may approach around 19% and 17% for monocrystalline and multicrystalline silicon solar cells, respectively, by the year 2009. A key area for new solar cell business opportunities is development of innovative cell structures and simplified process flows which may drive efficiencies up while lowering overall solar cell and module manufacturing costs. For alternative (e.g., thin-film PV) approaches to succeed over the mainstream wafer-based crystalline silicon solar cell technologies, they should provide higher efficiencies at even lower manufacturing costs compared to the projected efficiency and cost numbers for the mainstream wafer-based crystalline silicon solar cells when the new technology is fully commercialized.

[0013] Economy-of-scale fab cost reduction associated with high-volume solar fab capacities is a key factor impacting LCOE. The state-of-the-art high-volume solar photovoltaic fabs have annual production capacities on the order of or in excess of 50 MW_p to 100 MW_p (MW_p=1 million W_p). High-volume solar photovoltaic fab capacities are expected to increase substantially to annual production rates of several hundred MW_p or even approaching 1 GW_p (GW_p=1 billion W_p) in the coming decade. While very-high-volume solar fabs in the range of 100 MW_p to 1 GW_p should facilitate longer term cost reductions (including LCOE) through high-volume manufacturing economies of scale, the relatively high initial fab investment costs, which may easily exceed $100M, may impose certain limits on solar photovoltaic fab construction options. Ideally, the preference may be to develop innovative crystalline silicon solar cell designs and simplified manufacturing processes which facilitate substantial manufacturing cost reductions in solar cells and modules even in smaller-scale (and less capital intensive) fabs with modest production volumes (e.g., annual production volumes in the range of 5 MW_p to 50 MW_p). This type of technology would allow for modest-volume solar photovoltaic fabs with modest fab setup and operation costs. Reduced fab setup and operation costs would further facilitate global proliferation of cost-effective solar modules, enabling construction of a multitude of very affordable modest-volume fabs (in contrast to having to set up very expensive high-volume fabs in order to achieve sufficient economy of scale for manufacturing cost reduction). Of course, an innovative solar cell technology that meets the above-mentioned criteria for cost-effective, modest-volume fabs (i.e., meeting the LCOE roadmap requirements even at modest production volumes in low-cost fabs set up for simplified solar cell processing), may also be applicable to very-high-volume (e.g., greater than 100 MW_p) solar fabs. Such solar photovoltaic fabs can take further advantage of the economies of scale associated with increased volume.

[0014] Thin-film solar cell (TFSC) technologies (e.g., amorphous silicon, CdTe, and CIGS) require little absorber material (usually much less than 10 microns in thickness) to absorb typical standard "Air Mass 1.5" (AM-1.5) solar illumination due to absorption bands that are well matched to the

solar spectrum. The TFSC absorber material may be deposited on inexpensive substrates such as glass or flexible metallic or non-metallic substrates. TFSCs typically offer low cost, reduced module weight, reduced materials consumption, and a capability for using flexible substrates, but are usually much lower in efficiency (e.g., usually 5% to 12%). In the case of prior art thin crystalline silicon films, there are a number of major problems and challenges with the use of flat silicon films (such as epitaxially growth silicon films with thicknesses below 50 microns) for low-cost, high-performance solar cells. These include: relatively low solar module efficiencies (typically 7% to 12%), field degradation of module efficiencies, scarce and expensive absorber materials (e.g., In and Se for CIGS and Te for CdTe), limited validation of system field reliability, and adverse environmental impact of non-silicon technologies such as CIS/CIGS and CdTe.

[0015] Prior art FIG. **1** shows process flow **10** for fabricating c-Si TFSCs using planar silicon thin-film absorber layers produced by epitaxial silicon. This prior art TFSC fabrication process flow uses several shadow mask process steps to form the cell structure. The cell absorber is simply a thin planar film of c-Si formed by silicon epitaxial growth processing. The cell uses frontside silicon texturing to improve light trapping and a detached rear aluminum mirror to improve the cell efficiency. Step **12** starts with single-crystal p^+ CZ silicon. Step **14** involves electrochemical HF etching of silicon to form 2-layer porous silicon comprising a 1 micron top layer with 20% porosity and a 200 nanometer rear layer with greater than 50% porosity. Step **16** involves a hydrogen (H_2) anneal at 1100° C. for 30 minutes. Step **18** involves epitaxial silicon growth at 1100° C. using trichlorosilane or $SiHCl_3$ (deposition rate of 1 micron per minute), forming 2 microns of p^{+-}Si and 30 microns of p-Si. Step **20** involves frontside surface texturing by wet KOH etching to form upright surface pyramids. Step **22** involves the first shadow mask process, with LPCVD silicon nitride (SiN_x) deposition through a shadow mask to define emitter diffusion windows. Step **24** involves solid source phosphorus diffusion at 830° C. (to achieve **80** Ω/square for the n^+ doped junction). Step **26** involves the second shadow mask process, with frontside metallization (titanium/Pd/silver grid) by evaporation through shadow mask. Step **28** involves emitter surface passivation by hydrogenated PVD or PECVD SiN_x. Step **30** involves contact frontside busbar by a conductive adhesive. Step **32** involves gluing the cell frontside to MgF_2-coated glass using clear glue. Step **34** involves separating the cell from silicon wafer by mechanical stress. Step **36** involves the third shadow mask process, with backside aluminum metallization using evaporation through shadow mask. Finally, step **38** involves attaching an aluminum reflector at 200 micron spacing from the cell backside.

[0016] Prior art FIG. **2** shows another process flow method **40** for fabrication of solar cells on silicon wafers with self-aligned selective emitter and metallization. This prior art process uses laser processing to pattern the top cell dielectric layer while melting the underlying silicon to form the heavily-doped n^{++} emitter contact diffusion regions (after formation of the lightly diffused selective emitter regions by rapid thermal annealing). Step **42** starts with single-crystal p-type silicon. Step **44** involves saw damage removal etch and anisotropic texturing etch in dilute NaOH at 90° C. Step **46** involves spin-on application and drying of phosphorus diffusion source. Step **48** involves rapid thermal annealing to form lightly diffused emitter (80 to 200 Ω/square). Step **50** involves application of backside metal contact by vacuum evaporation or screen printing of aluminum or silver/aluminum alloy, followed by drying. Step **52** involves backside metal sintering/firing (e.g., at 820° C. in oxygen/nitrogen) for a screen-printed contact (fires the metal paste while oxidizing the dielectric to raise its resistance to the metal plating solution). Step **54** involves laser processing to pattern the top dielectric layer while melting the underlying silicon to form the n^{++} contact diffusion region. Step **56** involves dilute HF etch to prepare metal plating surface. Step **58** involves electroless nickel plating at 90° C. for five minutes. Step **60** involves nickel sintering at 350° C. to 450° C. (in nitrogen, argon, or forming gas). Step **62** involves an additional 2 minutes of nickel plating followed by long electroless copper plating to form thick high-conductivity copper film. Step **64** involves flash immersion silver (silver) deposition on copper surface. Finally, step **66** involves edged junction isolation (e.g., using laser grooving, edge cleavage, or plasma etching).

[0017] With regard to the prior art crystalline silicon (c-Si) thin-film solar cell (TFSC) technology, there are difficulties associated with sufficient surface texturing of the thin silicon film to reduce surface reflectance losses, while reducing the crystalline silicon film thickness. This places a limit on the minimum flat (co-planar) monocrystalline silicon thickness due to production yield and cell performance (efficiency) considerations. In the case of a flat or co-planar film, it is essential to use surface texturing since the reflectance of an untextured crystalline silicon film is quite excessive (can be greater than 30%) and results in substantial optical reflection losses and degradation of the external quantum efficiency. Thus, reduction of reflectance-induced photon losses in co-planar epitaxial silicon films requires effective surface texturing which itself places a limit on the minimum epitaxial silicon layer thickness. Depending on the film surface texturing requirements and processes, the minimum crystalline silicon layer thickness may be on the order of at least 10 microns (so that the texturing process does not break through any portions of the crystalline silicon layer).

[0018] In addition, substantially reduced mean optical path lengths in thin planar crystalline silicon films result in reduced photon absorption, particularly for photons with energies near the infrared bandgap of silicon (800 to 1100 nanometers), resulting in reduced solar cell quantum efficiency (reduced short-circuit current or J_{sc}). This results in serious degradation of the solar cell efficiency due to reduced cell quantum efficiency and reduced J_{sc}. For instance, in a co-planar (flat) crystalline silicon absorber layer with thickness of 20 microns, a solar light beam impacting the cell at a near-normal angle would have an effective path length equal to the film thickness, far too short for the solar radiation photons with energies near the infrared bandgap of silicon (i.e., with wavelengths of roughly 800 to 1100 nanometers) to be absorbed effectively in the silicon thin film. In fact, a reduction of the active cell silicon thickness to below roughly 50 microns results in appreciable reduction of J_{sc} and the resulting solar cell efficiency, with this degradation effect rapidly accelerating when the silicon film thickness is reduced below roughly 20 microns. Thus, a co-planar thin crystalline silicon film may also require effective light trapping using both top surface texturing and rear surface back reflection of the light exiting the back surface of the crystalline silicon film in order to create effective optical path lengths equal to a large multiple of the crystalline silicon film thickness.

[0019] The prior art technologies using this approach mostly use either back reflection through internal reflection of the light at the crystalline silicon film/silicon substrate, or reflection from a blanket backside contact (such as a back surface field aluminum contact/mirror). The back reflectance provided by these techniques may not be great (e.g., roughly 70% effective near-IR rear reflectance), constraining the performance gain that would have otherwise been achieved by an optimal back reflector. The problem with this approach is that the primary incident beam always passes the crystalline silicon film only once. Any subsequent second passes of the primary incident beam photons are dependent on the back surface reflection.

[0020] There is also the problem of lack of rigidity and mechanical support of the thin film during cell and module processing steps. This problem relates to the mechanical strength of a large-area (e.g., 200 mm×200 mm) thin silicon film. It is well known that reducing the large-area crystalline silicon wafer thickness to below 100 microns results in a substantial loss of cell substrate mechanical strength/rigidity, and such thin wafers tend to be flexible and very difficult to handle without breakage during cell fabrication process flow.

[0021] Large-area, co-planar (flat) crystalline silicon films thinner than, for instance, 50 microns must be properly mounted and supported on a cost-effective support or handle substrate in order to achieve acceptable yield for solar cell and module manufacturing. One approach is to grow and retain the thin epitaxial film on a relatively low-cost (e.g., metallurgical-grade) silicon substrate (over which the epitaxial layer is grown); however, this approach suffers from some inherent problems constraining the ultimate solar cell efficiency. Another approach is to release or lift off the epitaxial silicon film from its (reusable) parent silicon substrate and subsequently place it on a cheaper non-silicon support or handle substrate to provide mechanical strength through the solar cell process flow. This approach may suffer from any thermal coefficient of expansion (TCE) mismatch between the support/handle substrate and silicon film during any high-temperature oxidation and anneal processes, as well as potential contamination of the thin epitaxial silicon film from the non-silicon support substrate (both creating possible manufacturing yield and performance/efficiency degradation problems).

[0022] The cost of the monocrystalline silicon film growth process using silicon epitaxy, particularly for thicker epitaxial films with thicknesses in excess of 30 microns is an additional issue which should be addressed. Using a relatively small epitaxial film thickness (in one embodiment, much below 30 microns) may lower the cost of epitaxy to an attractive range. However, this would present various challenges for fabrication of planar silicon thin-film solar cells. As stated, thinner co-planar (flat) epitaxial films (e.g., in the range of much less than 30 microns) produce a number of problems and challenges, including a lack of film mechanical strength, constraints limiting effective surface texturing of thin silicon films for low surface reflectance and reduced optical reflectance losses, relatively short optical path lengths, and reduced cell quantum efficiencies. Effective light trapping is essential for enhanced thin-film c-Si solar cell efficiencies. The requirement for effective light trapping is based on a combination of front surface texturing and back surface mirror, while achieving sufficiently low surface recombination velocities (for high cell efficiencies). This is very difficult to achieve in the co-planar (flat) c-Si thin film solar cells.

[0023] High-performance c-Si thin-film solar cells require some patterning steps or patterned processing steps (e.g., for formation of selective emitter, frontside emitter or backside emitter wrap-through metallization contacts, backside base metallization contacts, etc.). These patterning steps are usually achieved using photolithography, screen printing, and/or shadow-mask deposition (e.g., shadow-mask sputtering or evaporation) processes. The use of photolithography and/or screen printing and/or shadow-mask deposition patterning steps usually increases the manufacturing process flow complexity and cost, and may also detrimentally impact the fabrication yield as well as the ultimate achievable solar cell efficiency.

[0024] Therefore a need has arisen for a thin-film solar cell (TFSC) which corrects the problems identified above.

[0025] Yet a further need exists to address shortcomings of existing mainstream c-Si solar cell technology. This includes reducing the amount of polysilicon feedstock consumed per peak watt of solar power, and eliminating the kerf losses associated with sawing and slicing; thus, substantially reducing the overall solar cell manufacturing cost.

[0026] A further need exists for innovative solar cell structures and simplified process flows, increasing cell and module efficiencies while significantly lowering the overall solar cell and module manufacturing costs. A still further need exists for innovative c-Si solar cell designs and simplified self-aligned manufacturing processes which facilitate substantial solar cell and module cost reduction even in fabs with modest production volumes, enabling low to mid-volume solar cell fabs with modest fab setup and operation costs (thus, achieving economies of scale for manufacturing cost reduction at substantially lower fab volumes than the prior art fabs).

[0027] A still further need exists to address shortcomings of existing TFSC technology. This includes addressing difficulties associated with sufficient surface texturing of the thin planar silicon films to reduce surface reflectance losses, which currently places a limit on the minimum flat (co-planar) crystalline silicon thickness due to production yield and cell performance considerations. A still further need exists for effective light trapping based on a combination of front surface texturing and back surface mirror, while achieving low surface recombination velocities (for high cell efficiencies).

[0028] A still further need exists to address additional shortcomings of existing TFSC technologies. This includes the problem of lack of rigidity and mechanical support of the thin film substrate during cell and module processing steps, thus, necessitating the use of support or handle substrates (made of silicon or another material) for the TFSC substrates. This further includes the cost of the epitaxial silicon film growth process, particularly for thicker epitaxial films required for planar crystalline silicon TFSCs. This further includes the requirement of multiple photolithography and/or screen printing and/or shadow-mask processing/patterning steps which usually increase the manufacturing process flow complexity and cost, and may also detrimentally impact the fabrication yield as well as the ultimate achievable solar cell efficiency.

SUMMARY

[0029] In accordance with the present disclosure, a template is provided which may be used to form a pyramidal three-dimensional thin-film solar cell substrate (3-D TFSC substrate). The 3-D TFSC substrates may be used to form pyramidal three-dimensional thin-film solar cells (3-D

TFSCs) and modules, substantially eliminating or reducing disadvantages and problems associated with previously developed semiconductor wafer-based solar cells as well as TFSCs, both in terms of conversion efficiency as well as cell and module manufacturing costs.

[0030] According to one aspect of the disclosed subject matter, there is a provided a template for pyramidal 3-D TFSC substrate formation. The template comprises a template substrate; the template substrate comprises a plurality of posts and a plurality of pyramid trenches between said plurality of posts. The template forms an environment for pyramidal 3-D TFSC substrate formation.

[0031] The template is preferably reused to fabricate a plurality of 3-D TFSC substrates without a need for substantial reconditioning of the template.

[0032] According to another aspect of the disclosed subject matter, there is a provided a method for fabrication of a template for pyramidal 3-D TFSC substrate formation. The method comprises removing semiconductor material from select regions of a semiconductor substrate to form a plurality of posts and a plurality of trenches.

[0033] More specifically, the disclosed subject matter includes removing semiconductor material from select regions of a semiconductor substrate by the steps of lithography patterning to produce a design on the semiconductor substrate and transferring the design onto the semiconductor substrate using an etching process.

[0034] More specifically, the disclosed subject matter includes removing semiconductor material from select regions of a semiconductor substrate by laser micromachining to produce a design on said semiconductor substrate.

[0035] These and other advantages of the disclosed subject matter, as well as additional novel features, will be apparent from the description provided herein. The intent of this summary is not to be a comprehensive description of the claimed subject matter, but rather to provide a short overview of some of the subject matter's functionality. Other systems, methods, features and advantages here provided will become apparent to one with skill in the art upon examination of the following FIGURES and detailed description. It is intended that all such additional systems, methods, features and advantages be included within this description, be within the scope of the accompanying claims.

BRIEF DESCRIPTIONS OF THE DRAWINGS

[0036] The features, nature, and advantages of the disclosed subject matter may become more apparent from the detailed description set forth below when taken in conjunction with the drawings in which like reference characters identify correspondingly throughout and wherein:

[0037] FIG. **1** (PRIOR ART) shows a prior art process flow for fabricating crystalline silicon (c-Si) thin-film solar cells (TFSCs) using planar silicon thin-film absorber layers produced by silicon epitaxy;

[0038] FIG. **2** (PRIOR ART) shows a prior art process flow for fabrication of solar cells on silicon wafers including self-aligned selective emitter and metallization;

[0039] FIG. **3** provides an overview of the 3-D TFSC substrate and solar cell fabrication process flow;

[0040] FIG. **4** (PRIOR ART) summarizes the key process steps eliminated by the current disclosure, compared to the prior art;

[0041] FIG. **5** summarizes the high-level process flow and the competitive advantages of the current disclosure, compared to the prior art;

[0042] FIGS. **6** and **7** outline embodiments of process flows for fabrication of a template using either direct laser micromachining or photolithography patterning;

[0043] FIG. **8** shows a Y-Y cross-sectional view of an embodiment of a template;

[0044] FIGS. **9** through **12** show embodiments of process flows for fabrication of pyramidal 3-D TFSC substrates;

[0045] FIGS. **13** and **14** show the Y-Y and Z-Z cross-sectional axes on an embodiment of a hexagonal-pyramidal (honeycomb) 3-D TFSC substrate;

[0046] FIG. **15** shows a 3-D view of a single unit cell in a hexagonal-pyramidal 3-D TFSC substrate;

[0047] FIG. **16** shows a schematic ZZ cross-sectional-view of an embodiment of a 3-D hexagonal-pyramid TFSC substrate;

[0048] FIG. **17** shows a schematic YY cross-sectional-view of an embodiment of a 3-D hexagonal-pyramid TFSC substrate;

[0049] FIG. **18** shows a top view of a honeycomb hexagonal-pyramid array design TFSC substrate, with a peripheral planar silicon frame;

[0050] FIG. **19** shows a YY cross-sectional view of an embodiment of a 3-D self-supporting hexagonal-pyramid TFSC substrate with thin square-shaped silicon frame;

[0051] FIG. **20** shows a top view of an alternative honeycomb hexagonal-pyramid array design TFSC substrate, with a larger thickness peripheral planar frame;

[0052] FIG. **21** shows a YY cross-sectional view of an embodiment of a 3-D self-supporting hexagonal-pyramid TFSC substrate with thick square-shaped silicon frame;

[0053] FIG. **22** shows a top view of a 3-D TFSC substrate with a square-pyramid unit cell structure;

[0054] FIG. **23** shows a top view of a 3-D TFSC substrate with a triangular-pyramid unit cell structure;

[0055] FIG. **24** shows a top view of a 3-D TFSC substrate with an orthogonal V-groove unit cell structure;

[0056] FIG. **25** shows alternative cross sectional views of the 3-D TFSC substrate with an orthogonal V-groove unit cell structure, shown in FIG. **24**;

[0057] FIG. **26** shows a top view of a 3-D TFSC substrate with an alternative orthogonal diagonal V-groove unit cell structure;

[0058] FIG. **27** shows alternative cross sectional views of the 3-D TFSC substrate with an orthogonal diagonal V-groove unit cell structure, shown in FIG. **26**;

[0059] FIGS. **28** through **30** describe process flows for fabrication of a 3-D TFSC using fire-through metallization;

[0060] FIGS. **31** through **35** describe process flows for fabrication of a 3-D TFSC using selective plating metallization;

[0061] FIG. **36** shows a schematic view of a double-sided coater setup for self-aligned application (coating) of dopant liquid or paste layers on 3-D TFSC substrate top ridges and rear surface or ridges by roller coating and in-line curing of the applied liquid/paste layers (shown in conjunction with an integrated belt-driven process equipment);

[0062] FIG. **37** shows a view of an alternative spray coater and curing setup to perform the same processes as the roller coater and curing setup of FIG. **36**;

[0063] FIG. **38** shows a view of another alternative setup design using liquid-dip coating or liquid-transfer coating to

perform the same processes as the roller coater and curing setup of FIG. **36** and the spray coater and curing setup of FIG. **37**;

[0064] FIG. **39** shows a cross-sectional view of a 3-D substrate (showing one of the hexagonal-pyramid cells) after the above-mentioned doping process step;

[0065] FIGS. **40** and **41** show YY cross-sectional views after self-aligned formation of the emitter and base contacts and solar cell interconnects;

[0066] FIGS. **42** and **43** show YY cross-sectional views of the 3-D hexagonal-pyramid solar cells (showing a single hexagonal-pyramid unit cell and several adjacent unit cells, respectively) after completion of the solar cell fabrication process and after soldering the rear base contacts to the rear cell mirror (and base interconnect) plate;

[0067] FIG. **44** shows a YY cross-sectional view of the 3-D hexagonal-pyramid TFSC substrate (showing one pyramid unit cell) after self-aligned roller coating of n-type dopant paste on the frontside honeycomb ridges, and after curing and furnace annealing to form the selective emitter regions and heavily-doped emitter contact regions;

[0068] FIG. **45** is similar to FIG. **44**, except FIG. **45** roller coating of a p-type dopant layer and subsequent curing and anneal;

[0069] FIG. **46** shows a cross-sectional view similar to the view shown in FIG. **39**. However, in the embodiment shown in FIG. **46** there is only coating of n-type dopant paste on the frontside honeycomb ridges;

[0070] FIG. **47** shows a YY cross-sectional view of a 3-D hexagonal-pyramid substrate after self-aligned formation of the frontside solid dopant source layer and selective emitter, while FIG. **48** shows a ZZ cross-sectional view;

[0071] FIG. **49** shows a YY cross-sectional view of a 3-D hexagonal-pyramid substrate after self-aligned formation of the frontside solid dopant source layer, selective emitter, as well as the self-aligned frontside emitter and rear base contacts, while FIG. **50** shows a ZZ cross-sectional view;

[0072] FIG. **51** shows a view of a 3-D self-supporting hexagonal-pyramid TFSC substrate with thick silicon frame, compared to the thin frame shown in FIG. **41**;

[0073] FIG. **52** shows a schematic quasi-3-D view of a hexagonal-pyramid unit cell after formation of the self-aligned frontside emitter contact and the rear base contact;

[0074] FIG. **53** shows a view of an alternative embodiment of solar cell assembly on the rear mirror and base interconnect (the first embodiment shown in FIG. **43**);

[0075] FIG. **54** illustrates a first embodiment of a process flow for fabrication of solar modules with top protective glass plates and embedded PCBs of this disclosure (corresponding to the solar module structure of FIG. **55** with a PCB and a TFSC mounted on the PCB);

[0076] FIG. **55** shows a cross-sectional view of a solar module (solar panel) structure (resulting from the process flow described in FIG. **54**);

[0077] FIG. **56** outlines an alternative embodiment of an assembly process flow for fabrication of solar modules (corresponding to the solar module structure of FIG. **57**);

[0078] FIG. **57** shows a cross-sectional view of another embodiment of a solar module structure (resulting from the process flow described in FIG. **56**);

[0079] FIG. **58** shows a view of a solar cell integrated or assembled in building windows;

[0080] FIG. **59** shows a view of a representative example of series connections of TFSCs of this disclosure in a solar module assembly;

[0081] FIG. **60** shows a view of the frontside layout of the printed-circuit board (PCB) used for solar module assembly;

[0082] FIG. **61** shows a top view of the backside layout of the printed-circuit board (PCB) used for solar module assembly, showing the series connection of the TFSCs;

[0083] FIG. **62** shows a backside view of the copper pattern on the PCB and is essentially similar to FIG. **61**;

[0084] FIG. **63**A shows an enlarged top view of the pattern on the frontside of the solar module printed-circuit board (PCB);

[0085] FIG. **63**B shows an enlarged top view of the interconnect pattern on the backside of the solar module printed-circuit board (PCB);

[0086] FIG. **64** shows various schematic views of a thick silicon frame, silicon frame slivers, and a representative method to produce (e.g., cut) silicon slivers;

[0087] FIG. **65** (similar to FIG. **15**) is provided for reference for calculations;

[0088] FIG. **66** shows the ratio of the hexagonal-pyramid sidewall area to the planar hexagonal base area (S_{hp}/S_{hb}) versus the height-to-base diagonal diameter ratio (H/d) of the hexagonal-pyramid unit cell;

[0089] FIGS. **67** and **68** shows calculated frontside aperture angles of the solar cell hexagonal-pyramid unit cell versus the height-to-base diagonal diameter ratio (H/d) of the hexagonal-pyramid unit cell;

[0090] FIG. **69** is provided for reference for calculations;

[0091] FIGS. **70** and **71** show the ratio of the cone-shaped unit cell sidewall area to the planar circular base area (S_{cp}/S_{cb}) versus the height-to-base diameter ratio (H/D) of the cone-shaped unit cell and calculated frontside aperture angle of the solar cell cone-shaped unit cell (approximation for hexagonal-pyramid units cells) versus the height-to-base diameter ratio (H/D) of the cone-shaped unit cell;

[0092] FIG. **72** may be used for reference with an approximate analytical calculation of the TFSC interconnect ohmic losses, assuming a circular substrate with hexagonal-pyramid array of unit cells;

[0093] FIGS. **73** and **74** plot the projected (calculated) interconnect-related solar cell power losses as a function of the ratio of the hexagonal-pyramid height to diagonal base dimension (H/d) for two different emitter interconnect area coverage ratios on the top of the 3-D solar cell substrate; while FIGS. **73** through **84** show plots for various values of R_{thm} and L/H.

DETAILED DESCRIPTION OF THE SPECIFIC EMBODIMENTS

[0094] Preferred embodiments of the present disclosure are illustrated in the drawings, like numbers being used to refer to like and corresponding parts of the various drawings. The innovative solar cell designs and technologies of the current disclosure are based on the use of a three-dimensional (3-D), self-supporting, doped (in one embodiment, in-situ-doped) semiconductor thin film, deposited on and released from a reusable crystalline (embodiments include monocrystalline or multicrystalline silicon) semiconductor template.

[0095] A preferred semiconductor material for the 3-D TFSC substrate is crystalline silicon (c-Si), although other semiconductor materials may also be used. One embodiment uses monocrystalline silicon as the thin film semiconductor

material. Other embodiments use multicrystalline silicon, polycrystalline silicon, microcrystalline silicon, amorphous silicon, porous silicon, and/or a combination thereof. The designs here are also applicable to other semiconductor materials such as germanium, silicon germanium, silicon carbide, a crystalline compound semiconductor, or a combination thereof. Additional applications include copper indium gallium selenide (CIGS) and cadmium telluride semiconductor thin films.

[0096] The 3-D TFSC designs and production technologies as well as associated module structures and assembly approaches of this disclosure effectively overcome the above-mentioned problems and challenges and enable cost-reduced fabrication of very-high-efficiency solar cells and modules using self-aligned cell process flows without the use of any photolithography patterning or screen printing or shadow-mask deposition process steps during cell fabrication (i.e., during 3-D TFSC substrate and cell fabrication after fabrication of the reusable 3-D template). The 3-D TFSC technologies of this disclosure are based on the formation of a 3-D pyramid-array TFSC substrate structure on a low-cost reusable template and its subsequent release and lift-off from the template to form a free-standing, self-supporting 3-D thin-film semiconductor substrate structure.

[0097] The current disclosure combines the benefits of TFSC fabrication on a proven high-efficiency crystalline silicon (c-Si) platform. The 3-D c-Si TFSC designs and technologies of this disclosure enable significant advancements in the areas of c-Si solar cell and module efficiency enhancement as well as manufacturing cost reduction. Based on innovative thin-film process steps, dependence on an expensive and constrained silicon wafer supply-chain is eliminated. Some of the unique advantages of the cells designs and technologies of this disclosure which enable achieving ultra-high-efficiency at reduced manufacturing cost are substantial decoupling from the traditional solar PV silicon supply chain, performance enhancement, cost reduction, and reliability improvement.

[0098] The disclosed subject matter improves solar cell efficiency by using a 3-D c-Si film as an absorber layer in conjunction with highly efficient light trapping. Use of the crystalline silicon absorber layer leverages known solar cell manufacturing techniques and supply chain, while reducing absorber layer thickness (e.g., reduced by a factor of ten or more compared to silicon wafers used for wafer-based solar cells). The disclosed method and system eliminates or substantially reduces photo-degradation and enhances open-circuit voltage (V_{oc}) of cells. In addition, the disclosed method and system provides efficient frontside and rear side light-trapping in conjunction with a highly reflective rear mirror for maximum absorption of incident solar flux. Also, the disclosed method and system provides a selective emitter to enhance blue response and external quantum efficiency, with minimal shadowing of the cell and reduced ohmic losses due to a unique folded emitter metallization contact design and improved module assembly.

[0099] Manufacturing cost is reduced by decreasing silicon usage (by a significant factor, e.g., 3× to over 10×), with thinner deposited c-Si films also reducing the finished solar module energy payback time to less than 1 to 2 years. Manufacturing cost is further reduced by eliminating wire sawing and related kerf losses associated with mainstream solar cell wafer manufacturing technology. Manufacturing cost is still further reduced by using self-aligned processing without any lithography or patterning steps used during the substrate and cell fabrication process flow, and a reduced number of fabrication process steps, with improved yield and cycle time. Production cost is still further reduced by using a simplified interconnection and cell-module assembly process and light-weight monolithic modules.

[0100] Operational reliability is improved by using thinner silicon films, eliminating photo-degradation and reducing temperature coefficients. Operational reliability is further improved by using a simple distributed high-conductance electrical interconnection, minimizing field failures. Operational reliability is still further improved by eliminating module glass cover (for glassless module assembly), thus reducing cost and facilitating field installation and operation. Operational reliability is still further improved by reducing the number of manufacturing process steps and process variations using in-line manufacturing process control.

[0101] The current disclosure reduces the solar module cost per watt for the user (by at least 30% to 50%) and cuts balance-of-system (BOS) and installation costs for the integrators and installers. This may offer major benefits to the global grid-tied end-users and solar system installers and integrators. The current disclosure reduces the module integration and installation cost and installed solar cell system cost per W_p for the user, thereby lowering finished system cost per W_p. The current disclosure increases module efficiency, with higher module efficiency resulting in lower BOS cost. The lower installed solar cell system cost results in reduction of the economic break-even time to a lower fraction of the system lifetime, from roughly ½ to ⅓ for current best-of-breed c-Si solar cell systems to less than ¼ to ⅛ for the embodiments of this disclosure. The current disclosure reduces energy pay-back time (EPBT) from 3 to 7 years for best-of-breed c-Si solar cell systems to less than 1 to 2 years for the embodiments of this disclosure. Reduced EPBT substantially increases the net lifetime energy output (in kWh) for field-installed modules. The cell designs and module assemblies of this disclosure also provide stable degradation-free field operation over an extended time (e.g., 30 to 40 year life of the module), further increasing the net lifetime electrical energy output. Module manufacturing costs are expected to be 30% to 65% lower than that of the leading high-performance c-Si solar cells/modules at the time of market entry. This may shorten the ROI break-even time for the users compared to the current industry roadmap and projections. Further benefits include increased field performance stability and reliability and reduced environmental impact (non-toxic materials and shortened EPBT). Further, the cell and module designs of this disclosure are ideal for grid-tied applications where it is advantageous to maximize electricity generation from a limited building rooftop or façade area.

[0102] The absorber silicon film thickness of the current disclosure may be a value in the range of roughly 1 to 30-microns, where a thinner silicon layer is preferred for less material consumption (in one embodiment, in the range of 1 to 10 microns). Even after taking into account the effective surface area increase due to the 3-D geometric structure of the 3-D TFSC substrates, the 3-D TFSC substrates of this disclosure consume substantially less silicon material than the state-of-the-art wafer-based c-Si solar cells. Moreover, there are no sawing or kerf losses. Similarly, there is no requirement for saw damage removal since the 3-D crystalline silicon film is process-ready upon release from the reusable template. This substantially reduces the solar cell cost associated with sili-

con consumption. The self-supporting 3-D epitaxial silicon thin film is deposited on and released from a low-cost reusable crystalline (monocrystalline or multicrystalline) silicon substrate (template). The template may be reused numerous times before being reconditioned or recycled. The template may even be chosen from the much lower cost metallurgical-grade c-Si since any metallic impurities are prevented from contaminating the 3-D crystalline silicon film.

[0103] FIG. **3** provides an overview of the 3-D TFSC substrate and cell fabrication process flow. Focusing on the top of FIG. **3** illustrating the 3-D TFSC substrate fabrication, note that the first step in this process flow uses a pre-fabricated template. The template with a pre-fabricated 3-D trench or groove pattern may be used for formation of 3-D TFSC substrates, which are then used in the formation of 3-D TFSCs, substantially eliminating or reducing disadvantages and problems associated with previously developed TFSCs and the wafer-based crystalline silicon cell technologies. The template is capable of being used numerous times (e.g., tens to hundreds of times) to fabricate numerous 3-D TFSC substrates before being reconditioned or recycled. In one embodiment, the template may be used hundreds of times to fabricate 3-D TFSC substrates before being recycled. The template may be reused for as long as it remains relatively free of dislocations and/or for as long as it maintains an acceptable trench or groove pattern with widths and surface conditions within acceptable control limits (e.g., as gauged by in-line metrology).

[0104] FIG. **4** summarizes the overall crystalline solar cell fabrication process flow of prior art techniques and highlights the specific steps eliminated by the current disclosure, compared to the prior art. FIG. **5** summarizes the overall cell and module fabrication process flow and the competitive advantages of the current disclosure, compared to the prior art. As highlighted here, the current disclosure enables fabrication of 3-D TFSC substrates and 3-D TFSCs, thus, substantially reducing consumption of semiconductor absorber material (e.g., silicon) and the cell and module manufacturing costs.

[0105] In the following section, alternative embodiments of process flows for fabricating templates using either lithography and etch techniques or laser micromachining (or laser drilling) are described. The templates are then used and reused numerous times to fabricate the 3-D TFSC substrates for 3-D TFSC fabrication.

[0106] Templates may be fabricated using electronic-grade silicon wafers, solar-grade silicon wafers, or lower-cost metallurgical-grade silicon wafers. Moreover, templates made of silicon can be fabricated either using monocrystalline or multicrystalline silicon wafers. The starting template wafer may either be a standard polished wafer (after saw damage removal) or even a lower grade wafer immediately after wire sawing (without saw damage removal). The latter may further reduce the cost of the templates. The relatively low cost of each template is spread over numerous 3-D TFSC substrates, resulting in much lower TFSC substrate and finished module costs compared to the standard state-of-the-art (e.g., 200 microns thick) solar-grade monocrystalline and multicrystalline silicon wafers and associated modules.

[0107] For further explaining how a template is fabricated, FIG. **6** shows an embodiment of a process flow **100**. The process begins with step **102**, where an unpatterned monocrystalline silicon or multicrystalline silicon, either square-shaped or round substrate (e.g., 200 mm×200 mm square or 200-mm round) is provided. The starting template wafer may be a wafer prepared by wire saw either with or without saw damage removal (the latter may further reduce the cost of template). The starting template wafer may also be made of a lower purity (and lower cost) metallurgical-grade silicon. In one embodiment, the substrate is roughly 200 to 800 microns thick. Optionally, step **102** includes performing gettering on a low-cost metallurgical-grade silicon and/or performing a surface texturing etch (e.g., using isotropic acid texturing by a mixture of nitric acid and hydrofluoric acid, or using alkaline texturing in KOH/IPA) to create an optional textured template surface. Step **104** involves the use of programmable precision laser micromachining to form the desired periodic array of deep trenches. This process may be performed in a controlled atmospheric ambient based on either physical ablation or a combination of physical ablation and laser-assisted chemical etching. Step **106** involves template surface preparation and cleaning. This process includes stripping the patterned photoresist layer from the substrate. The template substrate is then cleaned in a wet bench prior to subsequent thermal deposition processing to form the TFSC substrates. Such cleaning may involve DRIE-induced polymer removal (using a suitable wet etchant such as a mixture of sulfuric acid and hydrogen peroxide) followed by an isotropic silicon wet etch (such as in a mixture of nitric acid and hydrofluoric acid) in order to isotropically remove a thin layer (e.g., on the order of 10 to 500 nanometers) of silicon from the trench sidewalls and bottoms. This may remove any surface and buried contaminants, such as any surface and embedded metallic and/or polymeric/organic contaminants introduced by the deep RIE (DRIE) process, from the sidewalls and bottoms of the DRIE-produced template trenches. Template processing may complete after a deionized (DI) water rinse and drying. Optionally and if desired, the template wafer may also go through a standard pre-diffusion (or pre-thermal processing) wafer cleaning process such as a so-called RCA wet clean prior to the above-mentioned DI water rinsing and drying. Another optional surface preparation step (either performed instead of or after the wet isotropic silicon etch process) includes performing a short thermal oxidation (e.g., to grow 5 to 100 nanometers of sacrificial silicon dioxide), followed by wet hydrofluoric acid (HF) oxide strip (to remove any residual contaminants from the patterned template). If no optional oxide growth/HF strip is used, an optional dilute HF etch may performed to remove the native oxide layer and to passivate the surface with hydrogen (forming Si—H bonds) in preparation for subsequent 3-D TFSC substrate fabrication. After the completion of step **106**, the resulting template may then be used and reused multiple times to fabricate 3-D (e.g. hexagonal-pyramid) TFSC substrates.

[0108] An alternative embodiment of a process flow **110** for patterning of a template is outlined in FIG. **7**, which uses photolithography and etch instead of direct laser micromachining. Step **112** (providing an unpatterned substrate) corresponds to step **102** of FIG. **6**. Step **114** uses photolithography patterning (in one embodiment, using a relatively low-cost contact or proximity aligner/patterning) to produce a mask pattern such as hexagonal-pyramid pattern in photoresist (i.e., interconnected hexagonal openings in the photoresist layer). The process sequence includes the formation of an oxide and/or nitride (optional) layer, photoresist coating (e.g., spin-on or spray coating) and pre-bake, photolithography exposure through a hexagonal-array mask, and photoresist development and post-bake. One embodiment includes an optional hard mask layer (SiO_2 and/or SiN_x; for example, a

thin thermally grown oxide layer can be used as an optional hard mask) below the photoresist (although the process may be performed without the use of any hard mask layer by placing the photoresist coating directly on silicon). When using a hard mask layer, the exposed portions of the hard mask layer are etched after photoresist patterning (thus, forming hexagonal openings). Such etching of the exposed hard mask layer may be simply performed using a wet etchant such as hydrofluoric acid for oxide hard mask or using plasma etching. Step **116** involves formation of hexagonal-pyramids using anisotropic plasma etch; where a high-rate deep reactive ion etch (DRIE) process forms a closely-packed array of deep (e.g., 100 to 400 microns) hexagonal-pyramid shaped trenches (i.e., pyramidal trenches with sloped sidewalls) in silicon. The photoresist and/or oxide and/or nitride hard mask layer(s) are used for pattern transfer from the patterned photoresist layer to silicon substrate. In one embodiment, the deep RIE (DRIE) process parameters are set to produce a controlled-angle hexagonal-pyramid sidewall slope. The RIE is allowed to produce small-diameter (e.g., less than 5 microns) holes at the bottom of pyramids by punching through the substrate backside. Alternatively, separate small-diameter backside holes may be formed which connect to the bottom tips of the pyramidal trenches. Step **118** (surface preparation and cleaning) corresponds to step **106** of FIG. **6**. After the completion of step **118**, the resulting template may then be used and reused multiple times to fabricate 3-D (e.g. hexagonal-pyramid) TFSC substrates.

[0109] FIG. **8** shows a Y-Y cross-sectional view of a template **120** showing hexagonal-pyramid trenches **122** between posts **123**, formed in the substrate fronstide **124** using the process flows described above. The bottom **126** of the trenches **122** connects to through-wafer backside, preferably small-diameter, holes **128** which connect to the template backside **130**. In one embodiment, the holes **128** are 1 to 10 microns in diameter. The holes **128** are used for subsequent wet etching of the sacrificial layer and 3-D silicon film release and lift-off. The template **120** has dimensions of L **132** (in one embodiment, 0 to 25 microns although it may also be much larger up to several hundred microns), 3-D unit cell height H **134**, pyramidal angle α **136**, and unit cell aperture diameter h **138**.

[0110] The templates described above may be used to fabricate 3-D TFSC substrates for use in 3-D TFSCs. All of the embodiments shown in FIGS. **9** through **12** use sacrificial layer formation (e.g., porous silicon sacrificial layer) and trench-fill deposition processes (e.g., epitaxial silicon deposition) which may be highly conformal, for conformal formation of the sacrificial (porous silicon) layer and subsequent seamless void-free filling of the trenches with a semiconductor absorber layer such as in-situ-doped (e.g., in-situ boron doped) monocrystalline or multicrystalline silicon layer. One embodiment uses a patterned single-crystal (monocrystalline) silicon or multicrystalline silicon (mc-Si) square-shaped (or round) template, with dimensions of approximately 150 mm×150 mm to over 200 mm×200 mm. Alternative embodiments may use much lower cost metallurgical-grade or solar-grade silicon.

[0111] FIG. **9** shows an embodiment of a process flow for fabrication of self-supporting, free-standing 3-D hexagonal-pyramid TFSC substrates. The process uses a lift-off 3-D thin-film release process based on a highly selective etch process to remove an interfacial sacrificial layer (of $Ge_{1-x}Si_x$) without any appreciable etching of silicon. The $Ge_{1-x}Si_x$ layer may be a single layer with a constant Ge fraction or a multi-layer (e.g., 2 to 3 layers) structure with varying Ge fractions. In step **142**, a patterned square-shaped template is provided. This template has already been processed to form an array of hexagonal-pyramid trenches on its frontside **124** along with an array of through-wafer holes **128** from trench bottoms **126** to backside **130**. Step **144** involves a multi-layer blanket epi in an epitaxial reactor. Step **144** first involves an H_2 or GeH_4/H_2 in-situ cleaning, which is performed after a standard pre-epi wet clean. Next, a thin sacrificial epi layer is deposited on the frontside only. In one embodiment, Ge_xSi_{1-x} is used for the sacrificial epi layer and is between 10 and 200 nanometers. Next, a doped silicon epi layer is deposited on the frontside only. In one embodiment, the layer is p-type, boron-doped and has a thickness between 2 and 20 microns. Step **146** involves 3-D TFSC substrate release. A highly selective isotropic wet or dry etch of Ge_xSi_{1-x} is performed, with very high selectivity with respect to silicon. In one embodiment, a mixture of hydrofluoric acid, nitric acid and acetic acid (HNA) is used to etch the Ge_xSi_{1-x} layer. Alternatively, a mixture of ammonia, peroxide, and water ($NH_4OH+H_2O_2+H_2O$) may be used. This process releases the silicon epi layer as a hexagonal-pyramid 3-D TFSC substrate, which may then be used for subsequent 3-D TFSC fabrication.

[0112] Depending on the emitter doping type (n-type or p-type), the in-situ base doping type is chosen to be p-type (e.g., boron) or n-type (e.g., phosphorus). The embodiments shown provide examples of boron-doped hexagonal-pyramid 3-D TFSC substrates which may be used to fabricate TFSCs with n-type, phosphorus-doped selective emitters. In an alternative embodiment, all the doping polarities may be inverted, resulting in phosphorus-doped hexagonal-pyramid 3-D TFSC substrates which may be used for fabricating cells with boron-doped selective emitters.

[0113] FIG. **10** shows an alternative embodiment of a process flow **150** for fabrication of self-supporting, free-standing 3-D hexagonal-pyramid TFSC substrates. The same process flow may be used for fabrication of 3-D TFSC substrates with other unit cell structures (square pyramid, triangular pyramid, orthogonal V-grooves, orthogonal diagonal V-grooves, etc.). This process uses a suitable sacrificial material layer (e.g., silicon dioxide) to facilitate the 3-D TFSC substrate release and lift-off (or removal from the template). Laser crystallization may be used to crystallize the amorphous silicon or polysilicon layer. Step **152** (providing a template) corresponds to step **142** above. Step **154** involves sacrificial layer deposition, where a thin sacrificial layer (e.g., SiO_2) is deposited preferably by APCVD (alternatively, use LPCVD or PECVD or even thermal oxidation). In one embodiment, this layer is between 20 nm and 200 nm of SiO_2. In step **156**, doped (e.g., p-type) silicon layer (preferably doped amorphous silicon or polysilicon) is deposited on oxide-coated substrate (top only) by a CVD process such as PECVD (e.g., 2 to 20 microns thick; boron-doped). Step **158** involves depositing a thin sacrificial layer (e.g., SiO_2) as a top protective layer, preferably by chemical-vapor deposition process such as APCVD (alternatively, use LPCVD or PECVD or even thermal oxidation). In one embodiment, this layer may be 5 nm to 50 nm of SiO_2. In step **160**, laser crystallization (preferably starting from a silicon frame at substrate edge) of doped silicon layer is performed, using a preferably square-shaped single-crystal silicon frame as laser crystallization seed (edge-to-center crystallization). Step **162** involves releasing the 3-D TFSC substrate, by performing a highly

selective isotropic HF wet etching of the sacrificial SiO_2 layer (with high selectivity with respect to silicon) to etch off the oxide release layer between the p-type 3-D silicon film and the template (this process lifts the 3-D hexagonal-pyramid silicon film). For all embodiments, releasing the 3-D film may be aided by applying a small mechanical stress (e.g., wafer warpage) or applying ultrasonic or megasonic agitation during the release etch.

[0114] FIG. **11** shows an alternative embodiment of a process flow **170** for fabrication of self-supporting, free-standing 3-D hexagonal-pyramid TFSC substrates. The same process flow may be used for fabrication of 3-D TFSC substrates with other unit cell structures (square pyramid, triangular pyramid, orthogonal V-grooves, orthogonal diagonal V-grooves, other types of pyramids, etc.). This process uses a sacrificial or disposable material layer (e.g., silicon dioxide) to facilitate the 3-D TFSC substrate release and. Laser crystallization may be used to crystallize the amorphous silicon or polysilicon layer. Step **172** (providing a template) corresponds to step **142** above. Step **174** (sacrificial layer deposition) corresponds to step **154** above. Step **176** involves performing a backside wet etching of SiO_2 to re-open the oxide-filled substrate bottom holes. Step **178** (doped silicon deposition) corresponds to step **156** above; and step **180** (sacrificial layer deposition) corresponds to step **158**. In step **182**, laser crystallization of the doped silicon layer is performed, using the single-crystal islands at the bottom holes of hexagonal-pyramids as laser crystallization seeds. Step **184** (3-D TFSC substrate release) corresponds to step **162** above.

[0115] FIG. **12** shows an alternative embodiment of a process flow **190** for fabrication of self-supporting, free-standing 3-D hexagonal-pyramid TFSC substrates. The same process flow may be used for fabrication of 3-D TFSC substrates with other unit cell structures (square pyramid, triangular pyramid, orthogonal V-grooves, orthogonal diagonal V-grooves, other pyramidal unit cell structures, etc.). This process uses electrochemical silicon etching to form low and/or high porosity porous silicon layer(s) prior to semiconductor (e.g., silicon) epitaxy. Step **192** (providing a template) corresponds to step **142** above. Step **194** involves Electrochemical Silicon Etching in a Wet Bench to produce a single-layer porous silicon or a bilayer stack of a top layer of low-porosity porous silicon on a layer of high-porosity porous silicon, using electrochemical HF etching (also known as electrochemical anodization of silicon to form porous silicon). The porous silicon layer or layer stack may be formed either by direct electrochemical etching of the template substrate or by first depositing a thin layer of epitaxial silicon and then converting the thin silicon epi layer to sacrificial porous silicon using electrochemical etching. In step **196**, silicon epitaxy is performed in an epitaxial reactor to form preferably monocrystalline silicon on top of the porous silicon sacrificial layer or layer stack, with the following in-situ process steps performed: H_2 in-situ clean; deposition of doped (e.g., p-type) silicon epi (top only) (e.g., 2 to 20 microns thick; boron-doped). Finally, in step **198**, the 3-D TFSC substrate is released by either applying a mechanical stress to the substrate (e.g., by applying a slight warpage to the substrate), or simply by selective wet etching of the sacrificial porous silicon layer (or layer stack) using a suitable etchant (such as $HF+H_2O_2$ or TMAH or another suitable selective porous silicon etchant).

[0116] The following FIGURES show embodiments of 3-D TFSC substrate structures. The crystalline silicon film thickness is in the range of 2 to 30 microns, and preferably in the lower-end range of 2 to 10 microns. This is substantially less (by a factor of roughly 20× to 100×) than the state-of-the-art silicon solar cell wafer thickness (roughly 200 microns).

[0117] FIG. **13** shows a top view of a regular (equilateral) hexagonal-pyramid 3-D TFSC substrate **200**, formed using the process steps outlined above. Each hexagonal unit cell **202** contains hexagonal unit cell points (H_1, H_2, H_3, H_4, H_5, and H_6) **204**, **206**, **208**, **210**, **212**, and **214**, with the bottom tip (which will form the back contact) of the hexagonal-pyramid shown as point **216**. FIG. **13** further shows the hexagonal-pyramid 3-D TFSC substrate sidewalls **218**; the diagonal dimension of the unit cell hexagon (d) **220**; and hexagonal unit cell horizontal distance (h) **222**. In one embodiment, the hexagonal-pyramid 3-D TFSC substrate sidewalls **218** are between 2 and 30 microns thick.

[0118] FIG. **14** shows a bottom view of the TFSC substrate **200** shown in FIG. **13**. In this view, the hexagonal-pyramid rear (bottom) tips **216** are shown at the centers of the hexagons. The honeycomb hexagons are the bottom views of the top honeycomb ridges of the 3-D TFSC substrate.

[0119] FIG. **15** shows a quasi 3-D view **230** of an individual hexagonal-pyramid unit cell **202** of the TFSC substrate **200** shown above. The top hexagonal opening of the unit cell **202** forms the frontside self-aligned interconnected contacts of the thin-film solar cell (TFSC). Also shown in this view is the width (W) **231** of the semiconductor film forming the sidewalls of the hexagonal-pyramid cell **202** and the height (H) **232** of the cell **202**, and d/2 **234**.

[0120] When referring to the following FIGURES, the YY and ZZ axes are shown in FIGS. **13** and **14**. FIG. **16** shows a ZZ cross-sectional-view **240** of the 3-D hexagonal-pyramid TFSC substrate **200**, showing the hexagonal-pyramid top aperture angles β **242**. The bottom tips **216** of the triangles are the rear tips of the hexagonal-pyramids (where the base contacts will be placed). The solid line shows the 3-D TFSC substrate thin-film silicon layer, with thickness **231** (in one embodiment, roughly 1 to 25 microns thick). FIG. **17** shows a YY cross-sectional-view **250** of the hexagonal-pyramid TFSC substrate **200**, showing the hexagonal-pyramid top aperture angles α **252**.

[0121] FIG. **18** shows a top view **260** of a honeycomb hexagonal-pyramid array design TFSC substrate **200**, with a peripheral planar silicon frame **262**. The design includes a periodic array of high-aspect-ratio (or low-aperture-angle) hexagonal-pyramid unit cells **202**. In one embodiment, frame length (S) **264** is 125 mm to over 200 mm. Silicon Frame **262** may have the same thickness as the TFSC substrate **200** or may be much thicker (e.g., silicon frame thickness=5 to 500 microns). The top surface of the frame is also preferably used as the top solar cell interconnect (it is metallized along with the top honeycomb contacts, and is electrically connected to the honeycomb contacts). In one embodiment, the width **266** of the frame **262** is roughly 125 microns to 1 mm. The film thickness **231** of the TFSC substrate is roughly 2 to 30 microns, preferably 2 to 10 microns. Typically, there are millions (or as few as thousands) of these hexagonal-pyramid unit cells **202** form a large-area (e.g., 200 mm×200 mm) TFSC substrate **200**.

[0122] FIG. **19** shows a YY cross-sectional view **270** (not to scale) of an embodiment of a 3-D self-supporting hexagonal-pyramid TFSC substrate **200** with thin square-shaped silicon frame **262** (like the frame **262** shown in FIG. **18**), with thickness the same as the film thickness **231**. The silicon frame

width (W) **266** is between 50 and 250 microns. Note that the width of the top hexagonal honeycomb silicon ridges **272** is preferably much smaller than h **222** and H **232**. In one embodiment, the width of the top honeycomb ridges **272** is roughly 0.5 microns to less than 5 microns.

[0123] FIG. **20** shows a top view **280** of an alternative honeycomb hexagonal-pyramid array design TFSC substrate **200**, with a larger thickness **266** peripheral planar silicon frame **262**.

[0124] FIG. **21** shows a YY cross-sectional view **290** (not to scale) of an embodiment of a 3-D self-supporting hexagonal-pyramid TFSC substrate **200** with thicker square-shaped silicon frame **262** (like the frame **262** shown in FIG. **20**). Note that the thickness of the frame is not the same as the film thickness **231**. Instead, the thick silicon frame may be roughly 100 to 500 microns thick. The silicon frame width (W) **266** is between 50 and 250 microns. The thick peripheral silicon frame may be preferably made of low-cost metallurgical-grade silicon and may be attached to the 3-D TFSC substrate using one of the following methods: (i) thick silicon frame placed on the reusable silicon template and fused to the 3-D thin-film silicon film during the epitaxial silicon growth process; (ii) e-beam welding of the 3-D TFSC substrate to the thick silicon frame (after lift-off/release of the 3-D TFSC substrate from the reusable silicon template); or (iii) thermal bonding (under clamping pressure) of the thick silicon frame to the 3-D TFSC substrate. The thick silicon frame maybe used for enhanced mechanical support and rigidity of the 3-D TFSC substrate.

[0125] The previous section illustrated a preferred embodiment of a hexagonal-pyramid TFSC substrate. Alternative embodiments may use alternative designs for the unit cells such as inverted pyramid unit cells with polygon bases, including square pyramid, triangular pyramid, etc.; other embodiments may include 3-D TFSC substrates with V-groove or orthogonal V-groove patterns, etc. For example, FIG. **22** shows a top view **300** of a 3-D TFSC substrate with a square-pyramid unit cell structure. The primary difference between this pattern and the preferred embodiment hexagonal-pyramid unit cell pattern is the top base (or pyramid aperture) geometry (square base versus hexagonal base for the inverted pyramid unit cells). The vertical height and base area values of the square pyramid unit cells are comparable to those of the hexagonal-pyramid unit cells (similar considerations apply). Another example is shown in FIG. **23**, which shows a top view **310** of a 3-D TFSC substrate with a triangular-pyramid unit cell structure. The primary difference between this pattern and the preferred embodiment hexagonal-pyramid unit cell pattern is the top base or pyramid aperture geometry (triangular base versus hexagonal base for the inverted pyramid unit cells). The vertical height and base area values of the triangular pyramid unit cells are comparable to those of the hexagonal-pyramid unit cells (similar considerations apply).

[0126] FIG. **24** shows a top view **320** of a 3-D TFSC substrate with an orthogonal V-groove unit cell structure. The orthogonal V-groove unit cell preferably has four adjacent rectangular or square-shaped arrays of V-grooves, with the V-grooves in each pair of adjacent sub-unit cells running perpendicular to each other. A 3-D TFSC substrate uses a large number of the orthogonal unit cells shown above. The ranges for height and width of the V-grooves in the orthogonal V-groove unit cells are similar to the height and diameter ranges of the hexagonal-pyramid unit cells, respectively. Each square-shaped sub-unit cell (four sub-unit cells shown above produce one orthogonal V-groove unit cell) may have tens to hundreds of V-grooves. The orthogonal V-groove structure provides additional mechanical rigidity compared to the standard V-groove structure with parallel V-grooves on the entire substrate. The dotted lines depict the V-groove trench bottoms whereas the solid lines show the top ridges of the V-grooves. FIG. **25** shows XX **330**, YY **340**, and ZZ **350** cross sectional views of the 3-D TFSC substrate with an orthogonal V-groove unit cell structure, shown in FIG. **24**.

[0127] FIG. **26** shows a top view **360** of a 3-D TFSC substrate with an alternative orthogonal diagonal V-groove unit cell structure, compared to the orthogonal V-groove unit cell structure shown in FIG. **24**. The orthogonal diagonal V-groove unit cell preferably has four adjacent rectangular or square-shaped arrays of V-grooves, with the V-grooves in each pair of adjacent sub-unit cells running perpendicular to each other. The orthogonal V-groove structure provides additional mechanical rigidity compared to the standard V-groove structure with parallel V-grooves on the entire substrate. FIG. **27** shows YY **370**, XX **380**, and ZZ **390** cross sectional views of the 3-D TFSC substrate with an alternative orthogonal diagonal V-groove unit cell structure, shown in FIG. **26**.

[0128] The following section details the process of using the 3-D TFSC substrates described above to fabricate 3-D thin-film solar cells (TFSCs). Specifically, the following FIGURES illustrate embodiments of process flows using alternative methods of fire-through metallization and selective plating metallization. These process flows do not use any photolithography or screen printing processes. The 3-D hexagonal-pyramid structural design of the solar cell substrate enables self-aligned processing throughout the entire cell process flow. The emitter and base contacts and metallized regions cover relatively small fractions of the frontside emitter and backside base areas, respectively. As indicated, selective emitter and base doping is achieved by self-aligned application of the n-type and p-type dopant pastes to the top and bottom of the 3-D hexagonal-pyramid substrate, preferably using double-sided roller coating method. The 3-D substrate is then cured and moves on to a belt furnace to form the n^+ selective emitter on the frontside and the p^{+-}doped base on the rear side of the 3-D substrate. A preferred n-type dopant source is phosphorus and a preferred p-type dopant source is boron.

[0129] FIGS. **28** through **30** describe process flows using fire-through metallization, while FIGS. **31** through **35** describe process flows using selective plating metallization.

[0130] Process flow **400** shown in FIG. **28** describes an embodiment using fire-through metallization, with a forming gas anneal (FGA) step after copper (Cu) or silver (Ag) plating. Step **402** starts with a p-type 3-D silicon TFSC substrate. Step **404** involves selectively coating the top portions of the hexagonal-pyramids (in one embodiment, the top 2 to 10 microns in height) with n-type liquid or paste dopant source. Coating is performed by self-aligned roller coating using dopant paste/liquid, or liquid-dip coating by dipping in a controlled liquid dopant source depth. The dopant layer is then dried/cured (250° C. to 400° C. or UV). Step **406** involves formation of self-aligned emitter contacts. The bottom portions of the pyramid tips are selectively coated (in one embodiment, about 2 to 10 microns in height) with p-type liquid or paste dopant source. Coating is performed by self-aligned roller coating using dopant paste/liquid, or liquid-dip coating by dipping in a controlled liquid dopant source depth.

The dopant layer is then dried/cured (250° C. to 400° C. or UV). Step **408** involves self-aligned selective emitter formation, where the top n^+p and $n^{++}p$ junctions and rear p^+ tips are concurrently formed by an anneal (e.g., 800° C. to 950° C.). The dopant layer drying and annealing may be performed sequentially in a single belt furnace. Preferably, the substrate may be annealed face down on a heated planar surface, or with pairs of substrates in frontside face-to-face contact, in order to facilitate gas-phase doping formation of n^+ regions. In step **410** (Surface passivation and ARC), the dopant source layer and native oxide are stripped (in one embodiment, using dilute HF). Thin oxide is grown by steam oxidation (e.g., 3 to 10 nm @ 850° C. to 950° C.); and SiN_x ARC is then deposited by PECVD. Both layers are formed on both silicon sides, with PECVD-SiN_x also providing H passivation of silicon. In step **412** (Self-aligned metallization), the top portions of the hexagonal-pyramids are selectively coated (to a height less than the dopant source) with metal (Ag) paste using self-aligned roller coating, then dried and cured. The bottom tips of the hexagonal-pyramids are then selectively coated on the rear side with metal (Al or Ag) paste by self-aligned roller coating, then dried and cured. In step **414** (Self-aligned metallization (firing)), the front (Ag) and rear (Al, Ag) metallized regions are formed by firing through the thermal oxide/PECVD SiN_x layers. Step **416** involves an optional self-aligned metallization step, where an FGA is performed (e.g., 300° C. to 450° C.) to reduce front and rear interconnect resistance values and help with surface/bulk passivation. Step **418** involves an optional self-aligned metallization step, where Cu or Ag are selectively/concurrently deposited (e.g., 1 to 5 microns) on the metallized top honeycomb ridges and bottom hexagonal-pyramid tips by plating. Metallized regions are then flash coated with Ag. In step **420**, the solar cell backside metallized hexagonal-pyramid tips are soldered to a Cu or Ag mirror plate or foil (may be perforated), then flash coated with Ag. The rear mirror also serves as the rear electrical connector. Finally, in step **422**, the solar cells can be packaged into solar modules/panels.

[0131] An alternative fire-through metallization process flow **430** is described in FIG. **29**. Emitter contacts and interconnects are made on the top honeycomb ridges whereas the base contacts are made on rear hexagonal-pyramid tips. In this embodiment the rear base contact regions are heavily doped by Al during the fire-through process (no separate p^+ rear base doping used by boron dopant source). Forming gas anneal (FGA) performed after Cu and/or Ag plating. Step **432** (providing the substrate) corresponds to step **402** in FIG. **28**; and step **434** (selectively coating the top portions) corresponds to step **404**. However, step **406** (selective coating of bottom portions) is not performed next. Instead, subsequent steps **436** to **450** correspond to steps **408** to **422**.

[0132] Another alternative fire-through metallization process flow **460** is described in FIG. **30**. Compared to process flow **430** in FIG. **29**, the forming gas anneal (FGA) step is performed before Cu and/or Ag plating. Specifically, steps **444** and **446** from FIG. **29** are reversed, noted in steps **474** and **476** of FIG. **30**.

[0133] As noted above, FIGS. **31** through **35** describe process flows using selective plating metallization.

[0134] Process flow **490** shown in FIG. **31** describes an embodiment using selective plating metallization. Step **492** (providing a substrate) corresponds to step **402** in FIG. **28**; step **494** (selectively coating the top portions) corresponds to step **404**; step **496** (selectively coating the bottom portions) corresponds to step **406**; step **498** corresponds to step **408**; and step **500** corresponds to step **410**. However, step **502** (self-aligned metallization) involves selectively etching the top portions of the hexagonal-pyramids (to a height less than the dopant source) by self-aligned roller coating in etchant paste, followed by rinsing, and repeating the process on the rear hexagonal-pyramid tips. Step **504** (self-aligned metallization) involves concurrently forming the front and rear metallized regions by a single plating process (e.g., Ag, Ni, Pt, Ti, Co, Ta). Step **506** involves an optional self-aligned metallization step where a forming gas anneal (FGA) is performed (e.g., 300 to 450° C.), to reduce front and rear interconnect resistance values and help with surface/bulk passivation. Step **508** involves self-aligned metallization where Cu or Ag is selectively/concurrently deposited (e.g., 1 to 5 microns) on the metallized top honeycomb ridges and bottom hexagonal-pyramid tips by plating. Step **510** (solder) and step **512** (proceed with packaging) are the same as above.

[0135] An alternative selective plating metallization process flow **520** is described in FIG. **32**. No p^+ dopant paste coating is used for rear base contact doping. The rear base p^+ contact doping is performed by Al doping in the base contact regions using an anneal process after rear base tip Al metallization using plating. Step **522** (providing the substrate) corresponds to step **492** in FIG. **28**; and step **524** (selectively coating the top portions) corresponds to step **494**. However, step **496** (selective coating of bottom portions) is not performed next. Instead, step **526** (self-aligned selective emitter) is performed next, corresponding to step **498**. Step **528** (Surface passivation and ARC) corresponds to step **500**; and step **530** (self-aligned metallization) corresponds to step **502**. In step **532**, the rear metallized regions are selectively formed by an Al rear plating process (e.g., dip plate the rear/backside only). In step **534**, metal (Ag, Ni) is selectively plated on front exposed honeycomb n^{++} doped regions and rear Al-metallized regions. Step **536** involves performing an FGA (300 to 450° C.) to form Al-doped rear p^+ tips. The FGA reduces front and rear interconnect resistance values and helps with surface/bulk passivation. Step **538** (plating) corresponds to step **508**; step **540** (solder) corresponds to step **510**; and step **542** (proceed with packaging) corresponds to step **512**.

[0136] Another alternative selective plating metallization process flow **550** is described in FIG. **33**. In contrast to the embodiment is FIG. **31**, no roller paste etching process is used here. Instead the process here uses selective etching of dopant source layers. Steps **552** (providing a substrate), step **554** (selectively coating the top portions), and step **556** (selectively coating the bottom portions) correspond to steps **492** to **496** in FIG. **31**. Step **558** (self-aligned selective emitter) involves concurrently forming the top n^+p and $n^{++}p$ junctions and rear p^+ tips by an anneal (e.g., 800 to 950 C), sequentially first in an inert (Ar, N_2) and then oxidizing (steam) ambient to grow 5 to 50 nm of thermal oxide. The dopant layer drying and anneal may also be performed sequentially in a single belt furnace. Step **560** involves selectively etching the dopant source layers while removing only a small portion of oxide, using a wet etch with high etch selectivity compared to thermal oxide. Step **562** (plating) corresponds to step **504**; and step **564** (plating) corresponds to step **508**. Step **566** involves soldering (Pb-free solder) backside metallized hexagonal-pyramid tips to an Al mirror plate or foil (may be perforated), then flash coating with Ag. The rear mirror also serves as the rear electrical connector. Step **568** involves concurrently depositing ARC layer (e.g., low-temperature PECVD SiN_x)

on both front and rear surfaces. The ARC layer may also include spectral down-conversion. The ARC layer also helps with additional H passivation. Note that the peripheries of frontside solar cell and rear mirror should be masked during PECVD to facilitate cell/module interconnects. Step **570** (FGA) corresponds to step **504**, and step **572** (packaging) is the same as above.

[0137] Another alternative selective plating metallization process flow **580** is described in FIG. **34**. Compared to process flow **550** from FIG. **33**, this process uses only one high temperature (anneal and oxidation) process step. Steps **582** to **596** are the same as steps **552** to **566** in FIG. **33**. However, in step **598**, an ARC layer (e.g., low temperature PECVD SiN_x) is deposited on solar cell front surface only. Steps **600** and **602** are the same as steps **570** and **572** in FIG. **33**.

[0138] Another alternative selective plating metallization process flow **610** is described in FIG. **35**. Like process flow **580** from FIG. **34**, this process uses only one high temperature (anneal and oxidation) process step. Steps **612** to **620** correspond to steps **582** to **590** from FIG. **34**. However, step **592** (plating) is not performed. Instead, only plating step **594** is performed, corresponding to step **622**. Steps **624** to **630** correspond to steps **596** to **602** from FIG. **34**.

[0139] The above process steps may be performed on integrated in-line process equipment. For example, FIG. **36** shows a view **640** of a setup for performing the two process steps of liquid/paste coating and UV or IR curing prior to furnace anneal, allowing for subsequent formation of selective emitter and base regions after anneal in an in-line diffusion furnace. This integrated in-line process equipment allows for self-aligned formation of dopant liquid or paste coating on the 3-D TFSC substrate top ridges and rear ridges by roller coating. Roller coating may be performed using an atmospheric-pressure, belt-driven coating and curing equipment integrated in line with a diffusion furnace. In one embodiment, the top ridges are coated with n-type dopant liquid/paste; the rear ridges are coated with p-type dopant liquid/paste.

[0140] The 3-D TFSC substrate **642** is shown moving in **644** on input conveyor belt **646**. The rotating top rollers **648**, with top roller pads **650**, apply a controlled downward force to coat the top ridges with n-type paste. The rotating rear rollers **652**, with rear roller pads **654**, apply a controlled upward force to coat the rear ridges with p-type paste. Multilayer materials may be coated on each side of the 3-D TFSC substrate by applying (or flowing) a different liquid or paste material to each roller on the top **648** and/or rear **652** set of rollers. The 3-D TFSC substrate **642** next moves into the curing area where the dopant liquid/paste layers are concurrently formed using a curing lamp **656** which uses IR or UV curing beams **658**. The 3-D TFSC substrate **642** is next shown moving out **660** to the output conveyor belt **662**, which may move the substrate **642** to an in-line diffusion furnace, where the n^+ and p^+ contacts and selective emitter regions are concurrently formed.

[0141] A similar roller coater setup may be properly configured and used for applying metal liquid/paste coatings (e.g., silver and/or aluminum liquid or paste sources), curing the metal liquid/paste source, and performing subsequent thermal anneal in an in-line atmospheric furnace (resistively-heated or lam-heated furnace) for fire-through metallization in order to form the emitter and base contact metallization (and whenever applicable, also to form the aluminum-doped p^{++} base contact regions).

[0142] FIG. **37** shows a view **670** of an alternative setup design to perform the same processes as the roller coater/curing/furnace setup of FIG. **36**. The setup in FIG. **37** may be used for self-aligned formation of dopant source liquid/paste coating on the 3-D TFSC substrate top ridges and rear ridges by angled spray coating. This setup also may utilize an in-line atmospheric-pressure coating and curing and diffusion equipment configuration which can be easily integrated with an in-line diffusion furnace. As with the roller coater setup in FIG. **36**, multilayer materials may be coated on each side of the substrate by using multiple sets of spray nozzles connected to different liquid sources (not shown here) and applying (or flowing) a different liquid source material to each nozzle on the top and/or rear set of spray nozzles. This is an alternative technique to the roller coating system shown in FIG. **36**. In one embodiment, the top ridges are coated with n-type dopant liquid/paste (such as phosphorus); the rear ridges are coated with p-type dopant liquid/paste (such as boron). Referring to FIG. **37**, the 3-D TFSC substrate **642** is shown moving in **644** on input conveyor belt **646**. Angled nozzles **672** spray n-type dopant liquid onto the surface at a sharp angle with respect to the surface (nozzles cover wafer width). This n-type dopant liquid comes from an n-type liquid dopant source and nozzle reservoir/pump **674**. Angled nozzles **676** spray p-type dopant liquid onto the surface at a sharp angle with respect to the surface (nozzles cover wafer width). This p-type dopant liquid comes from a p-type liquid dopant source and nozzle pump **678**. The 3-D TFSC substrate **642** next moves into the curing area where the dopant liquid/paste layers are concurrently formed using a curing lamp **656** which uses IR or UV curing beams **658**. The 3-D TFSC substrate **642** is next shown moving out **660** to the output conveyor belt **662**, which may move the substrate **642** to an in-line diffusion furnace, where the n^+ and p^+ contacts and selective emitter regions are concurrently formed.

[0143] The angled spray technique limits the vertical height of the liquid/paste coating to a portion of the ridges and prevents the liquid source from coating the inner parts of the hexagonal pyramid cavity sidewalls and/or rears. This type of in-line (or another drive method) processing system may also be used for applying metal source liquid (e.g., silver and/or aluminum source liquid) for fire-through metallization applications as well as applying liquid etchant for selective etching of dielectrics (e.g., oxide and/or solid dopant source layer) from the top and/or rear hexagonal-pyramid ridges.

[0144] FIG. **38** shows a view **680** of another alternative setup to perform the same processes as the in-line roller coater/curing setup of FIG. **36** and the in-line spray coater/curing setup of FIG. **37**. The setup in FIG. **38** may be used for self-aligned formation of dopant liquid/paste coating on the 3-D TFSC substrate top ridges and rear ridges by liquid-dip coating. This setup also may utilize an in-line atmospheric-pressure coating and curing equipment configuration to be attached to the input stage of an in-line diffusion (or fire-through) furnace.

[0145] In one embodiment, the top ridges are coated with n-type dopant liquid/paste (such as phosphorus); the rear ridges are coated with p-type dopant liquid/paste (such as boron). The 3-D TFSC substrate **642** is shown moving in **644** on input conveyor belt **646**. Liquid film dispenser containing n-type liquid dopant source **682** applies a controlled thickness n-type liquid dopant film **684**. This n-type dopant liquid comes from n-type liquid dopant source and liquid level and depth controller **686**. Liquid film dispenser containing p-Type

liquid dopant source (with peripheral air levitation) **688** applies a controlled thickness p-type liquid dopant film **690**. This p-type dopant liquid comes from p-type liquid dopant source and liquid level and depth controller **692**. The 3-D TFSC substrate **642** next moves into the curing area where the dopant liquid/paste layers are concurrently formed using a curing lamp **656** which uses IR or UV curing beams **658**. The 3-D TFSC substrate **642** is next shown moving out **660** to the output conveyor belt **662**, which may move the substrate **642** to an in-line diffusion furnace, where the n^+ and p^+ contacts and selective emitter regions are concurrently formed.

[0146] As in the setups in FIGS. **36** and **37**, multilayer materials may be coated on each side of the 3-D TFSC substrate by using multiple sets of liquid-dip applicators (not shown here) and applying (or flowing) a different liquid source material to each liquid-dip applicator on the top and/or rear set of applicators. This type of processing system may also be used for applying metal liquid for fire-through metallization as well as applying liquid etchant for selective etching of dielectrics (e.g., oxide and/or solid dopant source layer) from the top and/or rear ridges.

[0147] The following section shows cross-sectional views of the TFSC substrate during various stages of the process flows outlined above. In the following FIGURES, the relative dimensions are not shown to scale.

[0148] FIG. **39** shows a cross-sectional view **700** of the 3-D substrate **200** (showing one of the hexagonal-pyramid cells **202**) after the above-mentioned doping process step in a suitable process equipment such as an in line belt-driven equipment (roller coating or spray coating or liquid-dip coating or another liquid/paste-transfer coating of dopant liquids/pastes, drying/curing, and diffusion furnace anneal). In regard to the n-type (e.g., phosphorus) dopant paste or liquid **702** covering the top portion of the hexagonal ridges **272**, the single furnace anneal process in the diffusion furnace (e.g., at roughly 800° C. to 950° C.) produces more heavily-doped contact diffusion regions **704** with higher surface phosphorus concentrations on the top silicon hexagonal ridges directly in contact with and underneath the cured n-type dopant solid source layer **702**. Through gas or vapor-phase transport of the vaporized dopant source to the adjacent frontside regions within the hexagonal-pyramid cavities, the furnace anneal/diffusion process concurrently dopes the remaining frontside surface regions **706** not covered with the solid dopant source layer with phosphorus with smaller surface concentration and smaller dose, thus, creating self-aligned selective emitter regions with lighter surface doping. These less heavily doped regions **706** improve the blue response of the solar cell, while the more heavily doped ridges **704** will minimize the frontside contact resistance of the solar cell for improved cell emitter contact metallization. Similarly, the same furnace anneal process produces more heavily doped p^{+-}doped **708** hexagonal-pyramid rear tips **216** for low base contact resistance, while the remaining backside base regions **710** are less heavily doped on the surface. In the embodiment shown in FIG. **39**, L **712** is much less than H **232** and much less than h **222**, with H **232** between 100 and 500 microns, while L **712** is between 2 and 20 microns. Also shown are l **714** and α **716**, where $l=L/\cos(\alpha/2)$ and $\alpha/2=\tan^{-1}(h/2H)$. Also shown are L' **718**, and l' **720**, where l' is the slanted height of heavily doped junction region.

[0149] FIGS. **40** and **41** show YY cross-sectional views **730** and **740** after self-aligned formation of the emitter and base contacts and solar cell interconnects. As shown, the emitter contact is preferably wrapped around (or it may be wrapped-through frame holes not shown) the 3-D substrate frame to make all the cell contacts on the rear side of the solar cell (for ease of solar module assembly automation). As shown in FIG. **40**, the self-aligned frontside honeycomb contacts **732** are placed within the more heavily n^+-doped top ridges **704** of the honeycomb structure (thus, producing very low contact resistance). The remaining top regions not covered by the emitter contacts (which is most of the hexagonal-pyramid sidewall area doped by proximity vapor-phase doping from the adjacent solid dopant source regions) has the less heavily doped n^+ selective emitter regions, enabling excellent solar cell blue response. The base metallization contacts **734** on the rear side hexagonal-pyramid tips cover the more heavily p^{+-}doped regions (formed by direct contact with the solid dopant source layer), resulting in low base contact metallization resistance. The remaining base surface regions on the rear side of the 3-D substrate are less heavily doped with boron (by proximity vapor-phase doping from the adjacent solid dopant source regions), enabling very low surface recombination velocity and improved cell performance. Also shown is surface passivation & ARC layers (thermal SiO_2 and PECVD or PVD hydrogenated SiN_x) **736**. FIG. **41** shows a view **740** of multiple unit cells **202**, with self-aligned peripheral emitter wrap-around contact **742** connected to the solar cell hexagonal frontside emitter contact at the frame edge. Note that both frontside **732** and backside contacts **734** are accessible on the rear side of the cell for ease of automated module assembly.

[0150] FIGS. **42** and **43** show YY cross-sectional views **750** and **760** of the 3-D hexagonal-pyramid solar cells (showing a single hexagonal-pyramid unit cell and several adjacent unit cells, respectively) after completion of the solar cell fabrication process and after soldering (or connecting with a suitable electrically conductive epoxy) **752** the rear base contacts **734** (rear hexagonal-pyramid metallized tips) to the rear cell mirror **754** (and base interconnect) plate. This mirror/interconnect plate may be made of a number of materials, preferably Ag-coated Cu or Ag-coated Al (or any other suitable electrically conductive and optically reflecting material). The combination of the highly reflective rear mirror and the 3-D hexagonal-pyramid structure of the solar cell (and the frontside honeycomb pattern aperture **762** of the solar cell) ensure extremely efficient light trapping, enabling ultra-high-efficiency solar cells using very thin crystalline silicon films.

[0151] The following FIGURES show alternative views, corresponding to various steps in the process flows for fabrication of TFSCs outlined above.

[0152] FIG. **44** shows a YY cross-sectional view **770** of the 3-D hexagonal-pyramid TFSC substrate **200** (showing one pyramid unit cell) after self-aligned roller coating (or spray coating or liquid-dip coating or another suitable liquid-transfer coating) of n-type dopant paste/liquid **702** on the frontside honeycomb ridges **272**, and after drying/curing and furnace annealing, preferably in an in-line belt furnace, to form the selective emitter regions and heavily-doped emitter contact diffusion regions (the preferred embodiment applies both n-type and p-type dopant pastes or liquids on the frontside and backside, respectively, before a single furnace anneal/diffusion process to form the doped diffusion regions, including selective emitter junction regions). This structure shows the unit cell after short thermal oxidation (e.g., to grow 5 nm to 100 nm thermal oxide) and PVD or PECVD ARC layer (SiN_x) formation. The dotted lines show the doped regions (after further processing, the unit cell structure is shown in

FIG. 39). This embodiment shows no prior p^+ base contact doping (it will be done by Al doping in conjunction with Al rear base contact formation using a base contact firing process).

[0153] FIG. 45 is similar to FIG. 44, except FIG. 45 shows p^+ base contact doping by roller coating (or spray coating or liquid-dip coating or another suitable liquid-transfer coating) of a p-type dopant layer and subsequent curing and anneal (same anneal as emitter). Self-aligned solid-dopant-source-doped rear p^+ contact regions **782** (for plated rear base contacts) are illustrated using dotted lines.

[0154] FIG. 46 shows a cross-sectional view **790** similar to the view **700** shown in FIG. 39. However, in the embodiment shown in FIG. 46 there is only coating of n-type dopant paste/liquid on the frontside honeycomb ridges. There is no p^+ dopant paste/liquid applied to the backside.

[0155] FIG. 47 shows a YY cross-sectional view **800** of a 3-D hexagonal-pyramid substrate **200** after self-aligned formation of the frontside (top) solid n^+ (e.g., doped with phosphorus) solid dopant source layer and selective emitter. This structure leads to the structure shown in FIG. 41. The frontside pattern consists of honeycomb ridges which will be subsequently used for formation of the emitter contacts/interconnects. FIG. 48 shows a ZZ cross-sectional view **810**.

[0156] FIG. 49 shows a YY cross-sectional view **820** of a 3-D hexagonal-pyramid substrate **200** after self-aligned formation of the frontside (top) solid n^+ (e.g., doped with phosphorus) and p^+ solid dopant source layer, selective emitter, as well as the self-aligned frontside emitter and rear base contacts (shown with fire-through metallization but selective plating may also be used to obtain the same structure). This structure leads to the structure shown in FIG. 41. The frontside pattern consists of honeycomb ridges which will be subsequently used for formation of the emitter contacts/interconnects. FIG. 50 shows a ZZ cross-sectional view **830**.

[0157] FIG. 51 shows a view **840** of a 3-D self-supporting hexagonal-pyramid TFSC substrate with thick silicon frame, compared to the thin frame shown in FIG. 41. The thick frame may have a width of roughly 500 to 1000 microns and may be fused to a 3-D TFSC substrate **200** during the epitaxial silicon deposition process (by placing the thick silicon frame on the reusable silicon template) or after silicon epitaxy and 3-D substrate release (by e-beam welding).

[0158] FIG. 52 shows a schematic quasi-3-D view **850** of a hexagonal-pyramid unit cell of one embodiment of a 3-D TFSC substrate structure of the disclosed subject matter after formation of the self-aligned frontside emitter contact (on the honeycomb ridges) and the rear base contact (on the hexagonal-pyramid rear tips). Solar light enter the solar cell from the topside into the hexagonal-pyramid unit cell cavities.

[0159] Finally, FIG. 53 shows a view **860** an alternative embodiment of solar cell assembly on the rear mirror and base interconnect (the first embodiment shown in FIG. 43). In contrast to FIG. 43 shown with a specular rear mirror, this embodiment uses a diffused rear base mirror **862** (with a roughened Ag-coated surface to scatter the reflected light back into the 3-D cell structure).

[0160] In the next section, various embodiments of this disclosure for making solar modules suitable for building rooftops and façades, centralized power generation, and other applications are described. Usually solar modules are made by arranging a plurality of solar cells and connecting them in series (series electrical connections) within a solar module assembly protected by a top glass layer and a rear protective material layer such as Tedlar. The cells may be connected in series in order to step up the DC voltage (while maintaining the solar module current at the same level at the level of the cell current) to facilitate high-efficiency DC-to-AC power conversion.

[0161] FIG. 54 illustrates a first embodiment of a process flow **900** for fabrication of solar modules with top protective glass plates and embedded PCBs of this disclosure (corresponding to the solar module structure of FIG. 55 with a PCB and a TFSC mounted on the PCB). This manufacturing flow is compatible with a fully automated module assembly line. This module assembly flow is based on the use of a double-sided printed-circuit board (PCB) with the cell rear mirrors/base interconnects on the PCB topside (silver-coated patterned copper on the PCB topside). For hexagonal-pyramid 3-D TFSCs with rear base layers and integrated/embedded (or attached) rear mirrors fabricated prior to module assembly (e.g., hexagonal-pyramid cells with rear base layers and thin-film rear mirrors deposited on the rear surfaces of the rear base layers using PVD or plating or roller coating/spray coating and curing), the patterned PCB copper layer does not have to be coated with a high-reflectivity mirror material (silver). In step **902**, module assembly starts with a double-sided PCB coated with copper foils on both frontside and backside. The PCB area should support the desired number/layout of TFSCs (e.g., $\geqq 1$ m^2, with a copper foil thickness on each side of roughly 10 to over 100 microns). Step **904** involves PCB interconnect patterning and silver flash coating (the latter if needed for PCB rear mirror). The PCB frontside and backside copper foils are patterned according to the desired frontside and backside interconnect layouts. Copper patterns are flash coated with a thin layer of highly reflective silver (and/or aluminum). A highly reflective diffuse mirror may be used, though a specular mirror may also be used. Step **906** involves cell preparation for automated TFSC placement and soldering. The rear metallized side of the TFSCs is roller coated (or spray coated or dip coated) with lead-free solder or an electrically conductive and thermally-conductive epoxy paste. Step **908** involves automated TFSC placement and soldering (or curing of epoxy). TFSCs are automatically picked and placed in a closely-packed array on the frontside of the PCB. The rear side of each cell sits on its designated site on the frontside of the double-sided PCB with patterned copper interconnects. The TFSC rear hexagonal-pyramid base interconnect is soldered to the PCB frontside silver-coated patterned copper islands using thermal or ultrasonic soldering. In case of using epoxy instead of solder, the epoxy layer is cured using thermal and/or IR/UV curing. The protective thin-film shunt diodes are mounted and soldered (or epoxied) on the PCB backside. An optional step is to flash coat the metal regions with a thin layer of highly reflective silver. Step **910** involves final solar module assembly and lamination. A stack of low-reflection tempered (in one embodiment, also textured) top glass, an encapsulant layer, the cell-mounted PCB, another encapsulant layer and a Tedlar or polyvinyl fluoride back sheet is prepared. Next, the module stack assembly is hermetically sealed and packaged, for instance, using vacuum-pressure lamination.

[0162] FIG. 55 shows a cross-sectional view **920** of a solar module (solar panel) structure (resulting from the process flow described in FIG. 54) with a protective back plate **922** made of a proven prior art material (e.g., Tedlar or polyvinyl fluoride film); a rear encapsulant layer **924** (EVA), a 2-sided printed-circuit board (PCB) **926** of this disclosure with rear

patterned electrical interconnects **928** and top patterned electrical interconnects **930**; cell rear mirrors and TFSCs **932** with rear base and wrap-around (or wrap-through) emitter contacts mounted on the frontside of the PCB, a top encapsulate layer (EVA) **934**, and an anti-reflection-coated (ARC) tempered glass (in one embodiment, textured tempered glass) **936** (from rear to top), with greater than 98% transmission, with sputtered or sprayed or liquid-coated anti-reflection coating). This module structure may be assembled as a hermetically sealed package either as a frameless module or with a frame (e.g., made of aluminum). In one embodiment, the module assembly is a frameless assembly (also for reduced materials energy content and reduced energy payback time).

[0163] FIG. **56** outlines an alternative embodiment of an assembly process flow **940** for fabrication of reduced cost and reduced weight (lightweight) solar modules (corresponding to the solar module structure of FIG. **57**). This flow is compatible with a fully automated module assembly. This process flow shows the assembly process without the use of a thick glass plate (thus, further reducing the weight, cost, and energy payback time of the solar modules of this disclosure) and without an EVA encapsulant layer on the top of the cells. The module topside (the frontside of assembled cells) is covered with a hard protective glass-type layer (if desired, also including a top ARC layer) with a combined thickness on the order of tens to hundreds of microns. As deposited, this frontside protective layer is effectively textured as a result of the 3-D structure of the TFSCs. The top layer may be formed by a liquid coating technique (e.g., spray coating, liquid-dip coating, or roller coating) following by a thermal or UV curing process. The thermal (or UV) cure for the liquid-spray-coated (or liquid-dip coated or roller coated) protective/AR layers may be performed as a single step together with the vacuum-pressure thermal lamination process. This embodiment results in a lightweight module assembly with reduced materials consumption, reduced cost, and reduced energy payback time. Step **942** (providing PCB) corresponds to step **902** in FIG. **54**; step **944** (PCB patterning and silver flash coat) corresponds to step **904**; step **946** (cell preparation) corresponds to step **906**; and step **948** (automated TFSC placement) corresponds to step **908**. Step **950** involves solar module lamination. A stack of the cell-mounted PCB, an encapsulant layer, and a back sheet is prepared. Next, a suitable hermetic sealing/packaging process such as vacuum-pressure lamination is performed. Step **952** involves deposition of the solar module frontside protective coating (which may be automatically textured as deposited and provides efficient light trapping for effective coupling to the TFSCs) layer and an optional ARC layer. The frontside of the solar panel is coated with a thin layer of protective material (e.g., a glass-type transparent material) and an optional top anti-reflection coating (ARC) layer using a suitable coating method. This coating (roughly tens to hundreds of microns) may be performed using liquid spray coating, liquid roller coating, liquid-dip coating, plasma spray coating or another suitable method. Next, a thermal/UV curing process is performed.

[0164] FIG. **57** shows a cross-sectional view **1960** of another embodiment of a solar module structure (resulting from the process flow described in FIG. **56**). Instead of a top encapsulate layer (EVA) **934**, and an anti-reflection-coated (ARC) tempered glass **936**, as shown in FIG. **55**, there is a single frontside protective layer and anti-reflective coating layer **962**. The frontside protective layer and anti-reflective coating (ARC) layer **962** is formed by liquid spray coating/curing, liquid roller coating/curing, liquid-dip coating/curing, plasma spray coating, or another suitable low-temperature coating technique. This frontside protective coating and ARC layer **962** is effectively textured for the coating layer as deposited as a result of the 3-D structure of the TFSCs (thus, no separate texturing process is needed). This is due to the fact that the coating layer may have dips (low points) over the TFSC hexagonal-pyramid cavities and peaks (high points) over the hexagonal-pyramid emitter ridges. The frontside protective layer and anti-reflective coating layer **962** may have a combined thickness in the range of tens to hundreds of microns. In one embodiment, the thickness may be approximately 30 to 300 microns. In addition to providing an anti-reflection coating (ARC) function, the stacked frontside protective/ARC layer provides excellent protection against weather/elements and force impact (e.g., hail impact) in actual outdoor field operation. Since the frontside coating is effectively and automatically textured as a result of the 3-D structure of the TFSCs, the use of a separate ARC layer on the frontside coating is optional. The textured coating may provide effective light trapping in the frontside coating for effective coupling of a very high fraction (e.g., greater than 95%) of the incident solar light intensity to the TFSCs. The frontside protective layers may also provide an optical waveguiding function to eliminate or reduce any reflection losses associated with the top emitter contact metallization.

[0165] FIG. **58** shows a view **970** of a solar cell integrated or assembled in building windows. The solar cell can allow partial visible light transmission (e.g., with transmission on the order of 10% to 30%) by creating an array of holes or slot openings in the 3-D hexagonal-pyramid solar cell substrate. In one embodiment, the cell has a regular array of holes or slot openings to allow for 5% to 20% light transmission. This FIGURE has a magnified view of a portion of the solar glass with the hexagonal-pyramid cells (thus, the relative dimensions of the hexagonal-pyramid cell and the solar glass are not shown to scale). FIG. **58** shows frontside TFSC hexagonal emitter interconnects **732** and self-aligned backside hexagonal base contact **734**. The distance **978** between the top glass plate **972** and bottom glass plate **974** may be between 1 and 12 millimeters. The hexagonal-pyramid cell parameters may be designed to allow for a desired level of light transmission through the cell (e.g., roughly 10% to 90%). The level of average light transmissivity can be controlled by the aspect ratio of the TFSCs.

[0166] FIG. **59** shows a view **980** of a representative example of series connections of TFSCs of this disclosure in a solar module assembly. This example shows 24 squared-shaped cells **982** connected in series (in a 6×4 array). The electrical connections in series are shown by arrows between the adjacent cells connected in series. Module power input **984** and output **986** leads are also shown. In actual module assemblies, the numbers of cells may be smaller or larger and the cells may be connected in series or in a combination of series and parallel. As mentioned earlier, series connection of the cells within the module assembly allows for stepping up the DC voltage for the DC-to-AC inverter (and also limiting the DC current of the solar modules for ease of module installation in the field and reliability of the module-to-module electrical connections). The printed-circuit-board (PCB) based module assembly of this disclosure supports any number of cells assembled in a module and any electrical connection configuration (series, series/parallel combination, or par-

allel). The TFSCs and modules of this disclosure may provide relatively lightweight solar modules with areas from less than 1 m^2 to several m^2 (e.g., 10 m^2) for various applications. The cells connected in series within a module assembly are chosen based on sorting to be matched in terms of their photogenerated current (e.g., short-circuit current I_{sc} and/or maximum-power current I_m).

[0167] The solar module structures and assembly methods of this disclosure are based on the use of a printed-circuit board (PCB) to assemble the 3-D TFSCs in a closely packed array and to connect the cells (in one embodiment in series) using the PCB plate within a module assembly. The PCB plate may have a single patterned metal (in one embodiment, copper) interconnect layer on the top of the PCB or two patterned copper layers on the top and rear surfaces of the PCB plate. FIG. **60** shows a view **990** of the frontside silver-coated copper layout of the printed-circuit board (PCB) used for solar module assembly (the square islands serve both as rear mirrors (if no integrated mirror is used with single-aperture cells, or if the cells are dual-aperture cells without base layers) and base interconnects; the peripheral square-shaped copper bands connect to the wrap-around emitter contact at the TFSC peripheral frame rear side; copper-filled via plugs connecting select regions of the PCB frontside and backside are shown as small circles). This example is shown for an array of 24 TFSCs arranged in 4 rows of 6 cells in each row (the PCB may be designed for any number and various arrangements of TFSCs). The PCB conductor (copper or aluminum) thickness may be in the range of roughly 10 to over 100 microns to provide high electrical and thermal conductivities. The PCB also serves as an effective heat sink to minimize temperature cycling of the TFSCs in operation. The PCB material may be selected to be a lightweight, high-strength material (such as carbon composite materials used in aerospace industry), or even a relatively thin flexible material. The larger-area square-shaped silver-coated copper regions **992** are connected to the TFSC rear base regions (bottoms of the rear base layers for the single-aperture cells or the bottom ridges of the dual-aperture cells for the dual-aperture cells). The peripheral silver-coated copper lines **994** are electrically connected to the TFSC emitter contact metallization regions.

[0168] FIG. **61** shows a top view **1000** of the backside (optionally silver-coated) copper layout of the printed-circuit board (PCB) used for solar module assembly, showing the series connection of the TFSCs. The PCB backside may also include thin-film shunt diodes for shade protection of the TFSCs (as shown in FIG. **60**). The copper-filled via plugs (shown as circles) connect the PCB frontside and backside metallization patterns in the corresponding areas. While the example shown here is for connecting 24 TFSCs in series on a solar panel, similar PCB design methodology may be applied to configure and connect any number of cells in any desired arrangements on the module. The frontside view of this PCB is shown in FIG. **60**. This example is shown for an array of 24 TFSCs arranged in 4 rows of 6 cells in each row (the PCB may be designed for any number and various arrangements of TFSCs), all connected in series. The PCB conductor (copper or aluminum) thickness may be in the range of roughly 10 to over 100 microns to provide high electrical and thermal conductivities. The PCB also serves as an effective heat sink to minimize temperature cycling of the TFSCs in operation. The PCB material may be selected to be a lightweight, high-strength material (such as suitable carbon composite materials used in aerospace industry). FIG. **61** also shows power input Lead **984** (first cell's p-lead) and power output lead **986** (last cell's n-lead).

[0169] FIG. **62** shows a backside view **1010** of the copper pattern on the PCB and is essentially similar to FIG. **61**. This picture also shows the use of protective thin-film shunt diodes mounted on the PCB backside pattern (for cell shadow protection).

[0170] FIG. **63**A shows an enlarged top view **1020** of the silver-coated copper pattern (the pad for mounting one cell) on the frontside of the solar module printed-circuit board (PCB) used for rear mirror and also emitter and base interconnects for one of the TFSCs (relative dimensions are not shown to scale). FIG. **63**A shows dimensions of L_1 **1022** and L_2 **1024** (in one embodiment, 150 millimeters to greater than 200 millimeters, where $L_2=L_1+2$ (W+S)). S **1026** may be on the order of 25 to 250 microns. The width of the peripheral copper conductor band (W) **1028** may be on the order of 50 to 500 microns. The copper-filled via plugs **1030** are shown as circles (connecting the interconnect patterns on the PCB frontside and backside in a pre-designed arrangement in order to connect the TFSCs in series or in any other desired arrangement such as series/parallel; the representative example shown here is for connecting all the cells in series in order to step up the module open-circuit voltage). The via plug **1030** diameters may be on the order of roughly 50 to 500 microns (and may be smaller than W **1028**). The large central square pad serves both as the rear cell mirror and also base interconnect plane (connecting to the hexagonal-pyramid base contact metallization). The number of vias in the center square (p-region contact) (N) **1032** may be on the order of hundreds to thousands. The number of vias in the peripheral line (n-region contact) (M) **1034** may be on the order of tens to hundreds (or even thousands). The vias on the peripheral line contacting the TFSC emitter (n) regions are placed on three sides. The PCB conductor (copper or aluminum) thickness may be in the range of roughly 10 to over 100 microns to provide high electrical and thermal conductivities. The PCB plate also serves as an effective heat sink to minimize temperature cycling of the TFSCs in field operation. This FIGURE shows one of the copper interconnect/mirror pads shown in the full module PCB array of FIG. **60**.

[0171] FIG. **63**B shows an enlarged top view **1040** of the silver-coated copper interconnect pattern on the backside of the solar module printed-circuit board (PCB) used for emitter and base electrical interconnects for a couple of adjacent TFSCs of this disclosure (a portion of the PCB view). FIG. **63**B shows the PCB backside silver-coated copper interconnect pattern for TFSCs **1** and **2** in the array. The copper pattern here is shown for connecting the TFSCs in series to step up the module open-circuit voltage. FIG. **63**B shows dimensions of L_1' **1042**; peripheral emitter (n-region) connector linewidth W' **1044** (in one embodiment, 2 to 10 millimeters); spacing between the center base (p-region) connector plate and the peripheral emitter (n-region) connector line S' **1046** (in one embodiment, 100 microns to 1 millimeter). Note that L_1' **1042** is less than L_1 from FIG. **63**A by roughly 2 to 10 millimeters. This enables larger peripheral emitter (n-region) connector linewidth and substantially reduced ohmic losses on the PCB backside.

[0172] The 3-D TFSC substrates of this disclosure may utilize peripheral thick silicon frames, both for added mechanical support and also to facilitate formation of wrap-through or wrap-around emitter contact metallization (for ease of solar module assembly). The thick silicon frame may

be separately made from very low-cost silicon material (such as metallurgical grade or reclaim silicon wafers). FIG. **64** shows various schematic views **1050** of the thick silicon frame, the silicon frame slivers, and representative method to produce (e.g., cut) silicon slivers from very-low-cost round (e.g., reject silicon from microelectronics) or square-shaped (or rectangular) cast silicon (or reclaim Si) substrates. The slivers may be made of very low-cost crystalline or multicrystalline silicon such as metallurgical-grade cast Si. A round **1052** or square-shaped **1054** silicon wafer (e.g., a 200 mm×200 mm cast metallurgical-grade silicon substrate) may be used to produce hundreds of silicon slivers **1056** by a cutting process such as laser cutting (four slivers used to make a thick silicon frame for a 3-D TFSC substrate by a welding process such as electron-beam welding).

[0173] These slivers **1056** may be used to make the thick silicon frames for the substrates shown above. The separately fabricated thick silicon frame may then be integrally attached to the 3-D TFSC substrates, in embodiment before 3-D thin-film cell processing, by one of the following techniques: electron-beam welding at several peripheral spots/junctions; attachment during the 3-D TFSC substrate fabrication silicon deposition by placing the peripheral thick silicon frame on the template and allowing seamless attachment of the thick silicon frame to the 3-D TFSC substrate by the silicon deposition process; or a clean cured epoxy.

[0174] Top view **1058** shows a thick silicon frame to be fused to the 3-D TFSC substrate. The silicon frame thickness **1060** is roughly 50 to 500 microns. There are welded (e.g., e-beam-welded) joints **1062** (four welded joints), where L **1064** is roughly 150 to 300 millimeters, and where W **1066** is roughly 100 to 1000 microns. The slivers **1056** may also have through-holes (shown in view **1068**) to help with the wrap-through/wrap-around emitter metallization contacts.

[0175] The following section outlines various calculations related to the disclosed subject matter.

[0176] For given thin silicon film thickness and substrate size (e.g., 200 mm×200 mm substrate size) values, the actual amount (e.g., amount as measured by the total silicon surface area, volume, or weight) of silicon material used in the 3-D hexagonal-pyramid substrate structure is actually larger than that of a co-planar (flat) substrate with the same dimensions (e.g., 200 mm×200 mm).

[0177] FIG. **65** (similar to FIG. **15**) is provided for reference for the following calculations. B is the mid-point between H_2 and H_3; A is the mid-point between H_5 and H_6; $H_1H_4=H_3H_6=H_2H_5=d$; and AB is the hexagonal unit cell aperture horizontal distance (h):

$$h=(\sqrt{3}/2)d$$

[0178] Frontside aperture angle α is the angle defined by A-T-B, and frontside aperture angle β is the angle defined by H_6-T-H_3, and can be calculated as follows:

$$\alpha=2\tan^{-1}[(\sqrt{3}\cdot d)/(4H)]$$

$$\beta=2\tan^{-1}[d/(2H)]$$

[0179] The surface area of the cone pyramid base (S_{hb}):

$$S_{hb}=[(3\sqrt{3})/8]\cdot d^2$$

[0180] The surface area of the cone pyramid sidewall (S_{hp}):

$$S_{hp}=[(3\sqrt{3})/8]\cdot d^2\cdot\sqrt{[1+(16/3)\cdot(H/D)^2]}$$

[0181] Therefore, the effective surface area enlargement factor (S_{hp}/S_{hb}) is:

$$S_{hp}/S_{hb}=\sqrt{[1+(16/3)\cdot(H/d)^2]}$$

[0182] To achieve very efficient light trapping within the 3-D TFSC structure and very low effective surface reflectance with a reasonable (i.e., not excessive) area enlargement factor of S_{hp}/S_{hb}, the aperture angles (α and β) are chosen to be preferably in the range of around 20° to around 40°.

[0183] FIG. **66** shows the ratio of the hexagonal-pyramid sidewall area to the planar hexagonal base area (S_{hp}/S_{hb}) versus the height-to-base diagonal diameter ratio (H/d) of the hexagonal-pyramid unit cell. The preferred H/d range for near-optimal aperture angles is shown between dashed lines (H/d roughly 1.5 to 3.0). This results in sidewall-to-base area ratio on the order of roughly 4 to 7.

[0184] FIGS. **67** and **68** shows calculated frontside aperture angles (α and β) of the solar cell hexagonal-pyramid unit cell versus the height-to-base diagonal diameter ratio (H/d) of the hexagonal-pyramid unit cell.

[0185] FIG. **69** is provided for reference for the following calculations. A hexagonal-pyramid unit cell of the 3-D substrate may be approximated by a cone (with the same height as a hexagonal-pyramid and the same base area as a hexagonal-pyramid). The aperture angle (ϕ) is:

$$\phi=2\tan^{-1}[D/(2H)]$$

[0186] The surface area of cone pyramid base (S_{cb}) is:

$$S_{cb}=(\pi D^2)/4$$

[0187] The surface area of cone pyramid sidewall (S_{cp}) is:

$$S_{cp}=[(\pi D^2)/4]\cdot\sqrt{[1+(2H/D)^2]}$$

[0188] Therefore, the ratio of the sidewall surface area S_{cp} to the top base surface area S_{cb} is:

$$S_{cp}/S_{cb}=\sqrt{[1+(2H/D)^2]}$$

[0189] FIGS. **70** and **71** show the ratio of the cone-shaped unit cell sidewall area to the planar circular base area (S_{cp}/S_{cb}) versus the height-to-base diameter ratio (H/D) of the cone-shaped unit cell and calculated frontside aperture angle ϕ of the solar cell cone-shaped unit cell (approximation for hexagonal-pyramid units cells) versus the height-to-base diameter ratio (H/D) of the cone-shaped unit cell. These FIGURES provide plots of aperture angle and surface area ratio for a cone-shaped pyramid, whereas FIGS. **66** to **68** show these plots for a hexagonal-pyramid unit cell. The results (plots) for a cone-shaped pyramid unit cell (approximation of a hexagonal-pyramid unit cell) are fairly comparable to those for the hexagonal-pyramid unit cell.

[0190] One important consideration in the TFSC and module interconnects is the total power loss associated with the electrical interconnects in the TFSCs and the solar module assembly. The hexagonal-pyramid 3-D c-Si TFSC and PCB-based module designs of this disclosure effectively address this issue, resulting in very low interconnect ohmic losses in the cells and within the module. This feature (in conjunction with the highly efficient packing of the TFSCs on the PCB-based solar module assembly) substantially narrows the efficiency gap between the TFSCs and the solar module assembly in the technology of this disclosure.

[0191] The next section relates to the basic calculations of the emitter contact metallization ohmic losses in the hexagonal-pyramid 3-D TFSCs of this disclosure. The calculations of ohmic losses for emitter contact metallization are also applicable to the base contact metallization. However, since several embodiments of this disclosure mount the 3-D TFSCs on patterned printed circuit boards (PCBs), the base contact

metallization is electrically connected in a planar format to a very high conductivity copper pad; this substantially reduces the base interconnect ohmic losses (compared to the emitter interconnect ohmic losses). Therefore, in practical embodiments of this disclosure, the interconnect ohmic losses are dominated by the emitter contact metallization.

[0192] FIG. **72** may be used for reference with an approximate analytical calculation of the TFSC interconnect ohmic losses, assuming a circular substrate with hexagonal-pyramid array of unit cells base on the cell design embodiments of this disclosure. Since the overall cell interconnect ohmic losses are dominated by the top emitter contact metallization, the ohmic power loss due to the hexagonal emitter contact metallization is calculated as a function of cell current at maximum power and emitter contact metal vertical height coverage ratio L/d (ratio of the height of emitter contact metal coverage on the pyramid sidewall to the pyramid unit cell long hexagonal diagonal dimension). The analytical calculations shown here were used to produce the plots shown in the following FIGURES (FIGS. **73**-**87**). The calculations performed and trends obtained for round substrates are also approximately applicable to square-shaped TFSC substrates.

[0193] For the following calculations: I_0 is the total cell current at peak power; $A=(\pi A^2)/4$, total cell area (shown for round cell); $J_0=(4\cdot I_0)/(\pi a^2)$, cell current density; R_{thm} is the sheet resistance of top honeycomb contact metal; C is the effective flat surface coverage of honeycomb contact with vertical height L; and $R_{eff}=R_{thm}/C$, where R_{eff} is the effective flat surface sheet resistance of top metal contact.

[0194] Based on this, the interconnect ohmic losses as maximum cell power are:

$$P_1 \cong (R_{thm}I_0^2)/\{8\pi(S_{hp}/S_{hb})[1-(1-L/H)^2]\}$$

$$P_1 \cong (R_{thm}I_0^2)\Big/\Big\{8\pi\big[\sqrt{1+(16/3)(H/d)^2}\,\big][1-(1-L/H)^2]\Big\}$$

[0195] FIGS. **73** and **74** plot the projected (calculated) interconnect-related solar cell power losses in the 3-D TFSCs of the disclosed subject matter as a function of the ratio of the hexagonal-pyramid height to diagonal base dimension (H/d) for two different emitter interconnect area coverage ratios on the top of the 3-D solar cell substrate. For H/d=2.0, the ohmic power loss experienced as a result of extracting the maximum power from a 400 cm^2 solar cell is projected to be around 0.1 to 0.2 W (depending on the emitter metal coverage shown for the two plots). Since the maximum solar cell power in this example is assumed to be around 8 W, the ohmic power losses for the solar cell interconnects (dominated by the emitter current collection) is projected to be between 1.25% and 2.5%. The PCB metal pattern can be designed such that the PCB interconnect ohmic power losses are much smaller than the above-mentioned solar cell interconnect power losses. Thus, the total ohmic power losses can be kept to well below 2%. This means that using the solar cell and module technology of the disclosed subject matter, the efficiency gap between the solar cells and the solar modules can be reduced to well below 2%. Thus, with a solar cell efficiency of 23%, we can have a high degree of confidence that we will achieve a solar module efficiency of at least 21%. Both FIGURES show the calculated solar cell ohmic power loss for large-area cells with 400 cm^2 area and 12 A current at maximum power (roughly 8 W_p max power assumed). R_{thm} is the sheet resistance of the emitter contact/metal layer (e.g., Ag layer or a stack of Ag on a refractory metal layer) on the honeycomb hexagonal ridges (0.0075 Ω/square for both graphs). The ratio L/H (here, 0.05 in FIG. **73** and 0.025 in FIG. **74**) is the ratio of the vertical coverage height of the emitter metallized contact on the honeycomb ridges to the height of the hexagonal-pyramid unit cell.

[0196] The following FIGURES show plots for various values of R_{thm} and L/H. FIG. **75** shows R_{thm} of 0.002 Ω/square and L/H of 0.05; and FIG. **76** shows R_{thm} of 0.002 Ω/square and L/H of 0.01. FIG. **77** shows R_{thm} of 0.005 Ω/square and L/H of 0.01; and FIG. **78** shows R_{thm} of 0.005 Ω/square and L/H of 0.02. FIG. **79** shows R_{thm} of 0.005 Ω/square and L/H of 0.05; and FIG. **80** shows R_{thm} of 0.005 Ω/square and L/H of 0.1. FIG. **81** shows R_{thm} of 0.01 Ω/square and L/H of 0.05; and FIG. **82** shows R_{thm} of 0.01 Ω/square and L/H of 0.02. FIG. **83** shows R_{thm} of 0.003 Ω/square and L/H of 0.02; and FIG. **84** shows R_{thm} of 0.003 Ω/square and L/H of 0.05.

[0197] In summary, the disclosed subject matter provides a template for pyramidal 3-D TFSC substrate formation. The template comprises a semiconductor substrate; the semiconductor substrate comprises a plurality of posts and a plurality of trenches between said plurality of posts. The template may be used as an environment for pyramidal three-dimensional TFSC substrate formation, through a plurality of template reuse iterations without a need for substantial reconditioning between each template reuse iteration. The pyramidal three-dimensional TFSC substrate may be formed by the steps of forming a sacrificial layer, depositing a semiconductor layer, selectively etching said sacrificial layer, and releasing said semiconductor layer. The pyramidal three-dimensional TFSC substrate may be used for fabricating a three-dimensional thin-film solar cell.

[0198] The foregoing description of the preferred embodiments is provided to enable any person skilled in the art to make or use the claimed subject matter. Various modifications to these embodiments will be readily apparent to those skilled in the art, and the generic principles defined herein may be applied to other embodiments without the use of the innovative faculty. Thus, the claimed subject matter is not intended to be limited to the embodiments shown herein but is to be accorded the widest scope consistent with the principles and novel features disclosed herein.

What is claimed is:

1. A template for pyramidal three-dimensional thin-film solar cell substrate formation, comprising:

a template substrate, said template substrate comprising:

a plurality of posts; and

a plurality of pyramid trenches between said plurality of posts,

wherein said template forms an environment for pyramidal three-dimensional thin-film solar cell substrate formation.

2. A template for pyramidal three-dimensional thin-film solar cell substrate formation of claim **1**, wherein said template forms an environment for pyramidal three-dimensional thin-film solar cell substrate formation through a plurality of iterations of pyramidal three-dimensional thin-film solar cell substrate formation without a need for substantial reconditioning of said template prior to each iteration.

3. A template for pyramidal three-dimensional thin-film solar cell substrate formation of claim **1**, wherein said template substrate comprises a semiconductor substrate.

4. A template for pyramidal three-dimensional thin-film solar cell substrate formation of claim **3**, wherein said semiconductor substrate comprises a silicon substrate.

5. A template for pyramidal three-dimensional thin-film solar cell substrate formation of claim **1**, wherein said plurality of pyramid trenches comprises a plurality of polygon-pyramid trenches.

6. A template for pyramidal three-dimensional thin-film solar cell substrate formation of claim **5**, wherein said plurality of polygon-pyramid trenches comprises a plurality of hexagonal-pyramid trenches.

7. A template for pyramidal three-dimensional thin-film solar cell substrate formation of claim **5**, wherein said plurality of polygon-pyramid trenches comprises a plurality of square-pyramid trenches.

8. A template for pyramidal three-dimensional thin-film solar cell substrate formation of claim **5**, wherein said plurality of polygon-pyramid trenches comprises a plurality of triangular-pyramid trenches.

9. A template for pyramidal three-dimensional thin-film solar cell substrate formation of claim **1**, wherein said plurality of pyramid trenches comprises a plurality of orthogonal V-groove pyramid trenches.

10. A template for pyramidal three-dimensional thin-film solar cell substrate formation of claim **1**, wherein said plurality of pyramid trenches between said plurality of posts further comprises a plurality of channels to provide etchant access.

11. A method for fabrication of a template for pyramidal three-dimensional thin-film solar cell substrate formation, the method comprising:

selectively removing semiconductor material from a semiconductor substrate to form a plurality of posts and a plurality of pyramid trenches,

wherein said template forms an environment for pyramidal three-dimensional thin-film solar cell substrate formation.

12. The method for fabrication of a template for pyramidal three-dimensional thin-film solar cell substrate formation of claim **11**, wherein said step of selectively removing semiconductor material from a semiconductor substrate to form a plurality of posts and a plurality of pyramid trenches comprises laser micromachining to produce a design on said semiconductor substrate.

13. The method for fabrication of a template for pyramidal three-dimensional thin-film solar cell substrate formation of claim **12**, wherein said design comprises a hexagonal-pyramid design.

14. The method for fabrication of a template for pyramidal three-dimensional thin-film solar cell substrate formation of claim **12**, wherein said design comprises a square-pyramid design.

15. The method for fabrication of a template for pyramidal three-dimensional thin-film solar cell substrate formation of claim **12**, wherein said design comprises a triangular-pyramid design.

16. The method for fabrication of a template for pyramidal three-dimensional thin-film solar cell substrate formation of claim **12**, wherein said design comprises an orthogonal V-groove pyramid design.

17. The method for fabrication of a template for pyramidal three-dimensional thin-film solar cell substrate formation of claim **11**, wherein said step of selectively removing semiconductor material from a semiconductor substrate to form a plurality of posts and a plurality of pyramid trenches comprises:

lithography patterning to produce a design on said semiconductor substrate; and

transferring said design onto said semiconductor substrate using an etching process.

18. The method for fabrication of a template for three-dimensional thin-film solar cell substrate formation of claim **17**, wherein said etching process comprises a deep reactive-ion etching process.

19. The method for fabrication of a template for pyramidal three-dimensional thin-film solar cell substrate formation of claim **17**, wherein said design comprises a hexagonal-pyramid design.

20. The method for fabrication of a template for pyramidal three-dimensional thin-film solar cell substrate formation of claim **17**, wherein said design comprises a square-pyramid design.

21. The method for fabrication of a template for pyramidal three-dimensional thin-film solar cell substrate formation of claim **17**, wherein said design comprises a triangular-pyramid design.

22. The method for fabrication of a template for pyramidal three-dimensional thin-film solar cell substrate formation of claim **17**, wherein said design comprises an orthogonal V-groove pyramid design.

23. The method for fabrication of a template for pyramidal three-dimensional thin-film solar cell substrate formation of claim **11**, wherein said step of selectively removing semiconductor material from a semiconductor substrate to form a plurality of posts and a plurality of pyramid trenches further comprises selectively removing semiconductor material to form channels in said plurality of pyramid trenches to provide etchant access.

24. The template for pyramidal three-dimensional thin-film solar cell substrate formation of claim **1**, wherein said template substrate can be reused to fabricate a plurality of pyramidal three-dimensional thin-film solar cell substrates.

25. The template for pyramidal three-dimensional thin-film solar cell substrate formation of claim **1**, wherein said template is a reusable template used for fabrication of a plurality of three-dimensional thin-film solar cell substrates.

26. The template for pyramidal three-dimensional thin-film solar cell substrate formation of claim **25**, wherein said template is reconditioned after a pre-specified number of reuse iterations in order to extend its ultimate iteration cycles.

27. The template for pyramidal three-dimensional thin-film solar cell substrate formation of claim **1**, wherein said plurality of posts comprises a honeycomb-shaped post pattern.

28. The template for pyramidal three-dimensional thin-film solar cell substrate formation of claim **1**, wherein said plurality of posts comprises a plurality of tapered posts.

29. The template for pyramidal three-dimensional thin-film solar cell substrate formation of claim **10**, wherein said plurality of channels to provide etchant access are formed through the template backside.

30. The template for pyramidal three-dimensional thin-film solar cell substrate formation of claim **10**, wherein said

plurality of channels to provide etchant access are formed through the template frontside.

31. The template for pyramidal three-dimensional thin-film solar cell substrate formation of claim **10**, wherein said plurality of channels to provide etchant access are through-wafer channels.

32. The template for pyramidal three-dimensional thin-film solar cell substrate formation of claim **10**, wherein at least a subset of said channels in said template substrate to provide etchant access directly connect to at least a subset of said plurality of trenches.

* * * * *